Copyright Warning & Restrictions

The copyright law of the United States (Title 17, United States Code) governs the making of photocopies or other reproductions of copyrighted material.

Under certain conditions specified in the law, libraries and archives are authorized to furnish a photocopy or other reproduction. One of these specified conditions is that the photocopy or reproduction is not to be "used for any purpose other than private study, scholarship, or research." If a, user makes a request for, or later uses, a photocopy or reproduction for purposes in excess of "fair use" that user may be liable for copyright infringement,

This institution reserves the right to refuse to accept a copying order if, in its judgment, fulfillment of the order would involve violation of copyright law.

Please Note: The author retains the copyright while the New Jersey Institute of Technology reserves the right to distribute this thesis or dissertation

Printing note: If you do not wish to print this page, then select "Pages from: first page # to: last page #" on the print dialog screen

ABSTRACT

HUMAN-ROBOT INTERACTION FOR ASSISTIVE ROBOTICS

by
Jiawei Li

This dissertation presents an in-depth study of human-robot interaction (HRI) with application to assistive robotics. In various studies, dexterous in-hand manipulation is included, assistive robots for Sit-To-stand (STS) assistance along with the human intention estimation. In Chapter 1, the background and issues of HRI are explicitly discussed. In Chapter 2, the literature review introduces the recent state-of-the-art research on HRI, such as physical Human-Robot Interaction (HRI), robot STS assistance, dexterous in hand manipulation and human intention estimation. In Chapter 3, various models and control algorithms are described in detail. Chapter 4 introduces the research equipment. Chapter 5 presents innovative theories and implementations of HRI in assistive robotics, including a general methodology of robotic assistance from the human perspective, novel hardware design, robotic sit-to-stand (STS) assistance, human intention estimation, and control.

HUMAN-ROBOT INTERACTION FOR ASSISTIVE ROBOTICS

by
Jiawei Li

A Dissertation
Submitted to the Faculty of
New Jersey Institute of Technology
in Partial Fulfillment of the Requirements for the Degree of
Doctor of Philosophy in Mechanical Engineering

Department of Mechanical and Industrial Engineering

December 2020

APPROVAL PAGE

HUMAN-ROBOT INTERACTION FOR ASSISTIVE ROBOTICS

Jiawei Li

Dr. Lu Lu, Dissertation Advisor — Date
Assistant Professor of Mechanical and Industrial Engineering, NJIT

Dr. Zhiming Ji, Committee Member — Date
Professor of Mechanical and Industrial Engineering, NJIT

Dr. Cong Wang, Committee Member — Date
Assistant Professor of Mechanical and Industrial Engineering, NJIT

Dr. Ian Fischer, Committee Member — Date
Professor of Mechanical and Industrial Engineering, NJIT

Dr. Sam Lieber, Committee Member — Date
Assistant Professor of Engineering Technology, NJIT

BIOGRAPHICAL SKETCH

Author: Jiawei Li

Degree: Doctor of Philosophy

Date: December 2020

Undergraduate and Graduate Education:

- Doctor of Philosophy in Mechanical Engineering,
  New Jersey Institute of Technology, Newark, NJ, 2020
- Master of Science in Mechanical Engineering,
  New Jersey Institute of Technology, Newark, NJ, 2016
- Master of Science in Mechanical Engineering,
  Universiti Technologi Malaysia, Skudai, Johor, 2012
- Bachelor of Science in Mechanical Engineering,
  Beijing University of Chemical Technology, Beijing, 2010

Major: Mechanical Engineering

Presentations and Publications:

L Lu, J Li, C Wang, D Strassberg, "A Novel Compliant Actuator With Load-Dependent Variable Stiffness: Design Concept and Control" *Dynamic Systems and Control Conference, Minneapolis, Minnesota*, 2016.

J Li, L Lu, C Wang, "Modeling and Precision Motion Control of Dexterous Object In-Hand Rotation" *IEEE International Conference on Mechatronics (ICM), Ilmenau, Germany*, 2019.

C Ding, L Lu, C Wang, J Li "6-DOF Automated Flight Testing Using a Humanoid Robot Arm" *International Conference on Automation Science and Engineering (CASE), Munich, Germany*, 2018.

J Li, L Lu, L Zhao, C Wang, X Huo "A Human-Centered Control Framework for Robotic Sit-to-Stand Assistance" *International Conference on Advanced Intelligent Mechatronics (AIM), Auckland, New Zealand*, 2018.

“When something is important enough, you do it even if the odds are not in your favor. I think it is possible for ordinary people to choose to be extraordinary.”

-Elon Musk

ACKNOWLEDGMENT

I would like to give my appreciation to my dissertation advisor Lu Lu for the guidance and teaching. I also want to give my thanks to all committee members: Zhiming Ji, Cong Wang, Ian Fischer and Sam Lieber for all assistance in my research. I appreciate the support of New Jersey Institute of Technology (NJIT) and National Science Foundation (NSF) award (No. 1625644) for the provided position of Research Assistant (RA) from 2016-2018 and the support from department of mechanical and industrial engineering for the provided position of Teaching Assistance (TA) from 2018-2020. I would like to give my biggest appreciation to my father Xiao Li, my mother Chunhua Duan, my wife Xiaoya Hai and my son Abdulla Li for their great support in my life.

TABLE OF CONTENTS

TABLE OF CONTENTS
(Continued)

TABLE OF CONTENTS
(Continued)

Chapter Page

LIST OF TABLES

LIST OF FIGURES

LIST OF FIGURES
(Continued)

LIST OF FIGURES
(Continued)

Figure **Page**

CHAPTER 1

INTRODUCTION

The increasing demands of Human-Robot Collaboration (HRC) in industrial field attracts great attentions of researchers to this area, such as: [1, 2]. The studies of HRC also show a large potential towards a wide range of home-automation tasks, such as: healthy lifestyle support, household and care support [3]. Traditionally, industrial robots are designed to complete a series of complicated tasks automatically. These tasks are usually simple and repetitive. In order to deal with increasingly complex and challenging tasks, recently researchers have brought the concept of the Human-Robot Collaboration (HRC) to this area. This allows the robot and the human work collectively to accomplish complicated tasks. In the field of healthy life care, the Human-Robot Interaction (HRI) has been implemented in nursing and medical assistance for years. The most common example is the movement support robots which are made for disabled people or elderly people. The applications of the surgical assistive robot and doctor collaboration in the hospital can be seen occasionally as well. With embedded the Artificial Intelligence (AI) in the robotic systems, scholars have boosted the technology to a higher level. Nowadays, researchers try to provide decision making abilities to robots so that these intelligent robots can be used for operating in houses or public places as agents of household support, care support and public services.

The Human-Robot Interaction/Collaboration (HRI/HRC) is a promising research field. However, the HRI/HRC has safety issues since robots are required to physically interact with humans in many applications. This could potentially endanger an operator who is adjacent to the robot. On the other hand, the robot could be damaged during operations as well. To ensure safety between operators and robots, many algorithms, control approaches and sensors have been invented. For example, optical sensors and

imaging techniques have been widely used in the HRI applications, such as gesture recognition and motion detection. These techniques provide a visual advantage for robots to adapt to the unpredictable environment. Acoustical sensors are also applied to the human-robot interaction as people can easily send their phonetic orders to the robots which decreases the chances of physically interacting with robots and increases the safety. Recently, a new approach has been created and applied in the HRI. Researchers attempt to combine the artificial intelligence and force/torque sensors together so that robots are able to perceive surroundings by its tactile sense.

An intelligent robot is not only capable of communicating with people but also capable of studying from people. The Machine Learning (ML) method and the Artificial Neural Networks (ANNs) are mostly used in robotics. One well-known example is the Google "Alpha-Go". This amazing AI has already defeated many professional GO players in the world. The reason of giving intelligence to robots is to improve the performance of human and robot collaboration rather than using it with a vicious purpose. If robots were to be able to obtain experience from people, then collaboration between human and robots would become more convenient, smoother and safer.

There are a lot of research on the Human-Robot Interaction (HRI) that have been done. However, researchers are facing some complicated and arduous issues as well. There are some unsolved problems as listed below:

First of all, many studies of home-automation and HRI stagnate at the state of kinematic and spatial relationship between a robot and surroundings. Although in these type of research, control problems are simplified, interactions between a moving robot and objects on dynamic level are neglected. Missing the dynamic feedback in pHRI and home-automation is non-trivial since the accuracy and safety are directly affected by the dynamics. Therefore, dynamic modelling in pHRI and home-automation is crucial.

Second, traditional studies on HRI, especially pHRI, make very simple problem formulations, such as set-point regulation, trajectory tracking, and impedance control for

human-robot contact. The reason why these assumptions are made to be extremely simple is that they can be easily converted into control problems, which are easily solved with guaranteed stability and performance. However, this type of "low-level" human-robot interaction has very limited applications. In reality, the collaboration between human and robot often involves various scenarios, changing environments, which can only be solved through high-level decision making. For example, when a robot helps an elderly people to put clothes on, the robot must make decision on how to change the orientation and position of the sleeves such that human can put their arms in easily. The robot should also decide whether human arm gets jammed in the sleeves and make a recovery strategy. The complicated scenarios involved in such type of tasks cannot be simply formulated as low-level control problems. Thus, more realistic problem formulation capturing all the complicated situations and uncertainties during human-robot interaction needs to be make, which should be addressed combining low-level control law and high-level planning/decision making algorithm together.

Third, the current state of the art of sensing, estimation, and prediction of human motion and intention is immature. To improve the collaborative performance in a human-robot task execution, the robot must read the human motion and understand its intention. Current human body sensing technique is not able to meet the stringent requirement of human-robot collaboration. For example, vision and time-of- flight sensors are subject to occlusion issue, while inertia sensors and potentiometers only measure the motion of the human skeleton without information on its exterior. More advanced sensing techniques need to be developed to capture human motion accurately. Besides, the prediction of human intention is also crucial to the success of human-robot collaborative task execution. Current methods on human motion prediction mainly focus on the application of extended Kalman filter, which is too simple to capture the decision process of human being during task execution.

Fourth, the safety between human and robot during their collaboration is not yet fully guaranteed. There have been various studies on human-robot safety issue. Each of them focuses on a particular aspect, such as hardware design, control design, motion planning, and decision making. However, human-robot safety is a complicated issue involving both low-level control and high-level intelligence. Failure to attack the safety problem from a holistic point of view leads to a trade-off between safety and performance, i.e., the robot has to move slowly and stay far enough to human to guarantee safety. How to ensure safety while maximizing the performance through the incorporation of physical control and decision making is yet to be studied.

The research aims to study physical Human-Robot Interaction (pHRI) with respect to how a robot helps the disabled and the elderly in their daily lives. This research field has extremely significant meanings for development and progress of modern human society since robotics, a promising technology, acts as an alternative, yet an very important tool for assisting people. In this dissertation, the study consists of seven chapters, which illustrates the research from various perspectives, such as dynamics modeling, apparatus construction and controller design. In the matter of script-writing, first of all, the study provides theoretical background and methodologies. Such as motion/trajectory planning, robot motion control method and robot force control algorithm, etc. The purpose of illustrating these algorithms is to give the theoretical support for safe and reliable physical Human-Robot Interaction (pHRI). Second, the research also provides several examples as well as information of assistive robot setups and current research as well as experimental results. For instance, design a human-centered control framework for robot assisted Sit-To-Stand (STS) and perform dexterous in-hand manipulation with a three-fingered robotic gripper. Third, the dissertation introduces the study results.

CHAPTER 2

LITERATURE REVIEW

2.1 Dexterous In-Hand Manipulation

In 2010, the population of aged Americans who have difficulty in grasping is $2,785,000$. Among this population, $334,000$ elderly people have a severe grasping issue [4].

Conventionally, medical science and neurology act as the major treatments for the patients. Nevertheless, in recent decades, with the prosperity of robotics, robots serve as alternative, yet effective tools for assisting those with difficulties in grasping [5]. Traditionally, robots are programmed, and are commanded for performing a series of simple, stiff and repetitive grasping motions in factories. Nowadays, as the application of robots to assistive living and home automation thrives, it is required that the new generation of assistive robots can perform elaborate and dexterous hand motions in human environment. Therefore, Dexterous Manipulation (DM), which is defined as the "object-oriented", multiple-fingers collaborative in-hand manipulation [6], has attracted significant attention in the study of assistive robotics.

Many tasks in home automation and assistive living environment require a robot to perform complicated rotational/cyclic grasping motions. For example, peeling the shell of a boiled egg for a patient who has Parkinson's Disease (PD), installing a bulb for a chandelier or pulling a circular duct tape for pipe repairing. To succeed in completing these tasks, a robot usually needs to take rolling, sliding as well as shifting motions into consideration. This type of tasks is intuitive and natural for a human, yet very challenging for robots as the contact modeling is extremely complicated. To bypass the difficulty, some researchers developed a variety of soft grippers, for instance, [7–9]. As a matter of fact, soft grippers have fine adaptive ability towards different objects and are usually easy to control. Nevertheless, compliant grippers are not designed for performing accurate and complicated

in-hand manipulation. Most of the compliant grippers are open-loop controlled, and the low stiffness between the actuator and the fingertip makes the precision contact motion control difficult.

In recent years, a fairly large number of researchers have started to use machine learning methods for complex dexterous in-hand manipulation, since the machine leaning methods are able to provide solutions based on massive data without the need of an explicit model which might be very complicated for robot in-hand manipulation, in [10–12]. It is worth noting that the machine learning methods usually reduce complexity in system modeling, whereas the system stability, robustness and performance cannot be testified by any means. Such a drawback may result in significant issues for assistive robots, as in home automation and assistive living environment, a failure operation of the robotic gripper may result in a severe injury to the human or damage to the object or home facilities. Therefore, the safety issue of using machine learning methods is still controversial.

Another group of researchers prefer modeling based control techniques for dexterous in-hand manipulation, as the force/dynamic model based approaches have outstanding performance in terms of accuracy, stability and robustness, [13, 14]. However, these research usually concern the problem of controlling the instantaneous motions of the object, yet ignoring finger-gaits planning for different types of dexterous in-hand manipulation tasks. Moreover, these studies usually involve complicated mathematical formulations of the physical movements in all degrees of freedom, which cannot be easily applied in practical tasks. In comparison, when a human executes this kind of manipulation, he/she only cares about the object movement in some of the "main" degrees of freedom, while other directions are controlled subconsciously. On the another hand, some researchers devote to certain specific areas of the dexterous manipulation, such as in-hand sliding manipulation or object re-grasping manipulation by using external contact. Some examples are given in [15, 16].

2.2 Robot STS Assistance

The increasing number of elderly Americans with chronic conditions or disabilities post significant challenge on public health as the chronic conditions as well as disabilities limit daily activities and reduce the quality of life of these people [17, 18]. Sit-To-Stand (STS), for example, is one of the fundamental and the most performed activities in people's daily lives. Achieving this action requires a sturdy and healthy muscle group to perform a series of complicated motions. According to the study [19], frequent repetition of knee movement may lead to wearing and degenerated knee functionality even for a healthy elderly individual, not to mention the impacts of STS motion to those with weak knees or those who suffer from various chronic conditions or disabilities. As for the latter, to accomplish this task successfully without giving any external assistance is incredibly difficult.

In the fields of bio-engineering and rehabilitation, a large quantity of research concentrates on designing and manufacturing mobile-based devices for STS assistance. For instance, [20–23]. In general, these mobile-based devices are time-consuming to design, expensive to manufacture and less intelligent to cope with any complicated tasks. Sometimes, the mobility of the devices is constrained by surroundings and terrains when the device operates at a narrow area. Additionally, an elderly or a disabled who accepts these types of assistive devices must confine himself/herself to it for most of the time.

A more intelligent and less constrained STS assistance requires the use of a mobile robot manipulator. A general purpose mobile robot manipulator also has potential to assist patients with varieties of daily activities in the future, which is more economic and efficient than having a myriad of assistive devices specific to different activities. However, the studies of using a mobile robot manipulator for STS assistance are very few. In [24], the authors propose an impedance controller to optimize interaction force between the human and the robot in STS assistance. However, it does not take into account the human body dynamics and optimize joint load of the human, which is a primary concern for people with

weak knees and back pains. In [25], an optimal control formulation is developed to resolve issues of task end-point accuracy, human balance, energy consumption and smoothness of motion according to the dynamic model constructed. Nevertheless, the research does not explicitly study different phases of STS motion as well as how to generate a robot trajectory to achieve the proposed optimal assistance. In fact, an STS process usually contains various stages (phases) [26]. For example, before getting up from a seated place, a person needs to adjust the center of weight so that he/she can successfully stand up. The study of how to control the robot movement that optimizes the joint muscle load of the human through the entire multi-stage STS process has been lacking.

On the other hand, human intention is also a critical factor in STS assistance that has been rarely taken into account. In most cases of physical Human-Robot Interaction (pHRI), due to the limitation of robots' intelligence, a human often plays as the leader, with a robot being the follower to assist the human. Therefore, in order to guarantee performance and safety, it is critical that a robot is able to estimate human intentions during any collaborative tasks. Some representative examples and methods, which are used for estimating human intention can be found in [27–30]. In a robotic STS assistance, the human intention also plays a significant role, since the human is not only the one who needs to be assisted, but also the master who naturally attempts to lead the entire STS motion, such as altering the stand-up speed, or sitting back down due to a sudden change of decision. Very limited research of robotic STS assistance has taken human intention into consideration. For example, [31,32]. Whereas, systematically predicting and using human intention to achieve a better STS assistance have not been investigated.

2.3 Human Intention Estimation

The increasing demands of Human-Robot Collaboration (HRC) in markets not only reveals an enormous efficacy of intelligent robots in mass production/manufacturing, but also exhibits a great potential in assistive tasks in people's daily lives [33, 34]. As a matter

of fact, the number of senile Americans who have disabilities is increasing in recent years that brings out an evident alert to the public health [18]. For the elderly who has gonitis or cervical osteoarthritis, for example are struggling with performing the most fundamental activities, such as walk as well as Sit-To-Stand (STS) in their daily lives since to accomplish these motions requires collaborations of both healthy muscles and joints. Therefore, it is believed that assistive robots can be an effective solution for these people in their daily lives.

Much research, for instance [20, 21, 24, 25] have studied the STS assistance. However, the issues of safe contact and human intention detection in STS assistance haven't been sufficiently studied. In fact, safe and dexterous STS assistance imposes a requirement of relatively high-level intelligence on the robot side to cope with various complicated situations. Such situations usually involve tasks re-planning and human intention estimation when the human partner suddenly changes his/her mind; maintaining the contact force between human and robot in order to achieve a safe and comfortable contact environment; Therefore, creating high efficient and intelligent robots is the pivotal issue for researchers and engineers.

In regard to human intention recognition, various approaches and models have been made to estimate human motion/intention using Artificial Neural Networks (ANNs). In [35], on the basis of a simplified joint position model, the authors propose a semi-adaptive neural network to predict human joint motions in real-time. In [36], a Recurrent Neural Network (RNN) is applied to estimate multiple and varying length action sequence using gaze and body posture data. In [37], a visual data driven Deep Convolutional Neural Network (DCNN) is investigated for recognition of human intended motions and context of human actions. A common feature of these studies is that the human intention estimation models are constructed on the similar structure which takes either current human limb/joint trajectories or human postures as the input. It takes the future joint trajectories or future human postures as the output. No doubt that this kind of framework is easy to understand

and convenient to apply in the research. However, it neglects contact forces between human and robots during the interaction process that may cause injuries of the human partner.

On the other hand, certain research, for instance [38, 39], adopts an alternative approach which uses force/pressure or tactile sensors to control the contact force and to anticipate human intention in HRC in consideration of simplicity of its underlying mechanism. Furthermore, bio-signal based sensors, such as Electromyography (EMG) or Electroencephalography (EEG) sensors are also utilized to forecast human intention in HRC, for example, [40, 41]. Despite the convenience of using these sensors to obtain contact force signals, its limitations are also evident. In reality, sensor readings are always tangled with uncertainties and disturbance which may result in less accurate performance [42].

In comparison with the above approaches, other scholars combine model-based control method, such as impedance model, with ANNs in the research of human intention recognition in order to involve more integrated contact models to the system meanwhile reduce the system sensitivity to the disturbance. For example, [43–46]. In spite of the advantages possessed in this approach, such as safe force control and real-time human intention recognition, these studies haven't considered a simultaneously recognition process of contact model identification and human intention estimation. In fact, when a person collaborates with another person in a task. The human workers are capable of figuring out what the partner intention is and how much force is applied by the another partner at the same time. Therefore, if the robot is able to achieve these functionalities in collaborative tasks. Then the safety and efficiency in robot assistance will be upgraded to a higher level.

CHAPTER 3

METHODOLOGY AND ALGORITHM

In this chapter, various algorithms that have been used in the research are introduced. First of all, a planar human body dynamic model that adopts a five-linked robot dynamics is presented. The model is applied in a series of studies of robot assisted Sit-To-Stand (STS) motion. Second, we explored the 2D frictional model for planar contact. This model is used for research of dexterous in-hand manipulation. Third, robot motion control, robot force control as well as hybrid control methods are introduced. Fourth, the principle of Artificial Neural Network (ANN) is explained.

3.1 Human Body Muscular Model

This model is constructed as a 2D model, which assumes that the human body can be depicted as a five-linked robotic system. The dynamics can be simply given as:

$$M(\theta)\ddot{\theta} + C(\theta,\dot{\theta})\dot{\theta} + G(\theta) = \tau + J(\theta)^T F, \tag{3.1}$$

where $M(\theta) \in R^{5\times5}$ is a positive definite symmetric matrix that represents the inertia of the robot, $C(\theta,\dot{\theta})\dot{\theta} \in R^5$ is the vector of Coriolis and centripetal forces, $G(\theta) \in R^5$ is the gravitational force vector, $\tau \in R^5$ represents the human joint torque. The interaction force $F \in R^2$ on the human's hand is generated indirectly from both the human joint torque and the robot motion. The matrix $J(\theta) \in R^{2\times5}$ is the Jacobian from the human joints to the human hand.

3.2 Planar Frictional Contact

The planar Coulomb friction for surface contact is given as a wrench, which the direction of the kinetic friction is in the same direction of the instantaneous velocity of the contact

region. The 2D kinetic friction is formulated as the integration over the contact area $\mathscr{A}$:

$$\mathbf{W} \triangleq \begin{bmatrix} f_x \\ f_y \\ \tau_f \end{bmatrix} = \begin{bmatrix} \mu p \int_{\mathscr{A}} \frac{v_x}{\sqrt{v_x^2+v_y^2}} dA \\ \mu p \int_{\mathscr{A}} \frac{v_y}{\sqrt{v_x^2+v_y^2}} dA \\ \mu p \int_{\mathscr{A}} \frac{v_x r_y - v_y r_x}{\sqrt{v_x^2+v_y^2}} dA \end{bmatrix} \tag{3.2}$$

Where $\overrightarrow{v_x}$ and $\overrightarrow{v_y}$ are velocities along x and y directions at each point within the contact region. We assume that the pressure p is isotropic in the area $\mathscr{A}$. Therefore, p can be taken out of the integration. (r_x, r_y) is coordinate of each point with in the area $\mathscr{A}$.

3.3 Robot Motion Control

The basic robot control follows the design procedure as below:

1. Tasks.
2. Desired Trajectory or Set Point Planning.
3. Desired Torque Evaluation.
4. Voltage/Current Input Calculation.

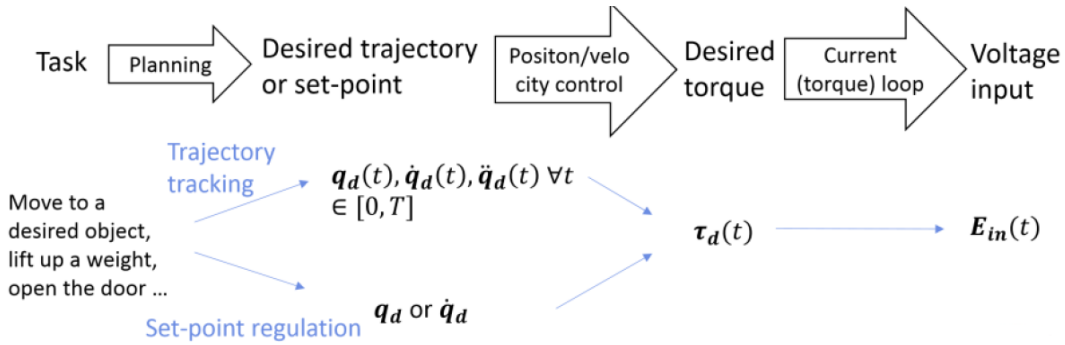

Figure 3.1 The basic robot control design procedure.

In robotic, the traditional motion control can be divided as three basic control approaches which are position control, velocity control and force/torque control. However, there exists another method which is combining the three previous methods together into a hybrid control algorithm. In position and velocity control, the objective can be divided into two

categories: the first one can be described as trajectory tracking. Namely, trajectory tracking task is to track a time vary desired trajectory with $q(t)$, $q\dot{(}t)$ and $q\ddot{(}t)$ in advance. The second one can be depicted as set-point regulation. The set-point regulation can be described as regulating the joint position or velocity towards a constant set-point $q(t)$ or $q\dot{(}t)$. To accomplish position or velocity tracking, there are two approaches:

1. *Decentralized Control*

Decentralized control is to control each joint variable independently without considering interaction.

$$B(q)q\ddot{(}t)+C(q,q\dot{(}t))+F_v q\dot{(}t)+g(q)=T+\delta \tag{3.3}$$

In which, $B(q)q\ddot{(}t)$ represents the inertia term, the $C(q,q\dot{(}t))$ is the Coriolis force term, $F_v q\dot{(}t)$ represents the viscous friction term, $g(q)$ is the gravity term, and T as well as δ are actuator force and disturbance. If the interacting forces can be ignored, then the terms $B(q)$ and F_v can be decomposed as diagonal matrices and disturbance terms. Therefore, the equation (3.3) can be transformed into:

$$\bar{B(q)}q\ddot{(}t)+\bar{F}_v q\dot{(}t)=T+d \tag{3.4}$$

Where, the term $\bar{B(q)}q\ddot{(}t)$ and $\bar{F}_v q\dot{(}t)$ are diagonal matrices. The disturbance term d can be written as:

$$d=\bar{B(q)}q\ddot{(}t)-B(q)q\ddot{(}t)-C(q,q\dot{(}t))-g(q)+\delta \tag{3.5}$$

Assuming that PID controller is applied to the robotic system, then for set-point regulation problem, the input torque can be designed as:

$$T = \bar{F}_v q(\dot{t}) + B(\bar{q})q(\ddot{t})(-K_p e - K_I \int e - K_d \dot{q}) \tag{3.6}$$

In which e equates to $q - q_d$, and q_d is the desired set-point.

In the trajectory tracking problems, the PID controller can be designed from designing $e = q - q_d$, $\dot{e} = \dot{q} - \dot{q_d}$, $\ddot{e} = \ddot{q} - \ddot{q_d}$. By substituting the equation (3.3) into $\ddot{e}$. The state equation is given as:

$$\ddot{e} + K_p e + K_I \int e + K_d \dot{e} = \bar{B}^{-1} d \tag{3.7}$$

If the term $\bar{B}^{-1}d$ is small enough, then the equation (3.7) will converge to zero, therefore the system will tends to stable.

2. *Centralized Control*

The centralized control is nearly equivalent to the decentralized control, however interactions are considered in each joint.

$$\ddot{e} = \bar{B}^{-1}(T - B(q)\ddot{q_d} - C(q, q(\dot{t})) - g(q) - F_v q(\dot{t}) + \delta) \tag{3.8}$$

The force T can be designed as:

$$T = B(q)\ddot{q_d} + C(q, q(\dot{t})) + g(q) + F_v q(\dot{t}) - B(q)(K_p e + K_I \int e + K_d \dot{e}) \tag{3.9}$$

Substituting equation (3.9) into (3.8), we have

$$\ddot{e} + K_p e + K_I \int e + K_d \dot{e} = \delta \tag{3.10}$$

If the value of δ is small enough, then equation (3.10) will converge to zero, therefore the system will tends to stable.

3.4 Force Control

The purpose of force control is to control the contact force between robot and environment. There are two basic force control methods: direct force control and indirect force control. Indirect force control is to construct a force-displacement model, then control the force through displacement, while direct force control is to synthesize a feedback controller to minimize the measured force tracking error.

1. *Direct Force Control*

The principle of direct force control is to design a controller to minimize the force tracking error. Suppose the desired force is F_d, the tracking error can be depicted as $\bar{F} = F - F_d$. Design a PID controller so that the state space equation can be transformed into:

$$\ddot{\bar{F}} + K_d\dot{\bar{F}} + K_p\bar{F} + K_i\int \bar{F} = 0 \tag{3.11}$$

2. *Indirect Force Control*

The purpose of indirect force control method is to minimize the trajectory tracking error or set-point tracking error. The tracking error can be described as $e = X - X_d$. The contact force can be designed as:

$$K_1(\ddot{X} - \ddot{X_d}) + K_2(\dot{X} - \dot{X_d}) + K_3(X - X_d) = -F \tag{3.12}$$

At steady-state, the equation (3.12) becomes as:

$$K_3(X - X_d) = -F \tag{3.13}$$

if the force F is nearly as the same as the desired force F_d, then the force control becomes a position control.

3. *Hybrid Control*

The hybrid control method focus on both force control and motion control simultaneously, but in different directions. Before the calculation, it is important to specify frame of interest and convert to a singular one. For example, as can be seen from the Figure 3.2.

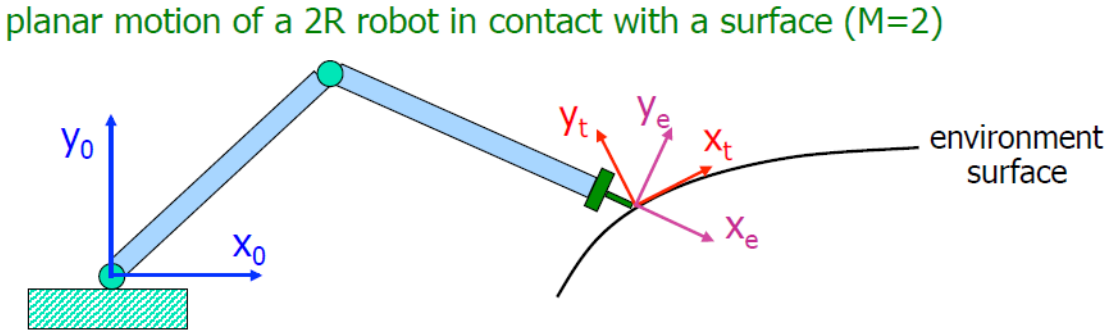

Figure 3.2 2D hybrid control.
Source:http://www.diag.uniroma1.it/ deluca/Teaching.php]

The task frame is represented by the red arrows, which is used for an independent definition of the the hybrid reference values and for computing the errors driving the feedback control law. The sensor frame is indicated by violet arrows, where the forces (F_{ex}, F_{ey}) on end-effector are measured. The base frame is at the origin, in which the velocity of the end-effector is expressed. All frames are required to be converted to the task frame.

$$\begin{bmatrix} W \\ V \end{bmatrix} = T(s)\dot{s} \tag{3.14}$$

In which, the equation (3.14) represents the free motions, W is the angular velocity and the V is the linear velocity.

$$\begin{bmatrix} F \\ M \end{bmatrix} = Y(s)\alpha \tag{3.15}$$

Where $T(s)$ and $Y(s)$ are the generalized directions of the task frame. F is the force and M is the torque.

The kinematics of the robot can be expressed as:

$$\begin{bmatrix} W \\ V \end{bmatrix} = J(q)\dot{q} \tag{3.16}$$

The dynamics of the robot can be represented by the equation:

$$B(q)\ddot{q(t)} + C(q,\dot{q(t)}) + g(q) = U + J^T(q) \begin{bmatrix} F \\ M \end{bmatrix} \tag{3.17}$$

The control objective is to impose $S(t)$ approaches as close as possible to the desired value $S_d(t)$, and $\alpha(t)$ approaches as close as possible to the desired value $\alpha_d(t)$ as well. The control law can be designed into two steps.

The first step is to exact linearization and decoupling in the task frame by feedback.

$$\begin{bmatrix} \ddot{s} \\ \alpha \end{bmatrix} = \begin{bmatrix} a_s \\ a_\alpha \end{bmatrix} \tag{3.18}$$

The second step is to design of a_s and a_α so as to impose the desired dynamic behavior to the errors $e_s = s_d - s$ and $e_\alpha = \alpha_d - \alpha$.

$$J(q)\dot{q} = T(s)\dot{s} \tag{3.19}$$

From equation (3.19), it can be transformed into:

$$\ddot{q} = J^{-1}(T\ddot{s} + \dot{T}\dot{s} - J\dot{q}) \tag{3.20}$$

Substituting the equation (3.20) into (3.17),

$$U = \begin{bmatrix} BJ^{-1}T & -J^TY \end{bmatrix} \begin{bmatrix} a_s \\ a_\alpha \end{bmatrix} + BJ^{-1}(\dot{T}\dot{s} - J\dot{q}) + s\dot{q} + g \tag{3.21}$$

It is sufficient to apply linear control techniques. Therefore, the equation (3.21) can be separated into motion control part and force control part:

$$a_s = \ddot{a_d} + K_d(\dot{s_d} - \dot{s}) + K_p(S_d - s) \tag{3.22}$$

$$a_\alpha = \ddot{\alpha_d} + K_I \int (\alpha_d - \alpha)dt \tag{3.23}$$

3.5 Artificial Neural Networks (ANN)

An Artificial Neural Network (ANN) is a type of computing model. It has layered structure that simulates the networked structure of biological neurons and connected nodes. A neural network is capable of learning from given data, therefore it is able to be trained to recognize patterns, classify data, and forecast future events. A neural network that work with less than three layers of connected neuron layers is treated as a shallow neural network. On the other hand, a deep learning network contains many layers. As can be seen from Figure 3.3.

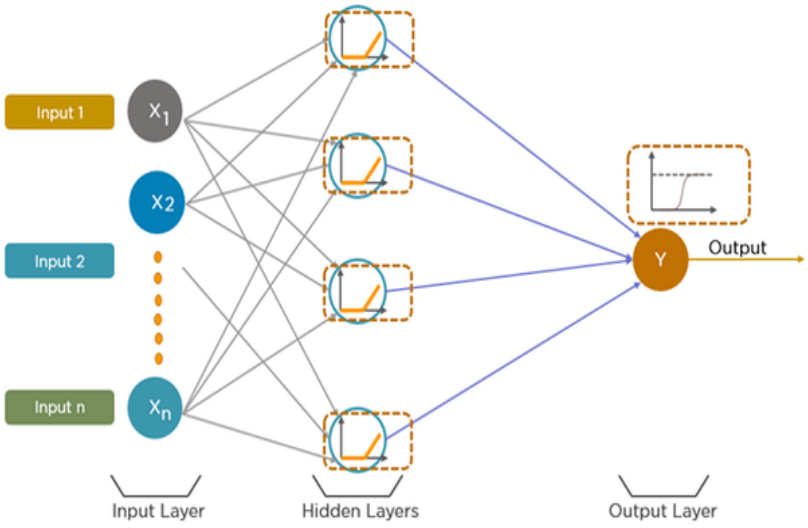

Figure 3.3 Typical neural network architecture.

3.5.1 Supervised Learning

Supervised learning is defined as training networks with given sample inputs and desired outputs. This method is particularly appropriate for system modeling, data classification, and future events prediction.

3.5.2 Classification

Classification is a kind of supervised learning method. This algorithm is used for identifying incoming data and labelling them into given categories.

3.5.3 Regression

Regression models construct the relationship of a output and one or more inputs.

3.5.4 Pattern Recognition

Pattern recognition is an indispensable method of Artificial Neural Networks (ANN) which is widely used in computer vision, character recognition, and data classification. The principle of pattern recognition can be depicted as classifying inputs into objects or classes on the basis of different unique features. This algorithm uses either supervised learning or unsupervised learning approaches.

3.5.5 Unsupervised Learning

Unsupervised learning is a type of training method that distinguishes from supervised learning. This learning approach let the ANN continually tune itself to new input data without using labeled responses.

3.5.6 Clustering

Clustering is a type of unsupervised learning method, where neural networks can be used for finding hidden patterns of data or grouping data.

CHAPTER 4

HARDWARE AND APPARATUS SETUP

In this section, the experimental apparatus and hardware are introduced. In particular, we give detailed descriptions on load dependent stiffness actuator, Movable Sawyer Arm Platform (MSAP), AUBO robot system, three-fingered robotic hand and motion capture system.

4.1 Load Dependent Stiffness Actuator

The load dependent stiffness actuator is designed to behave like a rigid actuator during normal operation and automatically switches to a compliant actuator in the event of an unexpected collision, without the need of additional force sensor/estimation. As shown in Figure 4.1. The system contains two parts, each part is driven individually by a motor. The

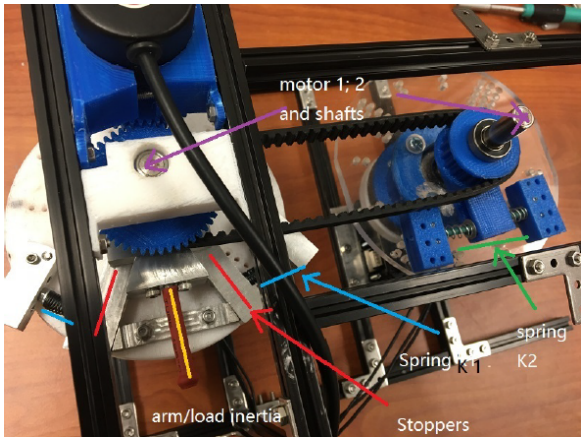

Figure 4.1 Prototype of semi-compliance load dependent actuator.

left part is driven by the initiative motor, and another part is driven by another motor. The prototype is consisted of two stoppers. The load inertia is clamped tightly by two stoppers, and the clamping force is generated by springs. The second/driven motor is connecting

with the initiative motor by using a belt and two springs. An encoder is used to record the rotational angles, angular velocities of the system.

4.2 Movable Sawyer Arm Platform

As can be seen from the Figure 4.2 the Movable Sawyer Arm Platform (MSASP) is

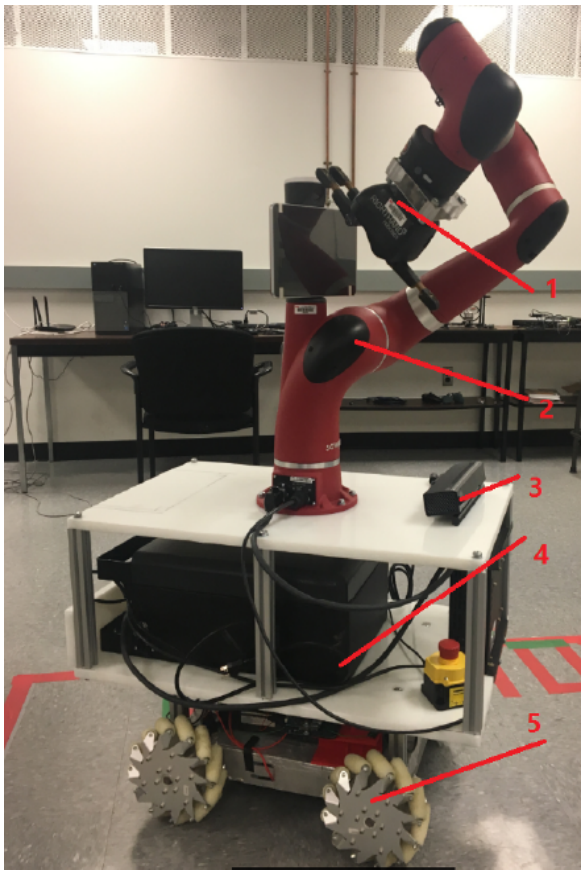

Figure 4.2 Movable Sawyer Arm Platform (MSAP).

a compound-typed robot that it contains five basic components: 'Right-Hand' gripper, Sawyer robot manipulator, 'Kinect' sensor, ROS as well as movable platform.

4.2.1 Right-Hand Gripper

The ReFlex Takktile hand is a underactuated hand with tactile sensors and joint feedback. The system consists of four actuators which are responsible for the movement of the three fingers. In there are nine tactile sensors embedded each finger. The collision-safe

mechanism is considered and designed with robust hardware. To ensure the simplicity of installation and operation, the Robotic Operating System (ROS) is served as the interface for the purposes of easy control and programming. As can be seen in Figure 4.3.

Figure 4.3 ReFlex Takktile hand.
Source:[https://cobotsguide.com/. Right Hand Robotics]

4.2.2 Sawyer Robotic Arm

Sawyer is a seven Degree Of Freedom (DOF), revolutionary collaborative robot designed to execute tasks that have been impractical to automate with traditional industrial robots. Sawyer gives manufacturers the high performance automation they need, while maintaining the flexibility, safety and affordability synonymous with the Rethink brand. As shown in Figure 4.4.

Figure 4.4 Sawyer robotic arm.
Source:[https://www.rethinkrobotics.com/sawyer.]

4.2.3 Microsoft-Kinect

$Microsoft - Kinect^{@}$ is an optical sensor that originally developed for video gaming. Recently, the Kinect sensor, which can be seedn from Figure 4.5, is utilized in robotics as it has a proprietary algorithms for feature selection, scene analysis, motion tracking, skeletal tracking, and gesture recognition.

Figure 4.5 Microsoft-Kinect.
Source:[https://en.wikipedia.org/wiki/Kinect.]

4.2.4 Robot Operating System

The Robot Operating System (ROS) is a flexible framework for writing robot software. It is a collection of tools, libraries, and conventions that aims to simplify the task of creating complex and robust robot behavior across a wide variety of robotic platforms.

4.2.5 Movable Platform

Figure 4.6 displays the mecanum wheeled robotic platform which is programmable with 'Arduino'. It is designed for driving the Sawyer robotic arm system moving in multi-directions. It includes the CNC cut 4WD base intended for the IG52 gear motors and nexus mecanum wheels or omni-directional wheels. The chassis is a rigid gusseted aluminum frame that is precisely fabricated using state of the art CNC equipment. Each wheel is supported by two angled, double-sealed ball bearing for extra support and chain driven. It is designed for any of planetary IG52 gear motors with or without encoders.

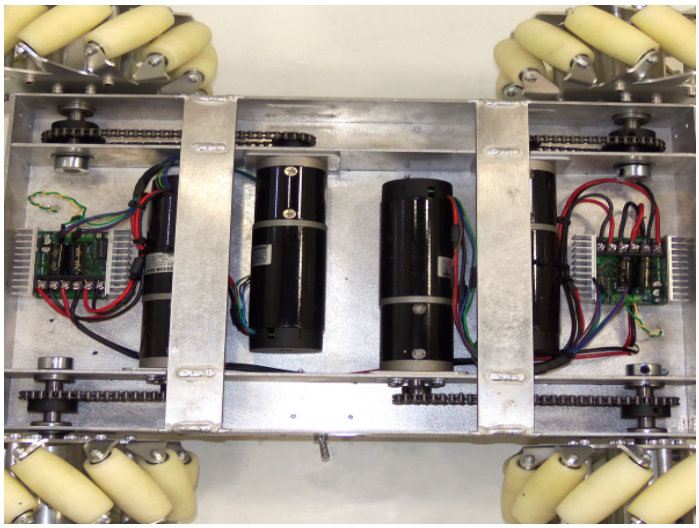

Figure 4.6 Mecanum wheel robot platform.

4.3 AUBO Robot System

AUBO robot, as shown in Figure 4.7 is a lightweight intelligent collaborative six degree of freedom robots (5 kg payload) that offers variety of functions and features. Specifically,

AUBO is easy to program and teach. It is able to work side by side with human operator without safety fence, laser or sensors. It also provides open source architecture which compatible with several communications, such CAN bus and ROS. The AUBO system consists of AUBO robotic arm, controller box, control pad as well as terminal computer.

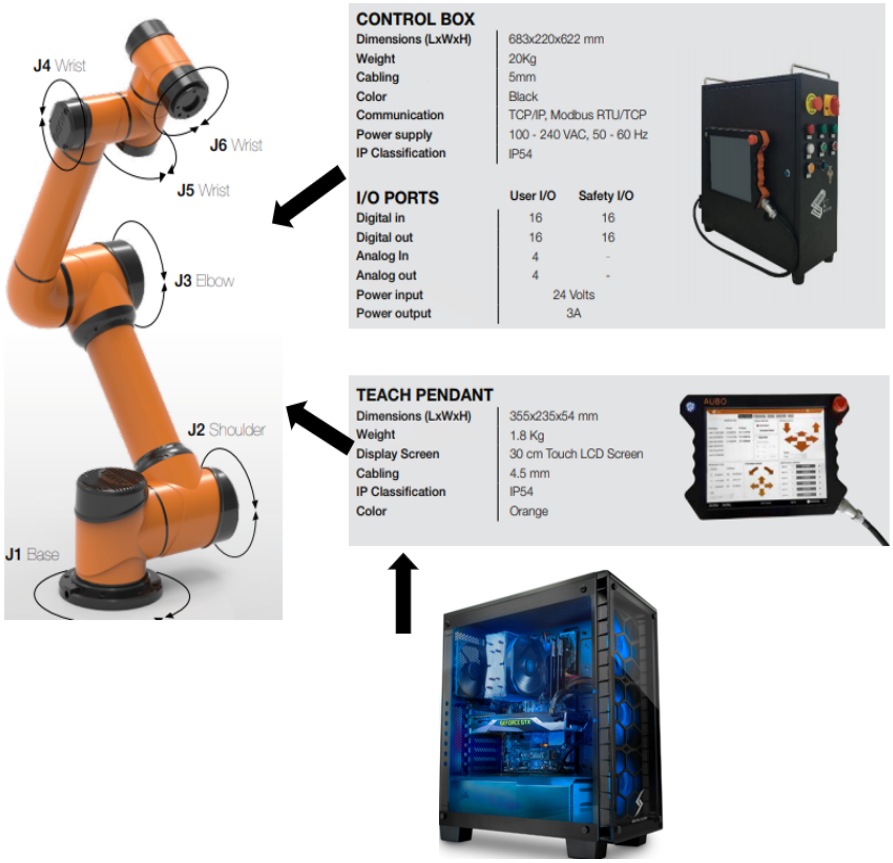

Figure 4.7 AUBO robot i5 system.
Source:[https://aubo-robotics.com/]

4.4 Three-fingered Gripper and ROBOTIS Actuator

The prototype of the three-fingered gripper is designed and manufactured to perform dexterous in-hand manipulation. As shown in Figure 4.8. It contains 9 ROBOTIS DYNAMIXEL motors, in which has 3 DYNAMIXEL motors that can be controlled under the velocity mode and 6 DYNAMIXEL motors that can be directly controlled on position level.

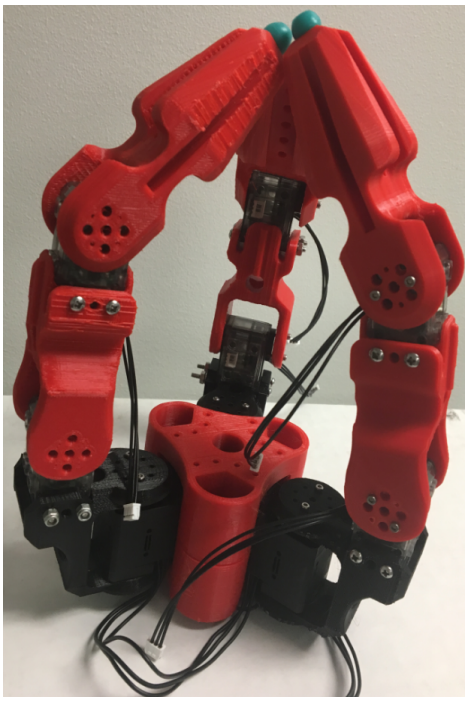

Figure 4.8 Prototype of three-fingered gripper.

'DYNAMIXEL' series servo motors are high performance actuators that are designed to be modular and daisy chained on robots or mechanical system for dexterous movements. A 'DYNAMIXEL' motor contains a fully integrated DC (Direct Current) motor, reduction gear-head, controller, driver and network, all in one servo module actuator. They are programmable and are capable of communicating through networks. The actuator status can be read and monitored through a data packet stream. In this gripper design, the motor is used for accurate robotic joint control.

4.5 Opti-Track Motion Capture System

'Optitrack' is a platform that designed for various motion tracking applications. As shown in Figure 4.9.

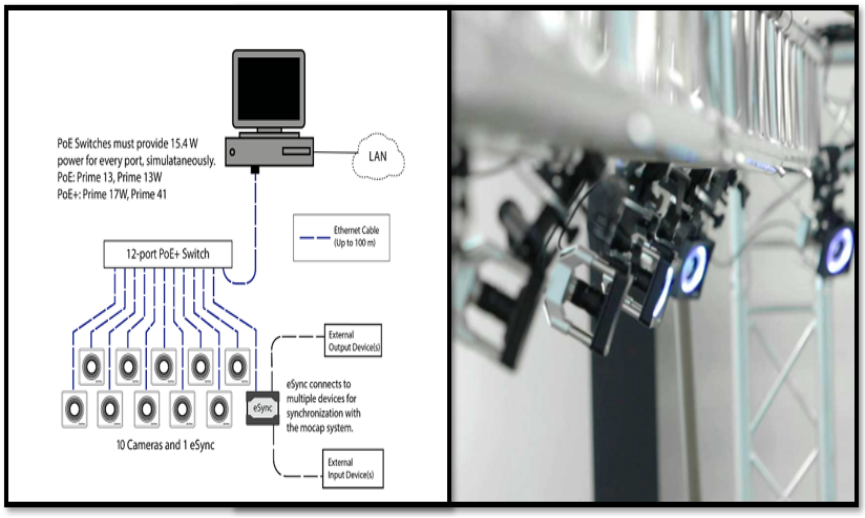

Figure 4.9 Opti-Track motion capture system.

Source:[https://optitrack.com/]

It not only allows the user to capture target motions and features, but it also provides interfaces, which is named as 'Motive', for both capturing and processing of 3D data. The captured data can be simultaneously recorded or live-streamed to other system. Motive obtains 3D information via data reconstruction, which is the procedure that compiles multiple 2D images of markers to get 3D coordinates. Applying 3D coordinates from tracked markers, Motive is able to obtain 6 Degree Of Freedom (DOF) data for multiple rigid bodies as well as skeletons. It is also able to track complex movements in the 3D space.

CHAPTER 5

SIMULATIONS AND EXPERIMENTAL RESULTS

In this section, the research results are introduced with respect to the following aspects:

1. Design and control a load dependent stiffness actuator.
2. Simulation of the Movable Sawyer Arm System and design of arm exoskeleton.
3. Dexterous in hand manipulation.
4. Robotic Sit-To-Stand Assistance and control framework design.

5.1 Design and Control a Load Dependent Stiffness Actuator

The actuator is designed to behave like a rigid actuator during normal operation and automatically switches to a compliant actuator in the event of an unexpected collision, without the need of additional force sensor/estimation. Therefore, both safety and performance requirements can be met simultaneously. As can be seen from Figure 5.1.

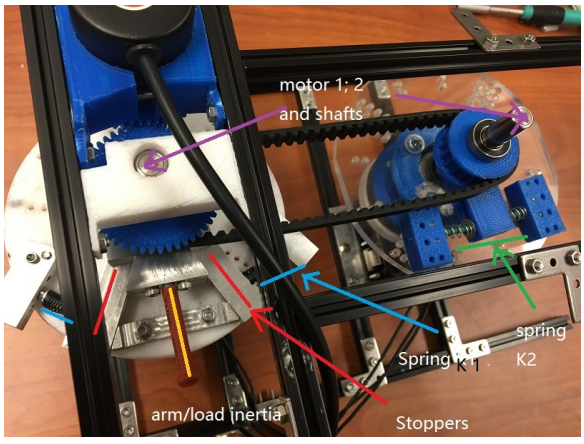

Figure 5.1 Prototype of semi-compliance load dependent actuator.

5.1.1 System Dynamics of the Actuator System

The dynamic equations of the prototype are given by:

$$
\begin{aligned}
\dot{\theta}_1 &= \omega_1, \\
J_1\dot{\omega}_1 &= T_1 + T_{SM}, \\
\dot{\theta}_2 &= \omega_2, \\
J_2\dot{\omega}_2 &= T_{SL} + T_{k2} + T_{comp} + T_{unexp}, \\
\theta_{3l} &= \min\{\theta_1, \theta_2\} - \theta_0, \\
\omega_{3l} &= \begin{cases} \omega_1 & \text{if } \theta_2 > \theta_1 \text{ or } \{\theta_1 = \theta_2 \text{ and } \omega_2 \geq \omega_1\}, \\ \omega_2 & \text{if } \theta_1 > \theta_2 \text{ or } \{\theta_1 = \theta_2 \text{ and } \omega_2 < \omega_1\}, \end{cases} \\
\theta_{3r} &= \max\{\theta_1, \theta_2\} + \theta_0, \\
\omega_{3r} &= \begin{cases} \omega_1 & \text{if } \theta_1 > \theta_2 \text{ or } \{\theta_1 = \theta_2 \text{ and } \omega_1 \geq \omega_2\}, \\ \omega_2 & \text{if } \theta_2 > \theta_1 \text{ or } \{\theta_1 = \theta_2 \text{ and } \omega_1 < \omega_2\}, \end{cases} \\
\dot{\theta}_4 &= \omega_4, \\
J_4\dot{\omega}_4 &= T_2 - T_{k2},
\end{aligned}
\tag{5.1}
$$

The actuator has ten continuous states: θ_1, θ_2, θ_{3l}, θ_{3r}, θ_4 and their derivatives (denoted by replacing "θ" with "ω" for each variable). Comparing to the moment of inertia J_1, the moment of inertia of two stoppers are small, therefore θ_{3l}, ω_{3l}, θ_{3r}, ω_{3r} do not have their own dynamics. The θ_0 is an angle that relates to pre-compression length of the two springs clamping the box when the system is at neutral position. J_4 is the moment of inertia of the secondary motor. T_{comp} is the torque term relates to the combination of external forces such as gravity and Coriolis force. The torque T_{unexp} is corresponding to the unexpected shock acting on the actuator. $T_{k2} = k_2(x_4 - x_2)r$ is the torque generated by the spring k_2 which rotates around central axis, where r is the distance from the spring k_1 to the central axis. T_{SM} is a net torque corresponding to the net force given by stoppers to the motor.

5.1.2 Position Tracking of the Actuator System

The position tracking algorithm (PID controller) to be designed for the proposed actuator (motor 1) must satisfy for the objective of tracking desired trajectory θ_d and the motor 2 should track the desired trajectory as close as possible. However during impacting, the θ_{1d} will deviate from θ_{2d}, therefore forcing θ_{1d} to be the same as θ_{2d} all the time is improper. Since the difference between θ_{2d} and θ_{1d} will eventually decrease towards zero due to the damping effect between motor inertia and load inertia, θ_{2d} will gradually converge to θ_d as well. As can be seen from the Figure 5.2, motor 2 is able to tack motor 1 during

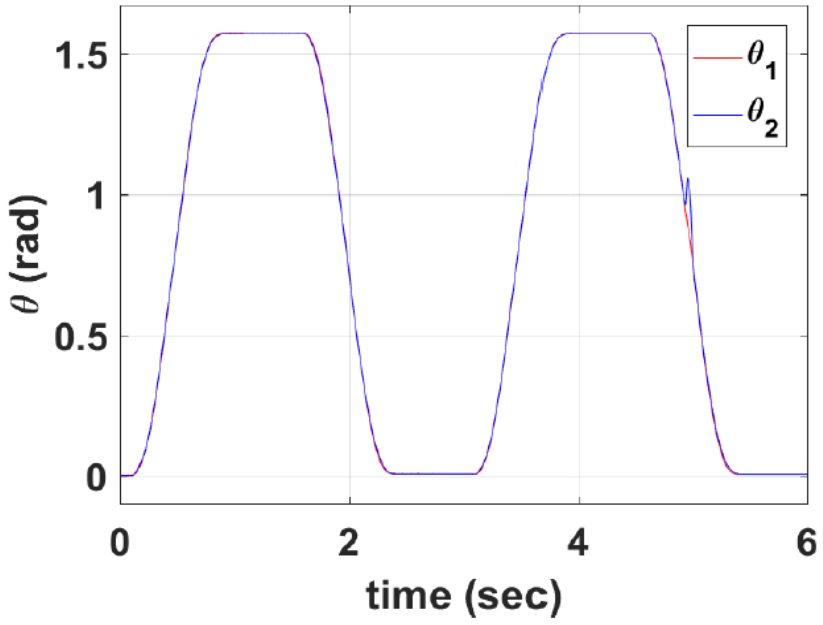

Figure 5.2 The tracking performance of θ_{1d} and θ_{2d}.

non-collision status and is able to absorb impacts during the collisions.

5.1.3 Simulation of Movable Sawyer Robot Arm System

In this subsection, the $MATLAB^{@}$ simulation of 7-DOF robot arm is described, the equation of inverse differential kinematics is given and preliminary results are demonstrated. In the

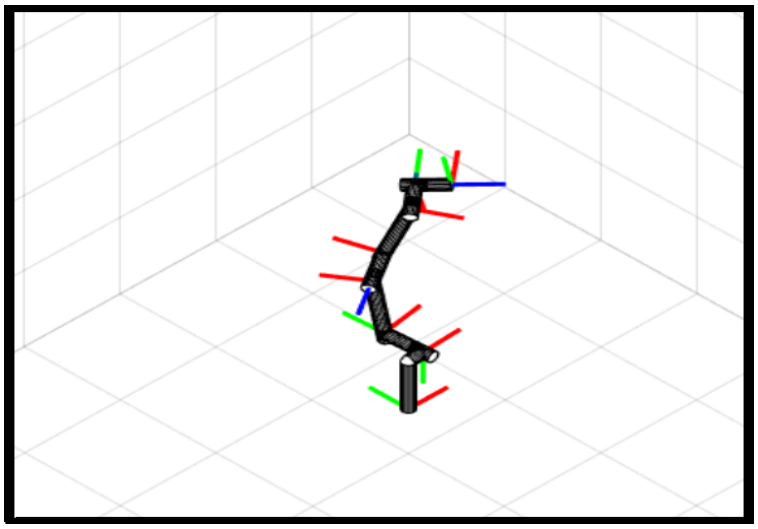

Figure 5.3 Simulation of 7 DOF Sawyer arm.

Figure 5.3, the virtual Sawyer robot arm is constructed base on the entity. At each joint, the coordinate is attached to identify the local direction. The control target is the velocity of the end-effector . As far as the humanoid robotic arm is concerned, it is logical to control the end-effector instead of joints since humans are naturally using their hands to touch, reach and grab objects. In this study, the inverse differential kinematics are applied and programmed into the robot arm. The inverse differential kinematics can be expressed as:

$$\dot{q} = J^T (JJ^T)^{-1} V_e \tag{5.2}$$

where the J is the Jacobian matrix and the V_e is the end-effector velocity matrix that represents the linear velocities and rotational velocities.

In the $MATLAB^{@}$ simulation, the velocities of end-effector are controlled by a XBOX controller and meanwhile, the movable Sawyer arm system is connected with $MATLAB^{@}$ as well, hence the system is operating under the commands of the XBOX controller. To illustrate the control algorithm, the control results are plotted in Figure 5.4.

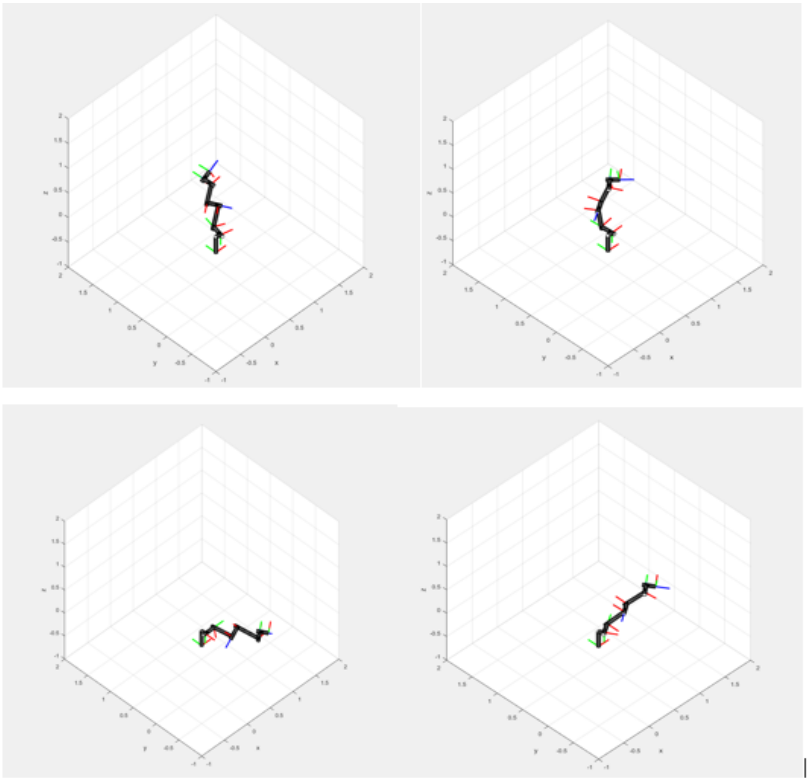

Figure 5.4 Demonstration of the simulation.

5.1.4 Design of Arm Exoskeleton

The arm exoskeleton is designed for controlling the Sawyer system. It contains 4 encoders and 1 leap motion optical sensor to record human arm joint movements. The human joint movements are real-time recorded and streamed from these devices to Arduino board, then at the same time, transmitted to the Sawyer robot. Therefore, an operator is able to manipulate the robot simultaneously with his/her arm movements. As can be seen in Figure 5.5. The design and manufacture process can be briefly described as: CREO simulation; 3D printer parts fabrication and electronic equipment setup.

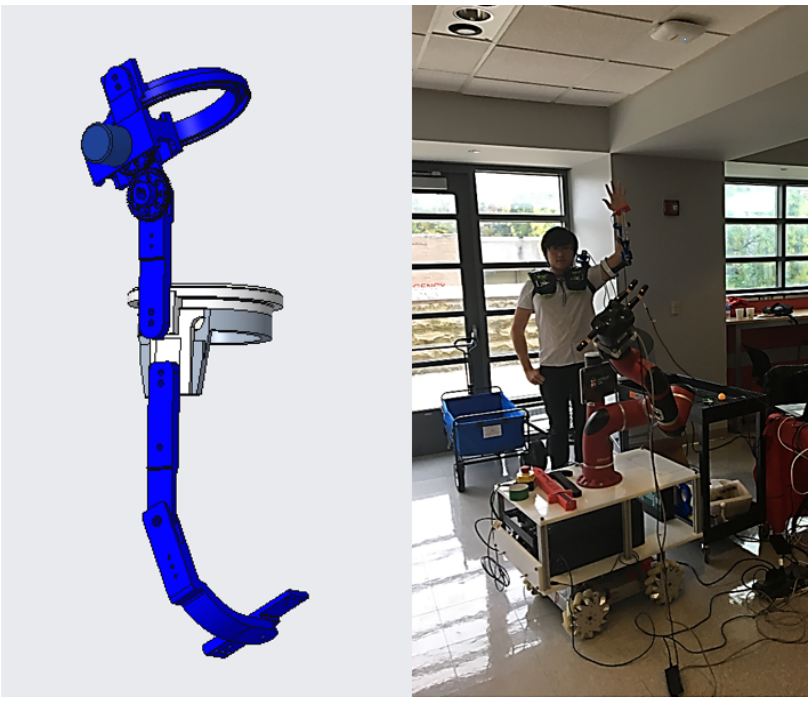

Figure 5.5 Arm exoskeleton.

5.2 Dexterous In-Hand Manipulation

Rotating an object in the hand accurately with fingers is a dexterous manipulation skill performed by humans everyday, and is a technique yet to be learned by robots towards home automation and assistive living. This study presents the modeling and precision motion control of an important class of dexterous object in-hand rotation by robots. It is assumed that the robot hand has three fingers, two of which clamping the object and the third one pushing the object to rotate to a desired angle. The contact friction between the fingertip and the object is explicitly modeled, based on which a simplified planar rigid body dynamic model is derived. To precisely regulate the object angle to its desired value while minimizing the deviation of the object center with respect to the fingertip, we propose a novel hybrid control structure consisting of two modules - regular tracking control module and the motion re-planning module. The regular module generates the clamp pressure and the pushing force of the fingers to let the object angle track a reference trajectory as accurately as possible while minimizing the object center deviation. When the object

center deviation is too large, the motion re-planning module is activated that optimizes a new pushing point for the third finger and generates a new reference trajectory for the object angle. The proposed approach naturally mimics the human motor behavior when rotating an object to a desired angle by pushing and re-positioning the fingers. A simulation study using a high-fidelity virtual physics engine "*mujoco*" is also performed that verifies the effectiveness of the proposed approach.

5.2.1 Observations of Object In-hand Rotation by Human

The system dynamics is constructed on the basis of observations of human in-hand manipulation. In particular, we conduct two human in-hand manipulation experiments which involve capping a bottle lid and peeling an orange by a human. As can be seen in Figure 5.6, in the first experiment, a human hand grasps a bottle lid with two fingers

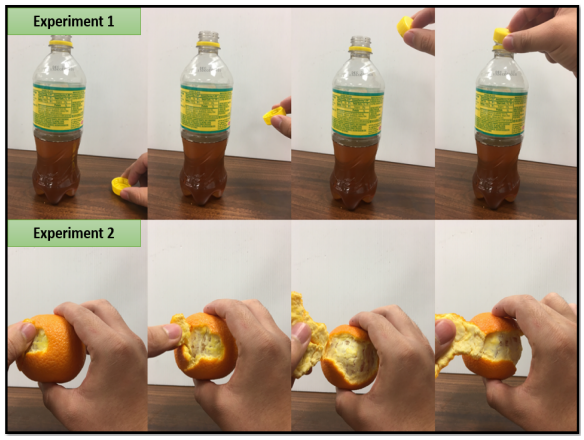

Figure 5.6 The experiments of human in-hand manipulation. Experiment 1: Capping a lid. Experiment 2: Peeling an orange.

clamping on the two sides. Another finger slightly pushes on the edge to rotate the lid till an appropriate angle. In the second experiment, a person uses two hands to peel an orange. Notice that the first two fingers are utilized as a clamp that grasps on both ends of the orange, while with the third finger slowly rotating and peeling. From the observations of two human in-hand manipulation experiments, we found that these type of in-hand manipulations share some common features. These common features can be concluded

as the followings. First, the grasped object experiences sliding motions as well as rolling motions during the operation. Second, at least three fingers are involved in doing the tasks. Specifically, two of the fingers act as a clamp that constrains the body, and with the third finger rolling and re-positioning the body. Third, the rotational motion of the object is constrained in a fixed virtual plane which is perpendicular to the line connecting the top and bottom fingertips.

5.2.2 Schematic Model of the System and Practical Assumptions

According to the observations from the above human experiments, we present the following schematic model of the system, as shown in Figure 5.7. In this model, we use an arbitrarily-

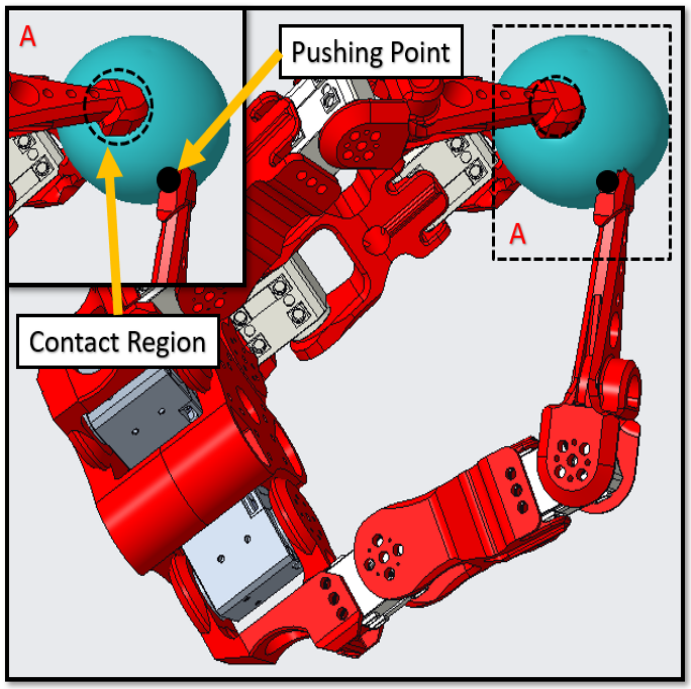

Figure 5.7 The schematic diagram of the proposed dynamic model.

shaped rigid body as the grasped object. Two fingers keep clamping the object from the top and the bottom, while a third finger of the robot pushes the object to rotate. This model can be used for representing a category of home automation tasks (or sub-tasks) that has the similar features, such as, capping lids, flipping coins and peeling oranges.

According to the experiments, we consider a class of planar in-hand rotation of light weight objects. For simplification and illustration purposes, we make the following assumptions. The rigid body translates and rotates in a 2D plane perpendicular to the gravity direction with no out-of-plane movement. The contact between the two clamping fingertips and the object is within an area $\mathscr{A} \subset \mathscr{O}$, where $\mathscr{O}$ is the projection of the object onto the 2D plane of movement. The contact between the third finger and the object is lumped at a single point C on the exterior of the object.

According to the assumptions, the contact area $\mathscr{A}$ between the two fingertips and the object creates linear friction force and rotational friction torque when the object is in motion, while the third finger only applies the pushing force (with no torque) to the object at point C. It is reasonable to simplify the system dynamic model in 2D space. The schematic diagram is shown in Figure 5.8:

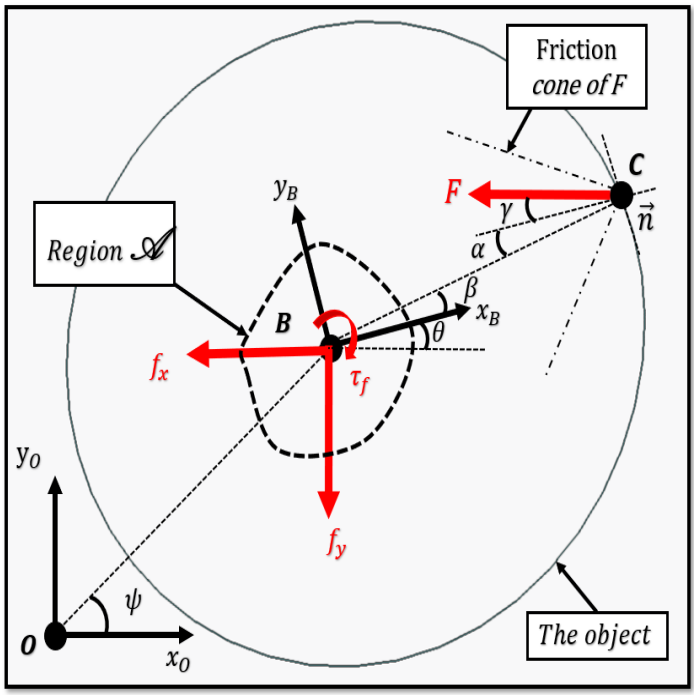

Figure 5.8 2D schematic diagram of the proposed dynamic model.

In the figure, $\{O - x_O y_O\}$ represents the inertia frame and $\{B - x_B y_B\}$ is the body frame. The origin of the body frame is defined at the center of mass of the object. $f_x \in R$

and $f_y \in R$ are the planar frictional forces along x_O and y_O directions. $\tau_f \in R$ is the frictional torque. It is worth noting that the friction forces and torque are generated passively after the pushing force F is applied. ψ is an angle between x_O axis and the vector $\overrightarrow{OB}$. $\theta \in R$ is the angle of rotation of the body frame with respect to the inertia frame. $\gamma \in R$ is the angle between F and the inward normal vector $\overrightarrow{n}$ at the contact point of the third finger. $\alpha \in R$ indicates the angle between the normal vector $\overrightarrow{n}$ and the vector $\overrightarrow{CB}$. $\beta \in R$ is the angle between the vector $\overrightarrow{BC}$ and the x_B axis.

5.2.3 Planar Friction Model

Frictional force plays an essential part in the study of dexterous manipulation. In this subsection, we first derive the frictional force condition at point C that needs to be satisfied by the pushing force, then we formulate a planar friction model for the clamping fingers which considers the static friction when the object is at rest and the kinetic friction when the object is in motion.

First of all, to ensure that maximum amount of the friction is applied to rotate the object, it is assumed that there is no relative sliding at contact point C. Thus, the static friction is calculated as:

$$f_c = F\sin(\gamma). \tag{5.3}$$

However, the maximum static friction value is roughly proportional to the normal force, i.e., $f_c \leq \mu F\cos(\gamma)$, where μ is the static friction coefficient. It follows that $\gamma \leq \gamma_{max}$, i.e., the total pushing force combining the friction force and the normal force should be within a "friction cone".

The planar frictional force at the region $\mathscr{A}$ is formulated depending upon whether the object is stationary or in motion. When the pushing force is insufficient to drive the object, the object is experiencing a static friction at the region $\mathscr{A}$. In this case, the static friction

has equal magnitude of the pushing force, yet in the opposite directions, i.e.,

$$\begin{aligned} f_x &= -F\cos(\theta+\beta-\alpha-\gamma), \\ f_y &= -F\sin(\theta+\beta-\alpha-\gamma), \\ \tau_f &= |\overrightarrow{BC}|\sin(\alpha+\gamma). \end{aligned} \tag{5.4}$$

When the pushing force overcomes the maximum force of static friction. The grasped object starts to move and the object experiences kinetic friction. In [47,48], the researchers proposed the planar Coulomb friction for surface contact as a wrench. Notice that the direction of the kinetic friction is in the same direction of the instantaneous velocity of the contact region. The two dimensional kinetic friction is formulated as the integration over the contact area:

$$\mathbf{W} \triangleq \begin{bmatrix} f_x \\ f_y \\ \tau_f \end{bmatrix} = \begin{bmatrix} \mu p \int_{\mathscr{A}} \frac{v_x}{\sqrt{v_x^2+v_y^2}} dA \\ \mu p \int_{\mathscr{A}} \frac{v_y}{\sqrt{v_x^2+v_y^2}} dA \\ \mu p \int_{\mathscr{A}} \frac{v_x r_y - v_y r_x}{\sqrt{v_x^2+v_y^2}} dA \end{bmatrix} \tag{5.5}$$

Where $\overrightarrow{v_x}$ and $\overrightarrow{v_y}$ are velocities along x and y directions at each point within the contact region. We assume that the pressure p is isotropic in the area $\mathscr{A}$, therefore p can be taken out of the integration. (r_x, r_y) is coordinate of each point with in the area $\mathscr{A}$. Notice that the frictional forces and torques are upper bounded, which satisfy:

$$\begin{aligned} |f_x| &\leq p f_s^{max}, \\ |f_y| &\leq p f_s^{max}, \\ |\tau_f| &\leq p \tau_f^{max}. \end{aligned} \tag{5.6}$$

5.2.4 Dynamic Modeling

The generalized dynamic model is given as:

$$\begin{aligned} m\ddot{x}(t) &= -F\cos(\theta+\beta-\alpha-\gamma)-f_x \\ m\ddot{y}(t) &= -F\sin(\theta+\beta-\alpha-\gamma)-f_y \\ J\ddot{\theta}(t) &= \tau_{in}-\tau_f \\ &= F\sin(\gamma+\alpha)|\overrightarrow{BC}|-p\mu\int_{\mathscr{A}}\frac{v_x r_y - v_y r_x}{\sqrt{v_x^2+v_y^2}}dA \end{aligned} \tag{5.7}$$

Where m is the mass of the rigid body, and J is the moment of inertia about the center of mass. $\ddot{x}(t) \in R$ and $\ddot{y}(t) \in R$ are the linear accelerations in the inertia frame. $\ddot{\theta}(t)$ is the angular acceleration. In the system, the control input variables are F (pushing force magnitude), γ (pushing force angle), and p (normal pressure of the clamping fingers).

5.2.5 Controller Design

We design a controller that meets the following control objectives:

(A) Let the object angle θ converge to the desired angle θ_d accurately and fast.

(B) Minimize the deviation of the object center $d = \sqrt{x^2+y^2}$.

In the human manipulation experiments, we notice that when the third finger pushes the object to rotate towards the target, the object center starts to deviate from the two clamping fingertips. As the pushing force of the third finger must lie in the friction cone, it can not "pull" the object back. Thus, after a certain amount of time, the third finger needs relocate to the other side of the object so that when a new cycle of pushing starts, the object center is gradually pushed back.

Based on the above observation, we propose a hybrid control structure as shown in Figure 5.9. The controller consists of two modules: a regular tracking control module and a motion re-planning module. The regular tracking control module implements a PID control followed by a constrained optimization algorithm to generate the pushing force magnitude,

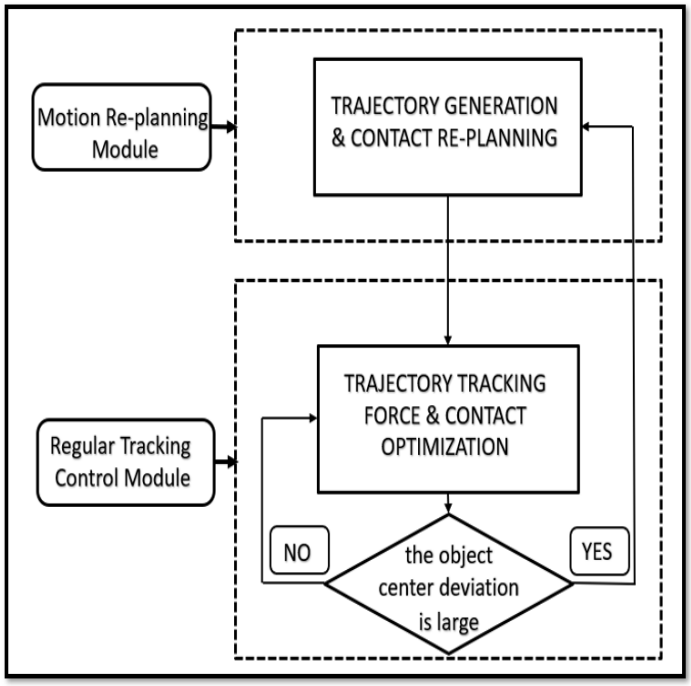

Figure 5.9 Flow chart of the proposed controller.

direction, and the clamping pressure force so that the object angle accurately tracks a reference trajectory while a combination of performance indices, such as the deviation rate of the object center, is minimized. When the object center deviation d is larger than a threshold d_{max}, the motion is stopped and a motion re-planning algorithm is implemented to generate an optimal new pushing point for the third finger, as well as the new trajectory for the angle θ, so that the object center is pushed back while angle still travels towards the target.

5.2.6 Simulations and Results

In this subsection, the simulations are performed to validate the proposed control framework. Specifically, we conduct two simulations. The result of the first simulation is used to verify the performance of the regular tracking control module. The second simulation is implemented to verify the functionality of the proposed motion re-planning module. That is, when the grasped object deviates away, the third finger automatically finds a new

contact point and pushes the object back in while still keeping the object rotating. The entire dynamic model construction and simulations are executed in '*mujoco*', a high-fidelity virtual physics simulation platform for multi-joint robotic systems with contact.

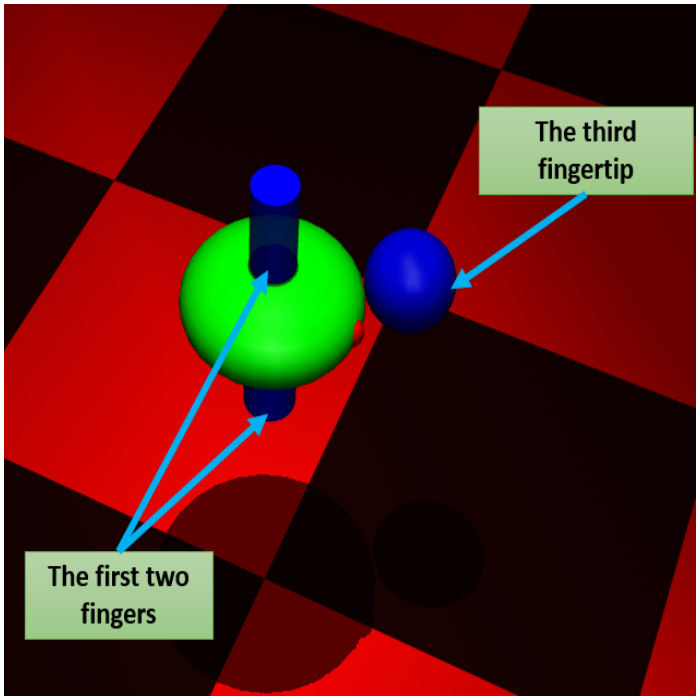

Figure 5.10 The diagram of *'mujoco'* model: Three-fingered gripper and the object.

The Simulation of Trajectory Tracking As shown in Figure 5.10, a simplified model of the three-fingered gripper is constructed by setting two cylinders (using prismatic joint in *'mujoco'* model) as the first and second fingers that clamp the object from the top and bottom. The third fingertip is represented by a sphere. At the contact points/areas between the fingers and object, normal forces, tangential friction forces and torsional friction torques are automatically generated assuming certain flexibility, damping, and friction coefficients in the mujoco system model. In this simulation, as shown in Figure 5.11, the third fingertip pushes the object to track a desired S-curve trajectory. In particular, the actuating force of the third fingertip is formulated by applying an impedance control, in such a way that the interacting force between the fingertip and the object is capable of driving the object to track the given angular trajectory.

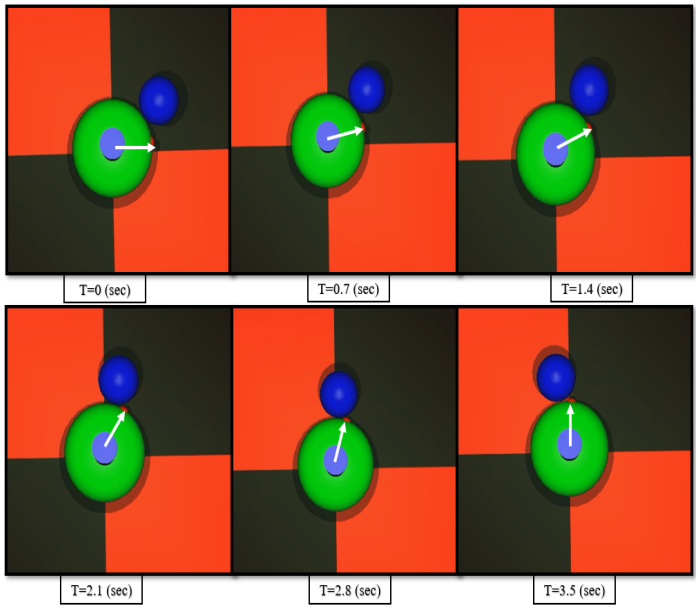

Figure 5.11 The demonstration of object trajectory tracking.

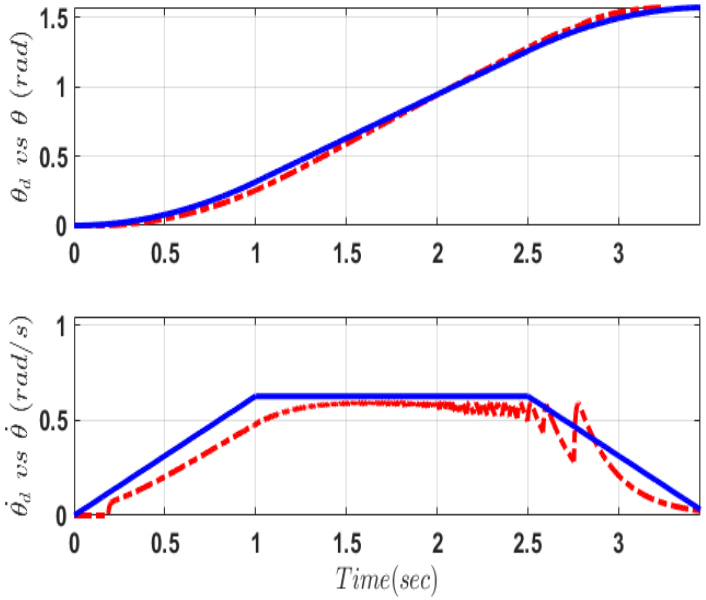

Figure 5.12 The performance of object trajectory tracking.

As can be seen from Figure 5.12, the rotation angle of the object is able to follow the desired signal precisely on position level and to approximately track the velocity signal on velocity level. The velocity tracking error is acceptable since most of the home automation tasks only demand high accuracy in position regulation, while the task may be executed in various speed levels. Additionally, the recorded planar frictions as well as torsional friction torque around the contact normal of the clamping fingers are given in Figure 5.13

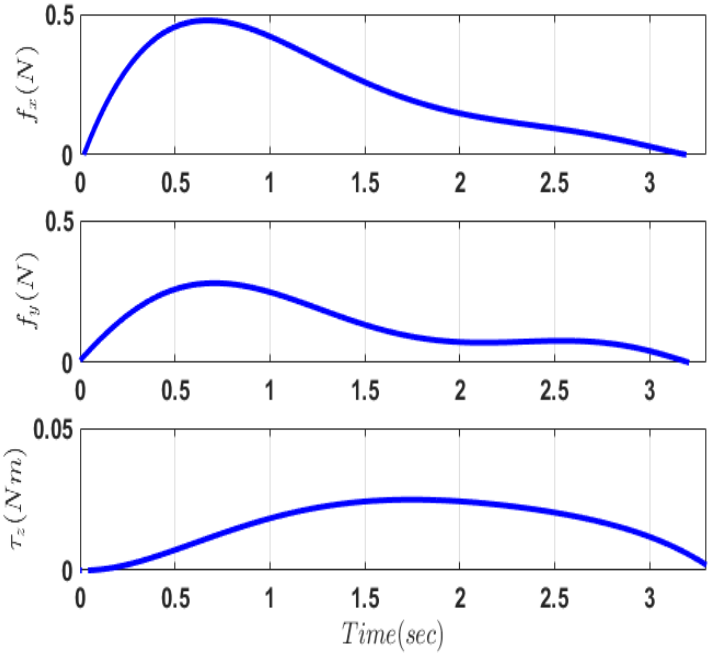

Figure 5.13 The planar friction wrench of the clamping fingers: $[f_x, f_y, \tau_z]$.

.

Simulation of Motion Re-planning The simulation demonstrates the motion re-planning procedures during an in-hand manipulation task. In particular, during the trajectory tracking task, the object gradually deviates away from the contact center. Once the center of the object crosses the bound of the default contact region, the clamping fingers increase the contact pressure to stop further deviation, as shown in Figure 5.14. A Then, as can be seen from Figure 5.14. B, the third finger retreats from the object and relocates to a new

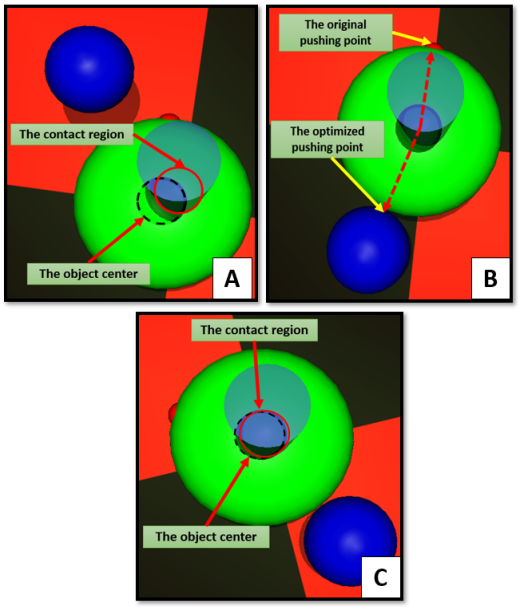

Figure 5.14 A The object deviates away while tracking the trajectory. B The third finger is re-positioned. C The object tracks the new trajectory and the center is pushed back in.

contact position. Next, the pushing finger tracks the new trajectory and push the object back in, as exhibited in Figure 5.14.

5.2.7 Conclusion

This study presented the modeling and precision motion control of an important class of dexterous object in-hand rotation by a three-fingered robotic gripper. First, on the basis of the observations of human in-hand manipulation, a simplified planar rigid body dynamics with contact friction modeling was derived. Then, a novel hybrid control framework was developed that consists of two modules: a regular tracking control module and a motion re-planning module. With the proposed control framework, it was demonstrated that the object angle is able to follow a desired trajectory while the object center deviation is minimized. Finally, the proposed dynamic model and the hybrid control framework were simulated by using a virtual physics engine *'mujoco'*. The simulation results successfully verified the effectiveness of the proposed dynamics and control method.

5.3 Robotic Sit-To-Stand Assistance: Preliminary Study

In this research, we propose a human-centered control framework for the Sit-To-Stand (STS) assistance by using a robot manipulator. The framework is designed to assist those with weak knees and feeble muscles to get out of a seated position. Compared to previous work on STS assistance, we develop a novel human-centered strategy that explicitly optimizes the human joint loads under the human body dynamics while taking care of the constantly-changing intention of the human during the actual STS assistance. Specifically, we first study the human-to-human STS process and construct a human dynamic model. Then, an optimal (nominal) robot end-effector trajectory is generated offline that minimizes the human joint loads under a nominal human body motion. During the actual STS process, the human may intend to move differently from the nominal motion. To deal with the changing human intention, we design an online switching controller for the robot end-effector. With such a controller, when the human intention is detected to be the same or close to the nominal one, the robot end-effector will track its nominal trajectory. Otherwise a modification is made to the end-effector trajectory to follow the detected human intention. The control framework is capable of reducing joint loads and estimating human decisions when the human intends to adjust his/her posture during the Sit-To-Stand (STS) assistance in real time. Simulations and experiments are conducted to validate the proposed control framework.

5.3.1 Formulation of the System Dynamics

The formulation of the system dynamics is based on a scenario in which a person attempts to rise from a seated position. However, a person's lower limbs can only output limited torque that may be insufficient to support his/her body. A humanoid robot arm is deployed nearby to assist the person in getting up with its end-effector clenched by the human hands. In such a way, the lack of human joint torque can be compensated by the interaction force between the human hand and the robot end-effector. We aim to design the motions

(velocities and accelerations, etc.) of the robot end-effector to assist people in getting up from a seated position instead of controlling the interaction force directly, since the interaction force is generated passively and is difficult to control directly. We use a five-link model to represent the human dynamics in a 2D plane, as shown in Figure 5.15. In this simplified model, the human hand is assumed to be rigidly attached to the robot

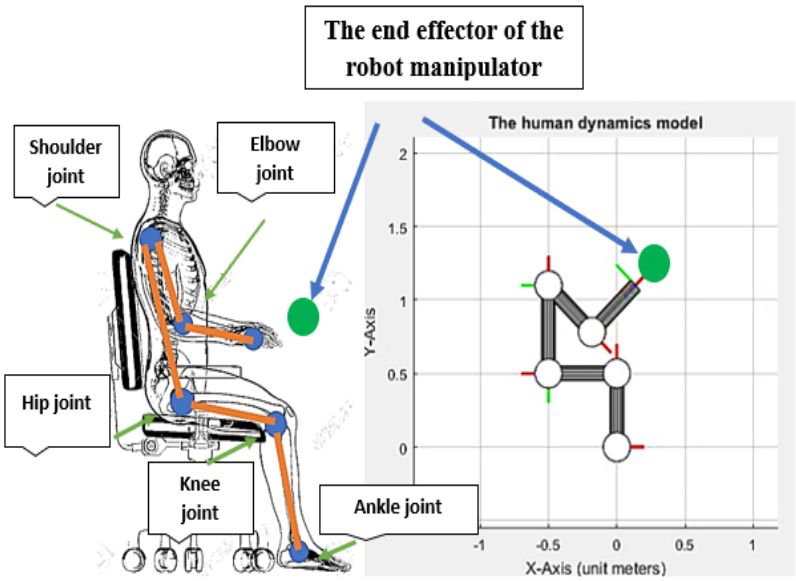

Figure 5.15 Illustration of the human dynamic model. The green dot represents the robot end-effector connected to the human hand.

end-effector, and the wrist joint moves passively with no actuation torque applied. This is a realistic assumption since compared to other major joints, the wrist usually exerts a much smaller torque, and is also more fragile. Thus, this local structure can be treated as the human hand "pinned" to the robot end-effector, whose horizontal and vertical movements can be freely controlled. The dynamics of the constrained five-link system is governed by the following equation:

$$M(\theta)\ddot{\theta} + C(\theta,\dot{\theta})\dot{\theta} + G(\theta) = \tau + J(\theta)^T F, \tag{5.8}$$

where $M(\theta) \in R^{5\times5}$ is a positive definite symmetric matrix that represents the inertia of the robot, $C(\theta,\dot{\theta})\dot{\theta} \in R^5$ is the vector of Coriolis and centripetal forces, $G(\theta) \in R^5$ is the gravitational force vector, $\tau \in R^5$ represents the human joint torque. The interaction force $F \in R^2$ on the human's hand is generated indirectly from both the human joint torque and the robot motion. The matrix $J(\theta) \in R^{2\times5}$ is the Jacobian from the human joints to the human hand.

To see how the human motion is determined from the human torque τ as well as the robot end-effector acceleration $\ddot{X}_e$, we need to eliminate the intermediate variable F by representing it as a function of τ and $\ddot{X}_e$. Specifically, taking the time derivative of the following differential kinematic equation representing the kinematic constraint of the five-link system

$$\dot{X}_e = J(\theta)\dot{\theta}, \tag{5.9}$$

we can get

$$\ddot{X}_e = J(\theta)\ddot{\theta} + J(\dot{\theta})\dot{\theta}, \tag{5.10}$$

where $J(\dot{\theta})$ is the matrix representing the differentiation of the Jacobian matrix. Then, we rewrite the human dynamics as:

$$\ddot{\theta} = M(\theta)^{-1}(\tau + J(\theta)^T F) - M(\theta)^{-1}(C(\theta,\dot{\theta})\dot{\theta} + G(\theta)) \tag{5.11}$$

From (5.10) and (5.11), the F term is represented as a function of τ and $\ddot{X}_e$ as:

$$F = (J(\theta)M(\theta)^{-1}J(\theta)^T)^{-1}[\ddot{X}_e - J(\dot{\theta})\dot{\theta} - J(\theta)M(\theta)^{-1}(C(\theta,\dot{\theta})\dot{\theta} + G(\theta) - \tau)] \tag{5.12}$$

Substitute (5.12) into the (5.8):

$$M(\theta)\ddot{\theta} = A_1\tau + A_2\ddot{X}_e + A_3\dot{\theta} - A_1(C(\theta,\dot{\theta})\dot{\theta} + G(\theta)) \tag{5.13}$$

where,

$A_1 = I - J(\theta)^T (J(\theta)M(\theta)^{-1}J(\theta)^T)^{-1}(J(\theta)M(\theta)^{-1})$;

$A_2 = J(\theta)^T (J(\theta)M(\theta)^{-1}J(\theta)^T)^{-1}$;

$A_3 = -J(\theta)^T (J(\theta)M(\theta)^{-1}J(\theta)^T)^{-1}J(\dot{\theta})$;

It is noted that the matrix A_1 is of rank 3 (not full rank), which means that the human joint torque cannot fully determine the body movement. In fact, Equation (5.13) indicates that during the STS assistance, the human body movement is affected by both the joint torque τ and the robot motion X_e, with $\ddot{X}_e$ determining the change of the kinematic constraint on the human body.

A specific human subject is used in our simulation and experiment. The weight of the subject is 74.2 kg and the standing height is 1.755 m. The geometric and inertia parameters of the human subject are estimated by referring to the table of body segment parameters [49]. The parameters are listed in Table 5.4. Where the $p(\%)$ is the segment

Table 5.1 Body Segment Parameters

Segment	$p(\%)$	$m(\%)$	$I_1(Kg-m^2)$	$I_3(Kg-m^2)$
Head	0.5358	0.0730	0.0248	0.3119
Upper arm	0.4360	0.0270	0.0213	0.3119
Forearm	0.4300	0.0160	0.0760	0.3119
Hand	0.5060	0.0066	0.0005	0.3119
Trunk	0.4383	0.5080	1.3080	0.3119
Thigh	0.4330	0.0988	0.1502	0.3119
Lower leg	0.4330	0.0465	0.0505	0.3119
Foot	0.4290	0.0145	0.0038	0.3119

length as a percentage of the whole body length, the $m(\%)$ represents the segment weight as a percentage of the whole body weight, I_1 is the mass moments of inertia of the segment

along the transverse axis, and I_3 is the mass moments of inertia of the segment along the longitudinal axis. In real applications, the geometric and inertia parameters can be set according to different individuals to be assisted, and fed into the control algorithm.

5.3.2 Human Joint Control Mechanism

Through various human-to-human STS assistance tests, we observed that, although a person could stand up with different speeds or with different upper body postures, the moving trajectory of the first three joint angles (the ankle joint, the knee joint, and the hip joint) stays almost on the same path in the 3D space. This is a natural phenomena since most of the weight of the human body concentrates on the trunk and lower limbs. Figure 5.16 shows the averaged 3D path that we have obtained from the first three joint angles from various STS assistance tests. Figure 5.17 shows how one person helps another in getting up. It can be seen from the figures that the first three joint angles stay close to the averaged path. According to such observation, we assume that during the STS process, human exerts torque on all the five joints to control his/her first three joints to reach a desired setpoint or to move along a fixed path in R^3. While the desired speed of the first three joints changes on the path according to the human's intention.

To mathematically model the control of the human joint torque τ, we pre-multiply (5.13) by $M(\theta)^{-1}$, and take the first three rows of the equation to represent the dynamics of the first three joints:

$$\ddot{\theta}_{123} = M(\theta)^{-1}_{123}[A_1\tau + A_2\ddot{X}_e + A_3\dot{\theta} + A_4(C(\theta,\dot{\theta})\dot{\theta} + G(\theta))], \tag{5.14}$$

where $M(\theta)^{-1}_{123}$ is a matrix that consists of the first three rows of $M(\theta)^{-1}$, θ_{123} is the vector of the first three joint angles of the human body.

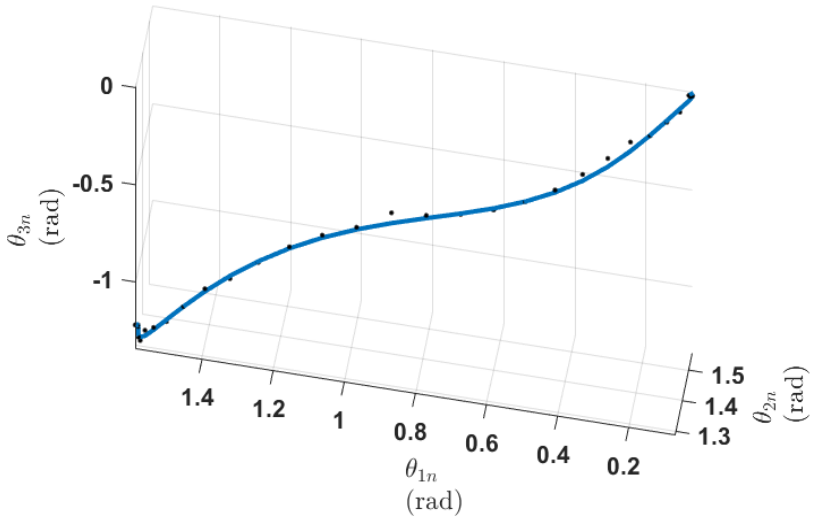

Figure 5.16 3D plot of the averaged path of the first three joint angles from various human-to-human STS experiments.

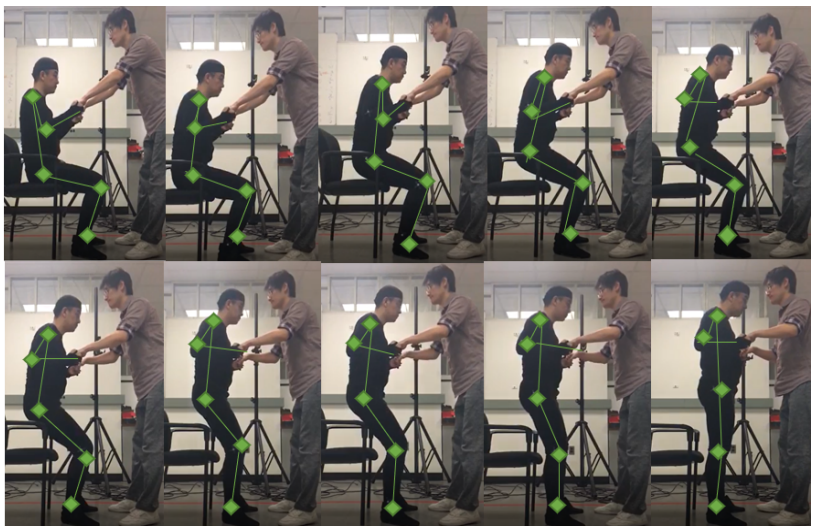

Figure 5.17 Screenshots of a particular human-to-human STS experiment.

We assume the human uses a PD controller with nonlinear compensation to regulate its first three joints [50], i.e., τ satisfies the following relationship:

$$A(\theta)\tau = B(\theta, \dot{\theta}, \theta_{123d}, \dot{\theta}_{123d}, \ddot{\theta}_{123d}), \tag{5.15}$$

where

$$\begin{aligned} A &= M(\theta)_{123}^{-1} A_1 \\ B &= -M(\theta)_{123}^{-1}[A_3\dot{\theta} + A_4(C(\theta,\dot{\theta})\dot{\theta} + G(\theta))] \\ &\quad -k_p(\theta_{123} - \theta_{123d}(t)) - k_d(\dot{\theta}_{123} - \dot{\theta}_{123d}(t)) + \ddot{\theta}_{123d}(t), \end{aligned} \tag{5.16}$$

where k_p and k_d are 3×3 diagonal matrices of proportional and derivative gains. $\theta_{123d}(t)$ is the time dependent desired trajectory of the first three joints determined from the human's intention. From the previous analysis, it is assumed that $\theta_{123d}(t) \in S$, where S is a 1-D curve with finite length in R^3, representing the fixed path of the first three joints for the STS motion.

Equation (5.15) has three equations but five undetermined entries in τ. It is well known that for such type of mechanical system with holonomic constraints, there exists infinite solutions of torque/force input that achieve the same physical movement. We assume that a human always chooses the set of torque values that minimizes its overall joint load instantaneously. Specifically, we define the objective function for this joint load minimization as

$$f(\tau) = \tau^T \Lambda \tau, \tag{5.17}$$

where Λ is a diagonal matrix consisting of the weight for each joint. Unfortunately, there is no way we can accurately know how a person intuitively "chooses" this weighting matrix for joint load minimization. However, based on our observation, we can formulate some sample versions of Λ for different types of people. For example, for people with very week knees, he or she may have a high weight on the knee joint. While for people with weak

upper extremity, the weights for the last two joints (upper limb joints) are high. In our research, we choose the weight of the knee joint to be 10 times the weight of other joints. This represents a common scenario when a human intends to minimize the load on the knees most, while still caring about other joints.

The human joint torque that minimizes $f(\tau)$ while satisfying (5.15) is given by

$$\begin{aligned} \tau &= \tau(\theta, \dot{\theta}, \theta_{123d}, \dot{\theta}_{123d}, \ddot{\theta}_{123d}) \\ &\triangleq \Lambda^{-1} A^T (A\Lambda^{-1} A^T)^{-1} B. \end{aligned} \tag{5.18}$$

The dynamics of θ_{123} with the assumed human torque control law becomes

$$\begin{aligned} \ddot{\theta}_{123} &= -k_p(\theta_{123} - \theta_{123d}(t)) - k_d(\dot{\theta}_{123} - \dot{\theta}_{123d}(t)) \\ &\quad + \ddot{\theta}_{123d}(t) + M(\theta)^{-1}_{123} A_2 \ddot{X}_e, \end{aligned} \tag{5.19}$$

5.3.3 Robot End-effector Control

From the analysis above, the human controls the first three joints along a known path while the robot end-effector changes its end-effector motion $X_e(t)$ that indirectly determines the motions of the 4^{th} and 5^{th} joints. The choice of the desired motion $X_e(t)$ of the robot should satisfy the following objectives:

1. The closed-loop system is stable with all the signals bounded.
2. The joint load $f(\tau)$ is minimized during the entire STS motion.
3. The human intention is followed.

It is known that human has excellent capability of preventing instability when interacting with the physical world. When an instability is about to happen, human can quickly detect it and switch to a conservative control strategy with stronger damping to dissipate the energy on his/her own side. Thus, the stability of the closed loop system is mainly determined by the robot motion. For objective 1, it can be verified that if X_e, $\dot{X}_e$ and $\ddot{X}_e$ are all bounded, the human joint positions and velocities will also be bounded under the

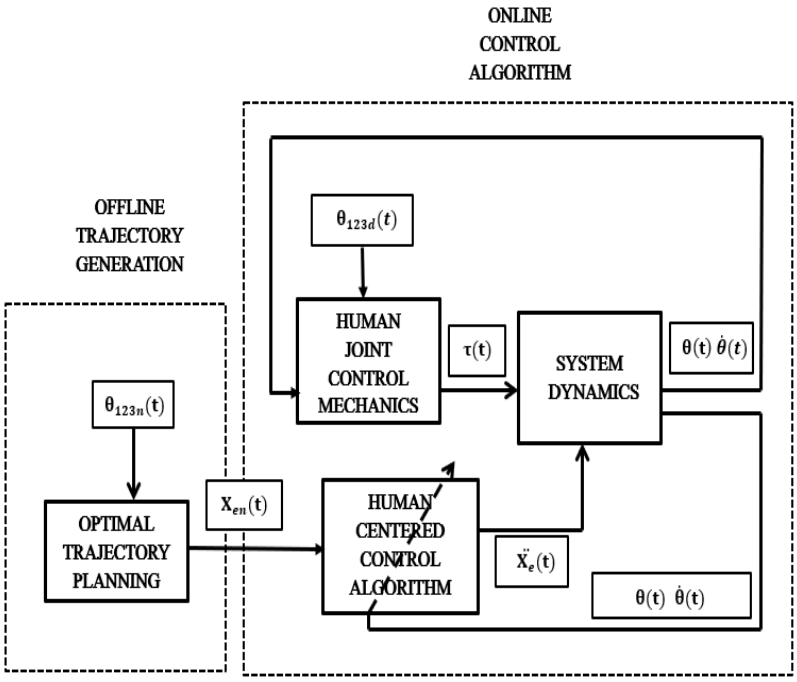

Figure 5.18 The schematics of the human-centered control framework.

human control law. Such a bounded end-effector trajectory will be generated later.

For objectives 2 and 3, since the human intention is time varying and unpredictable, it is impossible to generate a globally optimal control that minimizes the joint load with the human intention (the desired trajectory $\theta_{123d}(t)$) being a strong uncertainty. Thus, we adopt the following two-step strategy as in Figure 5.18: For step 1, a nominal robot end-effector trajectory $X_{en}(t)$ is generated offline to minimize the joint load under the nominal trajectory of the first three joints of human, i.e., $\theta_{123n}(t)$. For step 2, during online implementation, the human intention is detected in real time. If the detected human intention is close to the nominal one, then $\ddot{X}_e$ is designed to let $X_e(t)$ track the nominal trajectory $X_{en}(t)$. Otherwise $\ddot{X}_e(t)$ is modified to deal with the detected human intention.

The above two steps are referred to as the offline trajectory generation and online control.

5.3.4 Simulation and Experimental Results

In actual practice, it is very difficult to measure the human joint torque accurately. One approximative way of obtaining the joint torque is to calculate the torque through a dynamic model by assuming that the applied model is roughly close to the real human mechanics. Therefore, to validate the control framework, we estimate the human joint torque by implementing a numerical simulation under the proposed human dynamic model. Specifically, we implement three simulations under three different scenarios for the STS assistance:

(A) The human subject stands up by him/herself without any robotic assistance.

(B) The end-effector trajectory of the assistive robot is arbitrarily chosen which moves upward and forward to ensure a successful STS process.

(C) The end-effector trajectory of the assistive robot is the same as the optimized nominal one $X_{en}(t)$.

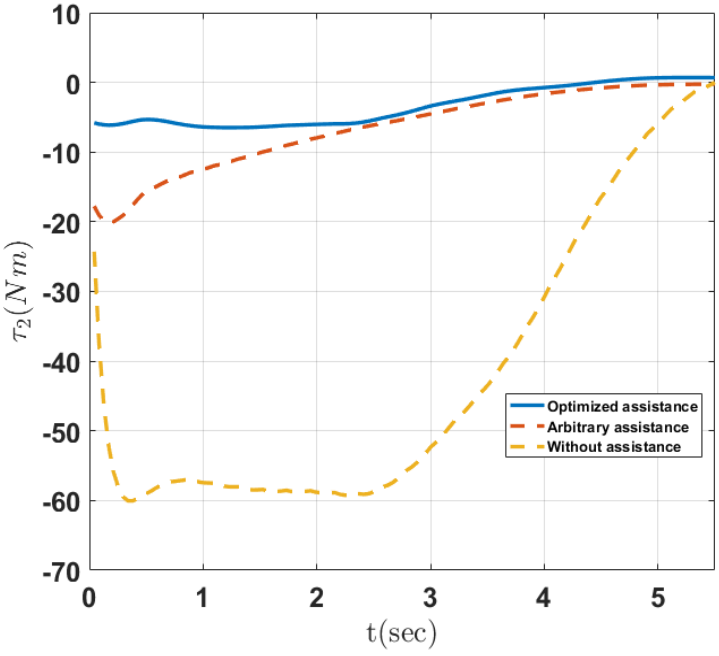

Figure 5.19 Comparison of the knee joint torque under three different scenarios.

In all the three scenarios, the desired trajectories of first three joints of the human are set to be $\theta_{123n}(t)$ for a fair comparison. The knee torque applied by human versus time is plotted in Figure 5.19. As can be seen from the figure, with an arbitrarily chosen end-effector trajectory, the human joint torque can be substantially reduced compared to the case when no assistance is given. However, with the proposed optimal assistance trajectory $X_{en}(t)$, the knee torque can be further reduced, which demonstrates the effectiveness of the joint load reduction under our proposed approach.

Next, we conduct a set of STS experiments to assess the applicability of the proposed human-centered control framework. A 6-DOF robot manipulator is placed steadily on a level surface to ensure that the robot has no tip-offs during the operations. The human subject sits naturally on a seat with two hands grabbing the robot end-effector firmly. An arm exoskeleton is put onto the subject for the purpose of real time elbow angle measurement. The measured angle value is used for calculating the angle difference, $\theta_5 - \theta_{5n}$ to determine the intention of human. Four STS tests are performed under four different types of human intentions:

(a) The human subject wants stands up normally (standard STS).

(b) The human subject wants to stand up faster than normal (fast STS).

(c) The human subject wants to stand up slower than normal (slow STS).

(d) The human subject changes his mind during the process and wants to sit back down.

The screenshots of the four tests are shown in Figure 5.20. The actual end-effector trajectories are plotted in Figure 5.21, while the paths followed by the end-effector (X_{ex} versus X_{ey}) are shown in Figure 5.22. First of all, as shown in Figure 5.22, the robot end-effector stays close to the nominal path S_{en} in all the four tests. However, the movements along the path are very different as can be seen in Figure 5.21. For (a), where the human subject intends to stand up normally, the actual end-effector trajectory is almost the same as the nominal one. For (b), the human subject intends to stand up faster. Such a

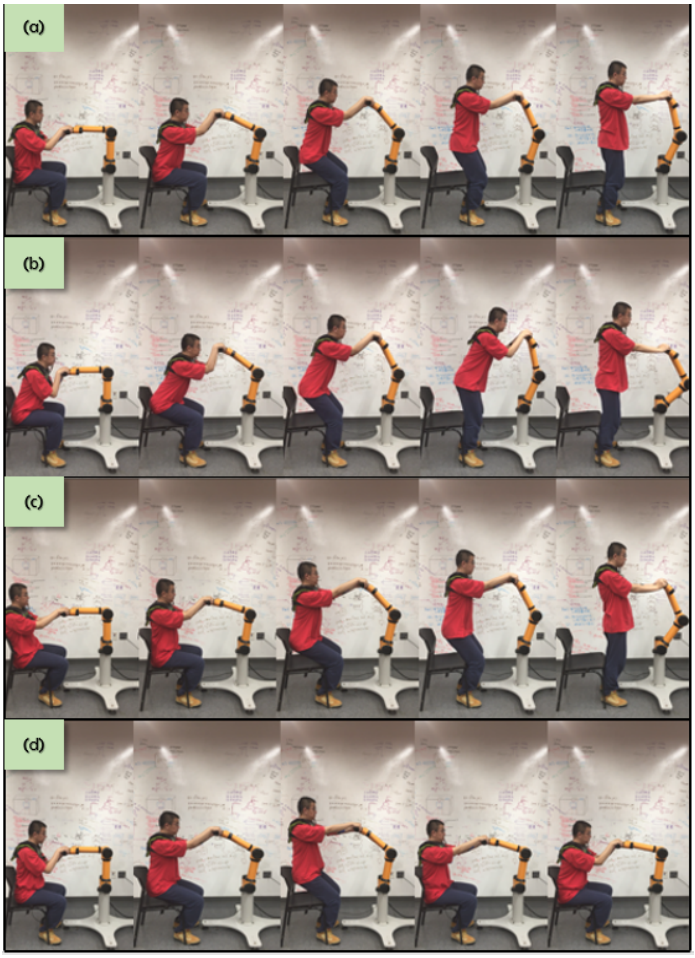

Figure 5.20 Four STS assistance with different human intentions: (a) Standard STS assistance, (b) Fast STS assistance, (c) Slow STS assistance and (d) Human refuses to stand up.

change in human intention is reflected physically by a faster trunk and leg movement, which leads to a smaller elbow angle compared to the nominal value during the STS process. As a result, the control law drives the robot end-effector faster to follow to trend of the human body movement. Similarly, for (c), the intention that human wants to stand up slower results in a slower movement of the robot end-effector. Finally, in (d), since the human wants to sit back down in the middle of the STS process, the elbow angle is much large than the nominal value. According to the control algorithm, the robot end-effector moves backward to capture the intention of the human. Eventually, the human subject successfully sits back to the seat with the robot end-effector staying just in front of him. These experimental results show that our proposed human-centered control algorithm can effectively capture the changing intention of the human subject during the STS process, which makes it succeed in every single STS operation.

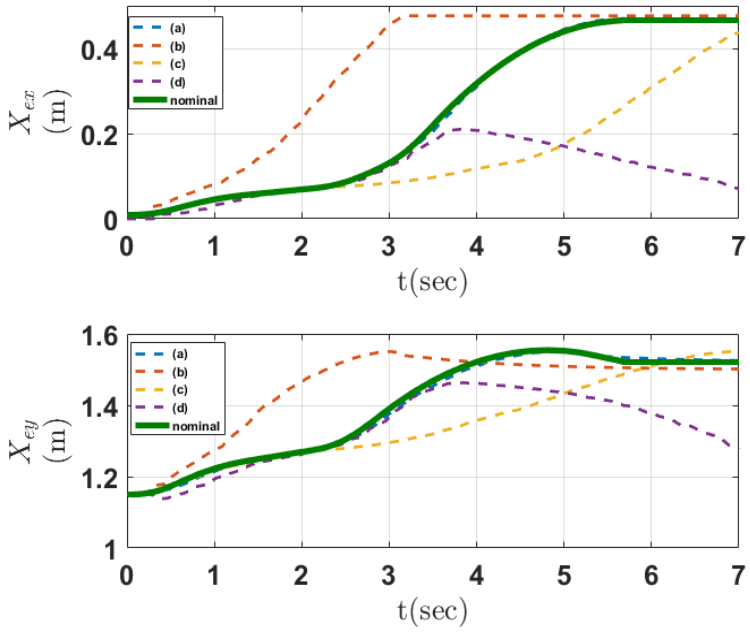

Figure 5.21 The end-effector trajectories $X_e(t)$ for the tests (a)-(d).

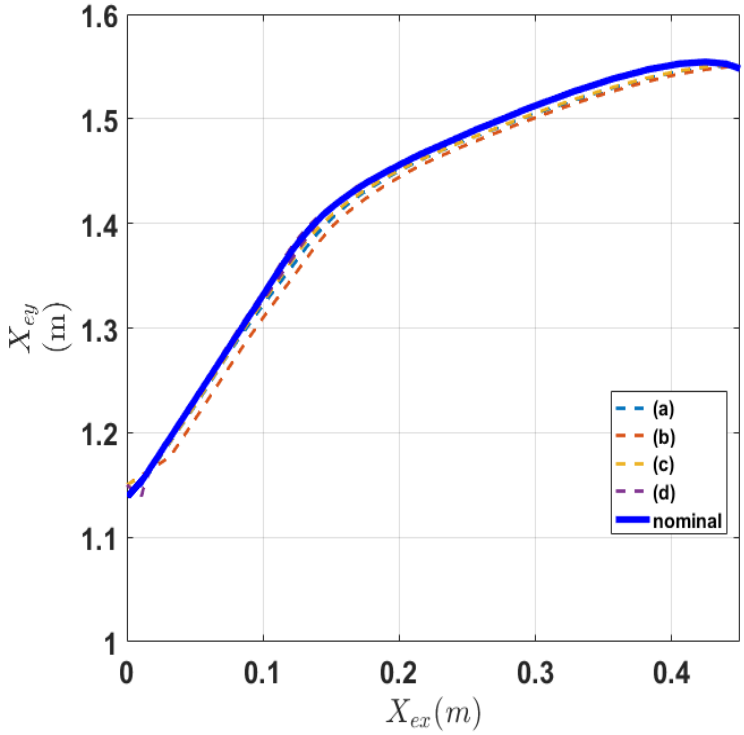

Figure 5.22 The actual paths ($X_{ex}(t)$ versus $X_{ey}(t)$) for the tests (a)-(d).

5.3.5 Conclusion

In this study, we proposed a human-centered control framework for the Sit-to-Stand (STS) assistance by using a robot manipulator. We first constructed a human dynamic model, based on which a human torque control law was assumed. Then, a two-step control strategy was developed to minimize the human joint load while taking care of the human intention under the assumed human torque control law. In Step 1, an optimal nominal trajectory for the robot end-effector that minimizes the nominal joint load was generated offline using dynamic programming. In Step 2, a real-time switching controller was constructed and implemented online to modify the nominal trajectory of the robot end-effector once a change of human's intention was detected. The proposed method was capable of minimizing the human joint load and following the constantly-changing human intention simultaneously during the STS assistance. Various simulation and experimental results validate the proposed design.

5.4 An Integrated Approach for Robotic Sit-To-Stand Assistance: Control Framework Design and Human Intention Recognition

5.4.1 Introduction

On the basis of our previous research [51], we propose an integrated approach which combines model based control method and deep learning based human intention recognition together for robotic STS assistance. The proposed algorithm features simultaneous motion control and optimization as well as human movement prediction which minimize the human joint loads and react to varying human intentions during the robotic STS assistance. In particular, we first implement various experiments of human-to-human STS assistance using motion capture sensors. Then, according to the experiments and the recorded data, we subdivide the entire STS process into two phases: Sit-To-Perch (STP) phase and Perch-To-Stand (PTS) phase. For each phase, we construct a human body dynamic model that maps the joint muscle forces and contact forces to the human body movement. To minimize the human joint muscle load while following the human's motion intention during the STS motion, we develop a two-step estimation/control strategy to generate the robot end-effector motion that combines traditional model-based tracking control, trajectory optimization, as well as a long-short term memory (LSTM) neural network for the prediction of human's intended velocity. Then this intended velocity is used to modify the moving velocity and the direction of the robot end-effector along its nominal path. Various simulations and experiments are also performed to validate the proposed approach.

5.4.2 Dynamic Modeling of STS Assistance

In this section, we implement various human-to-human STS assistance experiments. On account of observation and analysis of the human-to-human STS assistance, several assumptions are given. Finally, the system dynamic models are constructed based on the experimental results and assumptions.

Experiments of Human-To-Human STS Assistance It is reasonable that the way of how a robot assists a person in getting up from a seated place should learn from human beings, as human beings naturally possess the ability of interacting with other human beings efficiently and safely. On the other hand, the characteristics of how a human reacts and behaves during a human-to-human STS assistance can also be seized so that the entire system can be modeled appropriately in mathematical forms. Therefore, we conduct two groups of studies which are summarized as:

A) Observation of human-to-human STS assistance among various subjects.

B) Human joint trajectory recording of a weak knee subject.

In the first group of human-to-human STS assistance experiments, we invite various volunteers with different ages, genders and physical conditions to participate in the research, as shown in Figure 5.23. Specifically, subjects are asked to sit with different

Figure 5.23 Human-to-human STS assistance among various subjects. (A) assisting an elderly subject with STS motion; (B) assisting an male adult with STS motion; (C) assisting a female adult with STS motion.

postures comfortably on a seated place or a chair with two hands grasped tightly by an assistant. Then, the assistant pulls him/her up gradually to reach a proper stand-up posture.

In the second group of human-to-human STS assistance experiments, we apply motion capture sensors to record the joint angular trajectories of a human subject who

injured his left knee in basketball competition. The selected subject is asked to perform the STS motions with some featured initial sitting postures under the help of another person. As can be seen in Figure 5.24. 30 different tests are implemented, with 4650 data sets of

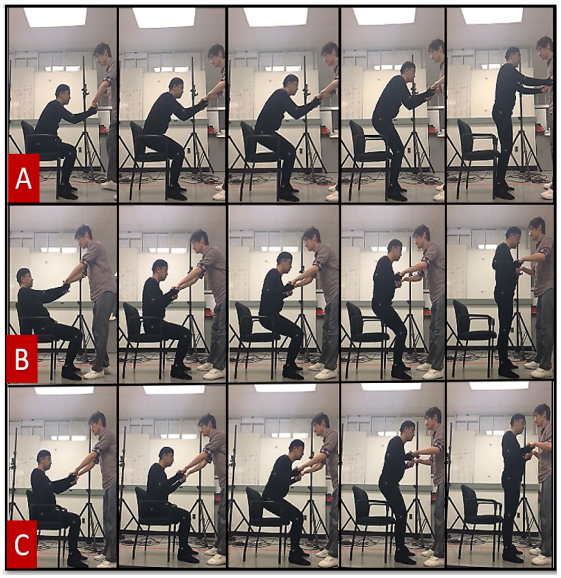

Figure 5.24 Human joint trajectory recording using motion capture sensors. A lean forward sitting posture; B lean backward sitting posture; C upright sitting posture.

the human joint angles collected. The purposes of conducting these human-to-human STS assistance experiments are to observe how the human subject behaves and reacts during the STS process as well as to investigate and record the characteristics of how the human joints move in the STS assistance. According to the observations as well as analysis of the human-to-human STS assistance, we found these experiments share some common features that can be concluded as:

- Feature 1: In the experiments, the subjects stand up in the sagittal plane as the out-of-plane waggling movement is very minimum.
- Feature 2: Regardless of any siting postures, the subjects need to adjust the centers of weight properly before their bodies take off from the chairs.
- Feature 3: Even though a person can get up with different speeds and upper body stances, the moving trajectories of the ankle joint, the knee joint and the hip joint remain almost unchanged when he/she stands up.

According to the obtained features, we make the following assumptions:

- *Assumption 1*: The human body is modeled by a five-link planar mechanism with one end (ankle joint) pinned to be ground and the other end (wrist joint) pinned to the robot end-effector.
- *Assumption 2*: The STS motion is divided into two phases: The Sit-To-Perch (STP) phase and Perch-To-Stand (PTS) phase. Particularly, STP phase is featured as a process of shifting the center of weight before standing up from a seated place, while PTS phase is characterized as a progress of standing up from the seated place.

Formulation of the System Dynamics for Two Phases We introduce a general scenario of STS assistance: a person intends to stand up from a seated place under the assistance of a robotic manipulator. The manipulator is placed adjacent to the human with the robot end-effector grasped firmly by the human's hands. Thus, we assume that the human wrist joint is pinned to the robot end-effector and its motion follows those of the other joints passively.

We first introduce the human dynamics in PTS phase since the PTS phase is the primary phase which takes up the most of time during STS assistance, while STP phase is considered as the transitional phase. The human body system can be treated as a five-link mechanism whose dynamic model is formulated as (Figure 5.25):

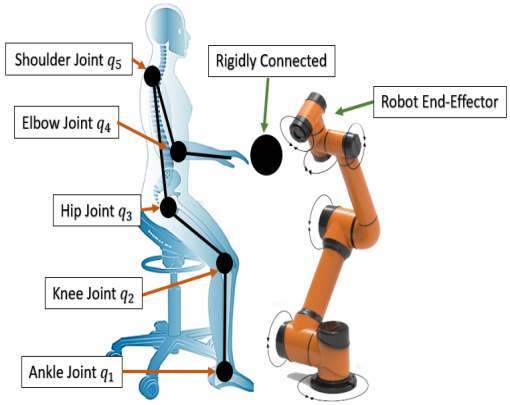

Figure 5.25 Schematic of the system dynamic model in PTS phase.

$$B(q)\ddot{q} + C(q,\dot{q})\dot{q} + G(q) = \tau + J(q)^T F. \tag{5.20}$$

Where $q = [q_1, q_2, q_3, q_4, q_5]^T$ is the vector of joint angles, including q_1 (ankle angle), q_2 (knee angle), q_3 (hip angle), q_4 (shoulder angle), q_5 (elbow angle). $B(q) \in R^{5\times5}$ is a positive-definite symmetric matrix, represents the inertia matrix of the human body system. $C(q,\dot{q})\dot{q} \in R^5$ is the vector of Coriolis as well as centripetal forces. $G(q) \in R^5$ represents the vector of gravitational force. $\tau \in R^5$ is the vector of human joint torques. $J(q) \in R^{2\times5}$ is the Jacobian matrix and $F \in R^2$ is the interactive force generated between the robot end-effector and the human hands along horizontal and vertical directions.

Since the assistive force F at the end-effector is indirectly determined by the human and robot motions, we need to eliminate it and represent the equation only in terms of the two control input variables: human joint torque τ and desired robot end-effector acceleration $\ddot{X}_e$. In particular, we first revise (5.20) as:

$$\ddot{q} = B(q)^{-1}[\tau + J(q)^T F - C(q,\dot{q})\dot{q} - G(q)] \tag{5.21}$$

Then, taking the time derivative of the equation $\dot{X}_e = J(q)\dot{q}$ that represents the kinematic relationship between joint space and work space, we obtain the end-effector acceleration $\ddot{X}_e$ as:

$$\ddot{X}_e = J(q)\ddot{q} + \dot{J}(q)\dot{q}, \tag{5.22}$$

Combining (5.21) and (5.22), the interaction force F, is formulation in terms of τ and $\ddot{X}_e$:

$$F = (J(q)B(q)^{-1}J(q)^T)^{-1}[\ddot{X}_e - \dot{J}(q)\dot{q} - J(q)B(q)^{-1}(C(q,\dot{q})\dot{q} + G(q) - \tau)] \tag{5.23}$$

Next, substitute (5.23) into the (5.20), we can get:

$$B(q)\ddot{q} = K_A\tau + K_B\ddot{X}_e + K_C\dot{q} - K_A(C(q,\dot{q})\dot{q} + G(q)) \tag{5.24}$$

In (5.24), the coefficients K_A, K_B and K_C are calculated as:

$$\begin{aligned} K_A &= I - J(q)^T (J(q)B(q)^{-1}J(q)^T)^{-1}(J(q)B(q)^{-1}); \\ K_B &= J(q)^T (J(q)B(q)^{-1}J(q)^T)^{-1}; \\ K_C &= -J(q)^T (J(q)B(q)^{-1}J(q)^T)^{-1}\dot{J}(q); \end{aligned} \tag{5.25}$$

(5.24) shows that the human body motion in the STS assistance is affected by the joint torque τ and the acceleration of the robot end-effector $\ddot{X}_e$.

In the STP phase, since the lower extremity rests on the chair, only the three upper links need to be considered in modeling the human body dynamics (Figure 5.26):

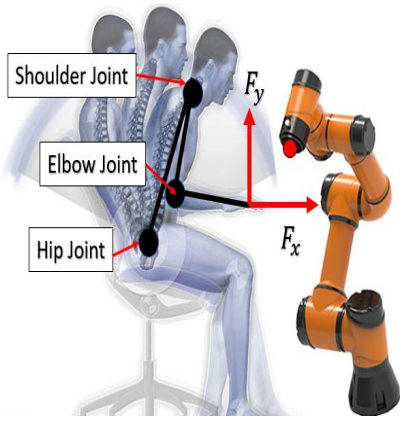

Figure 5.26 Schematic of the system dynamic model in the STP phase.

$$B_{345}(q_{345})\ddot{q}_{345} + C_{345}(q_{345}, \dot{q}_{345})\dot{q}_{345} + G_{345}(q_{345}) = \tau_{345} + J_{345}(q_{345})^T F. \tag{5.26}$$

where $q_{345} \in R^3$ is a vector that contains the hip angle q_3, the shoulder angle q_4 and the elbow angle q_5. $B_{345}(q_{345}) \in R^{3\times3}$ is the lower-right 3×3 matrix of B. $C_{345}(q_{345}, \dot{q}_{345}) \in R^3$ consists of the three lower rows of C. $G_{345}(q_{345})$ is vector of the third to fifth entries of G. $J_{345}(q_{345}) \in R^{2\times3}$ consists of the three lower rows of J.

Similar to the above derivation, the relationship between the human joint torque, the desired robot end-effector acceleration, and the human motion is obtained as:

$$B_{345}(q_{345})\ddot{q}_{345} = K_{A345}\tau_{345} + K_{B345}\ddot{X}_e + K_{C345}\dot{q}_{345} - K_{A345}(C_{345}(q_{345},\dot{q}_{345})\dot{q}_{345} + G_{345}(q_{345})) \quad (5.27)$$

Where K_{A345}, K_{B345} and K_{C345} have similar representations as in (5.25).

In the dynamic model, the B, C, G, and J matrices are determined by the joint position, joint velocity, as well as the kinematic and dynamic parameters of the particular human subject. In the experiments, the height and body weight of each individual can be directly measured, while the kinematic and dynamic parameters of each body segment cannot be easily determined. In this study, we use the table of body segment [49] as shown in Table 5.2 to calculate the unknown kinematic and dynamic parameters for each individual, and subsequently the B, C, G and J matrices.

Table 5.2 Parameters of Human Body Segment

SEGMENT	*P(male)*	*P(female)*	*M*	$I_{1(Kg-m^2)}$	$I_{3(Kg-m^2)}$
HEAD	0.138	0.138	0.0730	0.0248	0.3119
UPPER ARM	0.172	0.193	0.0270	0.0213	0.3119
FOREARM	0.157	0.166	0.0160	0.0760	0.3119
HAND	0.104	0.104	0.0066	0.0005	0.3119
TRUNK	0.3	0.3	0.5080	1.3080	0.3119
THIGH	0.232	0.247	0.0988	0.1502	0.3119
SHANK	0.247	0.256	0.0465	0.0505	0.3119
FOOT	0.042	0.042	0.0145	0.0038	0.3119

In this table, P represents the segment length of whole body and M is the segment weight of whole body. I_1 and I_3 are the mass moments of inertia of the segment along

transverse axis and longitudinal axis accordingly. In the STS assisting experiments, all the geometrical and inertia coefficients are selected on the basis of each individual who needs to be assisted and substitute to the dynamic model and the controller in real-time.

5.4.3 The Mechanism of Human Joint Control

For the design of a robot end-effector controller that optimizes the STS motion, the human joint control mechanism must be investigated first as the STS motion is a typical human-robot collaborative task. We assume the human generates his/her joint torques from a two-step planning and tracking strategy - a standard approach in automatic control. Specifically, the human intends to move his/her body along a specific path with a certain speed, which is referred to as the "planning" stage. Then, the body muscles generate joint torques that make the body track the trajectory generated, which is referred to as the "tracking" stage. In this section, we will conduct a full study of human joint control and propose the human joint control models for both the PTS and STP phases.

Modeling of Human Joint Control in PTS Phase In PTS phase as shown in Figure 5.25, from various experiments and data analyses, we notice that the moving paths of the first three joints - the ankle joint, the knee joint and the hip joint - stay almost the same every time a person is assisted to stand up. In Figure 5.27, we plot a nominal path for the first three joints in 3D space, which is obtained by taking average values of the first three joint data for all experiments. On the other hand, it is also observed that the shoulder joint and the elbow joint move passively along with the robot end-effector, and their trajectories vary across different experiments. Thus, it is natural to assume that human intends to control his/her first three joints in the lower extremity, while the upper extremity holds the end-effector to assist the lower extremity motion control. To mathematically model such a human joint control process, we multiply Equation (5.24) by $B(q)^{-1}$ and take the first three rows of the equation:

$$\ddot{q}_{123} = B_{123}(q)^{-1}[K_A\tau + K_B\ddot{X}_e + K_C\dot{q} - K_A(C(q,\dot{q})\dot{q} + G(q))], \tag{5.28}$$

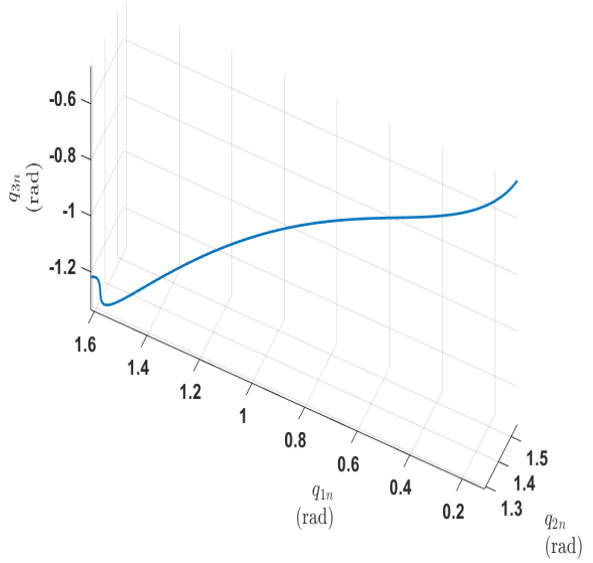

Figure 5.27 The nominal motion path of the first three joints in STS assistance.

Where $q_{123} \in R^3$ is a vector of the first three joint angles. $B_{123}(q)^{-1}$ is a matrix contains the first three rows of $B(q)^{-1}$. As in [50], the PD controller is assumed to be used by human to regulate and stabilize his/her lower extremity motion.

$$X\tau = Y(q, \dot{q}, q_{123n}(t), \dot{q}_{123n}(t), \ddot{q}_{123n}(t)), \tag{5.29}$$

where

$$\begin{aligned} X &= B_{123}(q)^{-1}K_A \\ Y &= -B_{123}(q)^{-1}[K_C\dot{q} - K_A(C(q,\dot{q})\dot{q} + G(q))] \\ &\quad -k_p(q_{123} - q_{123n}(t)) - k_d(\dot{q}_{123} - \dot{q}_{123n}(t)) + \ddot{q}_{123n}(t), \end{aligned} \tag{5.30}$$

k_p and k_d are 3×3 diagonal matrices consisting of proportional and derivative gains. $q_{123n}(t)$, $\dot{q}_{123n}(t)$ as well as $\ddot{q}_{123n}(t)$ represent the nominal trajectories of the positions, velocities and accelerations of the first three joints individually. From the above observation and analysis, $q_{123n}(t) \in S$, where S is a 1D curve with finite length in R^3, representing the nominal path of the first three joints. Notice that (5.29) includes three equations with five undetermined entries. Hence to solve the equation, we assume the human tries to minimize

the following quadratic objective function:

$$\min\ \tau^T \Lambda_1 \tau \tag{5.31}$$

Where Λ_1 is a positive definite diagonal matrix representing the joint weights. Different patients intuitively choose different Λ_1 matrix. For example, a person with knee injury may have a high penalty on the knee joint, while a person with waist pain may increase the weight of the waist joint. The human joint torque that minimizes (5.31) while satisfying (5.29) is given by:

$$\begin{aligned} \tau &= \tau_{PTS}(q, \dot{q}, q_{123n}(t), \dot{q}_{123n}(t), \ddot{q}_{123n}(t)) \\ &\triangleq \Lambda_1^{-1} X^T (X \Lambda_1^{-1} X^T)^{-1} Y. \end{aligned} \tag{5.32}$$

Therefore the dynamics of q_{123} with the assumed human torque control mechanism becomes:

$$\begin{aligned} \ddot{q}_{123} &= -k_p(q_{123} - q_{123n}(t)) - k_d(\dot{q}_{123} - \dot{q}_{123n}(t)) \\ &\quad + \ddot{q}_{123n}(t) + B_{123}(q)^{-1} K_B \ddot{X}_e, \end{aligned} \tag{5.33}$$

Modeling the Human Joint Dynamics for STP Phase The schematic diagram of the system in STP phase is shown in Figure 5.26. According to the above analyses, the system dynamics of STP phase is formulated without taking the movements of the lower extremities into consideration. Therefore, it is natural to assume that human only focuses on the motion control of the waist joint to tilt the upper body forward, whose dynamics is given as:

$$\begin{aligned} \ddot{q}_3 = B_{345}(q_{345})_3^{-1} [K_{A345}\tau_{345} + K_{B345}\ddot{X}_e + K_{C345}\dot{q}_{345} \\ - K_{A345}(C(q_{345}, \dot{q}_{345})\dot{q}_{345} + G(q_{345}))]. \end{aligned} \tag{5.34}$$

where q_3 is the hip joint angle. $q_{345} \in R^3$ is a vector that contains the hip joint angle q_3, the shoulder joint angle q_4 and the elbow joint angle q_5. $B_{345}(q_{345})_3$ indicates the first row of the matrix $B_{345}(q_{345})$. It represents the inertia terms of the hip joint. τ_{345} is the vector

consisting of τ_3, τ_4 and τ_5. Similar to the PTS phase, it is assumed that the human uses a PD controller with nonlinear compensation terms to control the hip joint to track a desired angle profile:

$$M\tau_{345} = N(q_{345}, \dot{q}_{345}, q_{3n}(t), \dot{q}_{3n}(t), \ddot{q}_{3n}(t)), \tag{5.35}$$

where

$$\begin{aligned} M &= B_{345}(q_{345})_3^{-1} K_{A345} \\ N &= -B_{345}(q_{345})_3^{-1}[K_{C345}\dot{q}_{345} - K_{A345}(C(q_{345}, \dot{q}_{345})\dot{q}_{345} \\ &\quad + G(q_{345}))] - k'_p(q_3 - q_{3n}(t)) - k'_d(\dot{q}_3 - \dot{q}_{3n}(t)) + \ddot{q}_{3n}(t) \end{aligned} \tag{5.36}$$

where k'_p and k'_d are defined as proportional and derivative gains. $q_{3n}(t)$ is the nominal trajectory of the human hip joint.

The redundancy resolution in STP phase is achieved by minimizing the following objective function:

$$\min \ \tau_{345}^T \Lambda_2 \tau_{345}, \tag{5.37}$$

Where Λ_2 is a positive definite matrix that contains the weights of each joint. The human joint torque that minimizes (5.37) while satisfying (5.35) is given by:

$$\begin{aligned} \tau_{345} &= \tau_{STP}(q_{345}, \dot{q}_{345}, q_{3n}(t), \dot{q}_{3n}(t), \ddot{q}_{3n}(t)) \\ &\triangleq \Lambda_2^{-1} M^T (M\Lambda_2^{-1} M^T)^{-1} N. \end{aligned} \tag{5.38}$$

And the closed-loop dynamics of q_3 becomes:

$$\begin{aligned} \ddot{q}_3 &= -k'_p(q_3 - q_{3n}(t)) - k'_d(\dot{q}_3 - \dot{q}_{3n}(t)) \\ &\quad + \ddot{q}_{3n}(t) + B_{345}(q_{345})_3^{-1} K_{B345} \ddot{X}_e, \end{aligned} \tag{5.39}$$

5.4.4 Robot End-effector Control and Online Human Intention Estimation

According to the system dynamic Equations (5.28) and (5.34), human controls the lower extremity to follow the intended desired trajectory during entire STS assistance, meanwhile the motion of robot end-effector $X_e(t)$ indirectly determines the movements of the upper

limbs and supplies the external force to assist the person in standing up. Therefore, we intend to design the motion of $X_e(t)$ to achieve the following objectives:

(1) All signals are bounded and stability of the system is maintained.

(2) Joint loads are optimized during STS assistance.

(3) The assisting robot reacts to human's intention during STS assistance.

As for the objective (1), it is well known that human beings possess outstanding ability of maintaining stability when interacting with the physical world. Thus, the system stability is primarily determined by the robot side. As seen from the closed-loop system dynamics with PD controller assumed in the last section, if the robot end-effector motion signals X_e, $\dot{X}_e$ and $\ddot{X}_e$ are all bounded, then the human joint positions and velocities will be bounded as well.

As the human intention is elusive and time-varying, the human's desired joint trajectories ($q_{123n}(t)$ in PTS phase and $q_{3n}(t)$ in STP phase) may vary a lot in real time along their nominal paths. It is thus extremely difficult to design a globally optimal control algorithm which optimizes the joint loads while taking care of any possible human intention change during the STS assistance. To accomplish the objectives (2) and (3), we construct a two-step control strategy as shown in Figure 5.28:

- Step 1: Given body and joint control parameters of the particular human subject to be assisted, a nominal robot end-effector trajectory $X_{en}(t)$ is generated offline to minimize the joint loads under the nominal human motion trajectory $q_{123n}(t)$ in PTS phase and $q_{3n}(t)$ in STP phase.
- Step 2: During the implementation, the human's intention is estimated by feeding the real-time human posture which is detected by motion capture sensors to a trained long short-term memory (LSTM) network. Based on this information, a simple proportional control law is developed to adjust the velocity of the robot end-effector along its nominal path.

The detailed design procedure is illustrated in the following subsections.

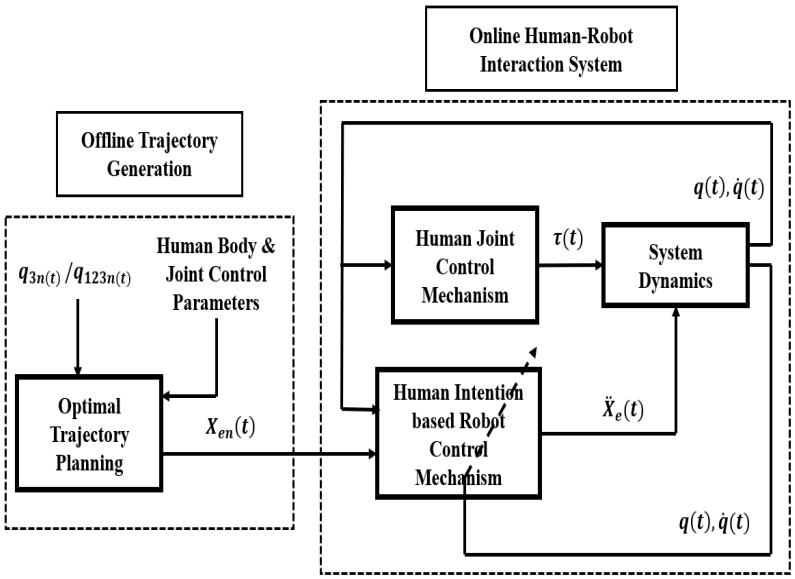

Figure 5.28 Schematic diagram of human intention based control framework.

Offline Trajectory Generation As mentioned above, on the basis of the experimental data, we assume a nominal time-varying trajectory of the hip joint $q_{3n}(t)$, to represent the averaged motion of how a person perches before standing up in STP phase. As can be seen from Figure 5.29. We also assume a nominal human intended time-varying trajectory of

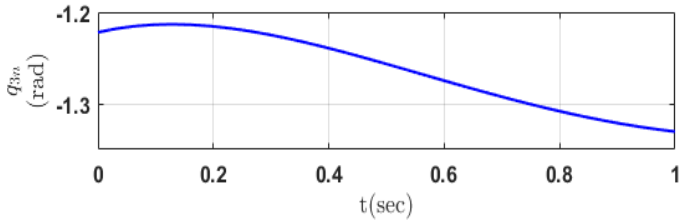

Figure 5.29 The angular trajectory of the hip joint in STP phase.

the first three joints $q_{123n}(t)$ to represent their averaged motions in PTS phase. As can be seen from Figure 5.30.

Therefore, according to the system dynamics and the human joint control mechanism, we construct the following optimal control problem to generate the nominal robot end-

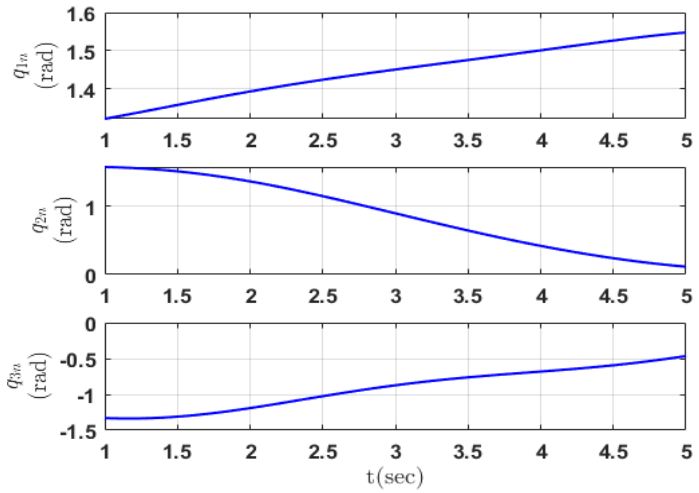

Figure 5.30 The angular trajectory of the first three joints in PTS phase.

effector trajectory $X_{en}(t)$:

$$\min_{X_{en}(t)} \int_0^T f(\tau_n(t))dt$$

$$s.t.$$

$$\begin{cases}
\text{In STP phase} \\
f(\cdot) = f_{STP}(\cdot), \\
\tau_n(t) = \tau_{STP}(q_{345}(t), \dot{q}_{345}(t), q_{3n}(t), \dot{q}_{3n}(t), \ddot{q}_{3n}(t)), \\
B_{345}(q_{345}(t))_3\ddot{q}_{345}(t) = K_{A345}\tau_{345}(t) + K_{B345}\ddot{X}_{en}(t) \\
+K_{C345}\dot{q}_{345}(t) - K_{A345}(C_{345}(q_{345}(t), \dot{q}_{345}(t))\dot{q}_{345}(t) \\
+G_{345}(q_{345}(t))), \\
\text{In PTS phase} \\
f(\cdot) = f_{PTS}(\cdot), \\
\tau_n(t) = \tau_{PTS}(q(t), \dot{q}(t), q_{123n}(t), \dot{q}_{123n}(t), \ddot{q}_{123n}(t)), \\
B_{123}(q(t))\ddot{q}(t) = K_A\tau + K_B\ddot{X}_{en}(t) + K_C\dot{q}(t) \\
-K_A(C(q(t), \dot{q}(t))\dot{q}(t) + G(q(t))),
\end{cases} \tag{5.40}$$

$$\forall t \in [0, T],$$

$$\dot{X}_{en}(0) = 0,\ \ddot{X}_{en}(0) = 0,\ \dot{X}_{en}(T) = 0\ \&\ \ddot{X}_{en}(T) = 0.$$

It is noted that $q_{123n}(t)$ in PTS phase and $q_{3n}(t)$ in STP phase are predetermined, while $q_{45n}(t)$ are determined indirectly given a particular $X_{en}(t)$ under the system dynamics and human joint control law discussed in Section 5.4.3. The objective function is simply the total joint load during the entire STS assistance process. To solve the above optimization problem, various methods can be applied, such as dynamic programming (DP) [52, 53] or iterative linear quadratic regulator (ILQR) [54]. In this case, we use nonlinear programming method [55] to obtain the nominal trajectory of the end-effector in the y-direction and the z-direction. The result obtained for assisting a particular human subject with given body and joint control parameters is shown in Figure 5.31.

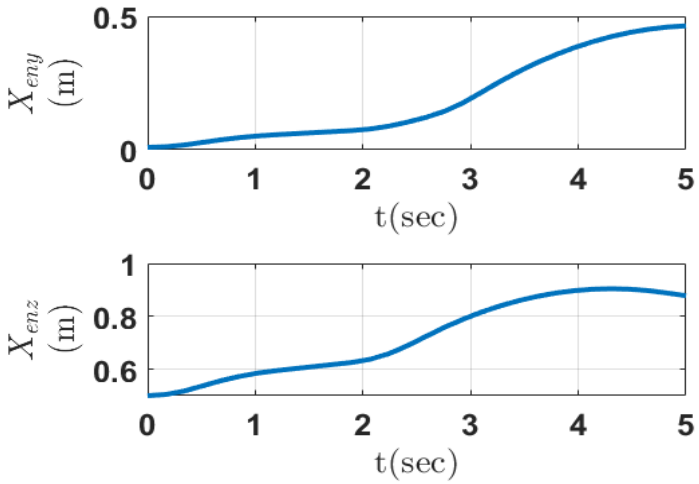

Figure 5.31 The nominal trajectory of the end-effector in y and z directions.

LSTM and Human Intention Estimation $X_{en}(t)$ is defined as a nominal trajectory of the robot end-effector that is generated under the optimization law (5.40). However, it merely represents an average and an idealized STS motion of a human. Yet a human may attempt to move differently from the default path, $X_{en}(t)$ in reality. For instance, a person may stand up faster or slower, or even sit back down due to a sudden alternation of intention. Suppose that the assistive robot is incapable of responding to the varying human intention during an

STS process. Then the person may end up with an awkward posture or even get injured. Therefore, an agile control mechanism is needed to deal with changing human intentions.

In this research, we use Long-Short Term Memory (LSTM) network for human intention prediction, as LSTM network is excellent in holding long term memories, or in other words, the prediction of future state/output based on a sequence of historical data [56–58]. In our application, the LSTM network is trained with a combination of historical (time series) data of the ankle, knee and hip joint trajectories. In particular, we invite human subjects to perform variety of STS motions, such as getting up from a seated place regularly, quickly, slowly and sit back down in the middle of the STS process. The joint trajectories are recorded by 'Motive' motion capture cameras and are treated as different intentions of STS motions. It is worth mentioning that the input data are partitioned and normalized into numerous arrays before training.

In the training process, as can be seen from Figure 5.32., the information goes

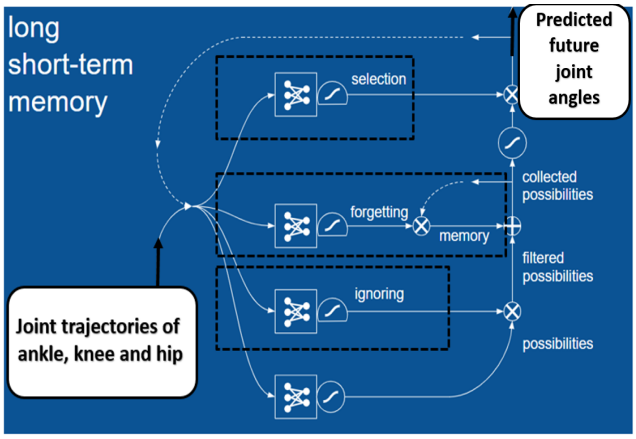

Figure 5.32 Schematic diagram of LSTM structure.

through basically three gates which are 'forgetting gate', 'ignoring gate' and 'selection gate'. Each gate has its own independent neuron network [59]. 'Forgetting gate' and 'memory' decide what information to be memorized and what to be forgotten. The compact

forms of the formulations of the 'forgetting gate' are given as:

$$\begin{cases} f_t = \sigma_g(W_f x_t + U_f h_{t-1} + b_f) \\ i_t = \sigma_g(W_i x_t + U_i h_{t-1} + b_i) \\ c_t = f_t \; o \; c_{t-1} = i_t \; o \; \sigma_c(W_c x_t + U_c h_{t-1} + b_c) \end{cases} \tag{5.41}$$

Where, f_t is the activation vector, i_t is the input activation vector and c_t is the cell state vector. σ_g is a sigmoid function, σ_c is a tangent function. Matrices W and U are the weights of the networks. x_t and h_{t-1} represents the input vector to the LSTM unit and the hidden state vector respectively. b is the bias. The operator 'o' denotes the element-wise product. The subscript t indicates the time step.

'Ignoring gate' and 'selection gate' decide what information or predictions need to be released for the moment.

$$o_t = \sigma_g(W_o x_t + U_o h_{t-1} + b_o) \tag{5.42}$$

Here, o_t represents the output activation vector. It is worthwhile to mention that the objective of the entire training process is to adjust weights to get the minimized error between the target and the prediction. This can be achieved by taking the gradient of the error in the direction of weights. Detailed formulations are given in [60, 61].

Finally, the trained LSTM network is used to predict transitory joint trajectory in future when the robot is assisting human in STS process. Specifically, during application, the current joint trajectory is collected and sent into the trained network. Then, the network estimates the future joint trajectory in every few mill-seconds. By calculating the gradient of the predicted joint trajectory, we are able to get the human intended velocity of STS motions in advance which indicates the human intention. Finally, this intended velocity is utilized to adjust the velocity of the robot end-effector online. So that the robot is able to cope with the varying human intentions during STS assistance. The entire process is given in Figure 5.33.

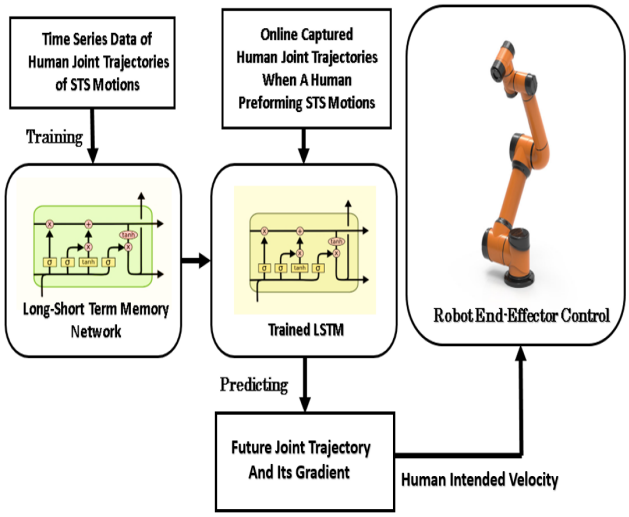

Figure 5.33 Flow-chart of human intention recognition mechanism.

Robot End-effector Control In this final step, we design a switching control algorithm for the robot end-effector to effectively follow the human's intended motion velocity, with the additional condition that both the end-effector acceleration and velocity are bounded to guarantee stability. Particularly, we enforce that the position of robot end-effector $X_e(t)$ always stays on the 2D curve formed by its nominal trajectory $X_{en}(t)$, denoted by S_{en} (which can be easily achieved by using various contour tracking algorithms in the direction normal to the curve), while the velocity along the curve is varying to deal with the detected human's intention. At every time instance, the position of the robot end-effector stays on S_{en}, and the arc length to the beginning of the curve is denoted as s_e. Now, the objective becomes to design the acceleration of the arc length variable $\ddot{s}_e$ such that the resulting $\dot{s}_e$ and s_e generated from this acceleration follows the human's intention. To achieve this, we first design $\ddot{s}_e$ to let $\dot{s}_e$ track a target velocity profile v_e:

$$\ddot{s}_e = \begin{cases} \ddot{s}_{emax}, & \text{if } \dot{s}_e > v_e, \\ -\ddot{s}_{emax}, & \text{if } \dot{s}_e < v_e, \\ \dot{v}_{en}(s_e) & \text{if } \dot{s}_e = v_e. \end{cases} \tag{5.43}$$

Where, $\ddot{s}_{emax}$ is the maximum acceleration of the robot end-effector. $v_{en}(s_e)$ and $\dot{v}_{en}(s_e)$ are the nominal velocity as well as nominal acceleration at the point s_e, which are obtained from re-parameterizing the tangential velocity and acceleration of the nominal trajectory $X_{en}(t)$ in terms of the arc length variable s_e.

On the velocity level, we construct the target velocity profile v_e as a function of an error between the human intended velocity v_i and the nominal human motion velocity. We first denote the 3D curve formed by the nominal trajectory of the first three joints q_{123} as S_{hn}. The current position of the human's first three joints in 3D space is projected onto S_{hn} and its arc length to the beginning of the curve is denoted as s_h. The nominal human motion velocity along S_{hn} at s_h is denoted as $v_{hn}(s_h)$, which is obtained by re-parameterizing the velocity of the nominal joint trajectory $\dot{q}_{123n}(t)$ in terms of the arc length variable s_h. Then, the target velocity profile of the robot end-effector is designed as (5.44), which is shown in Figure. 5.34.

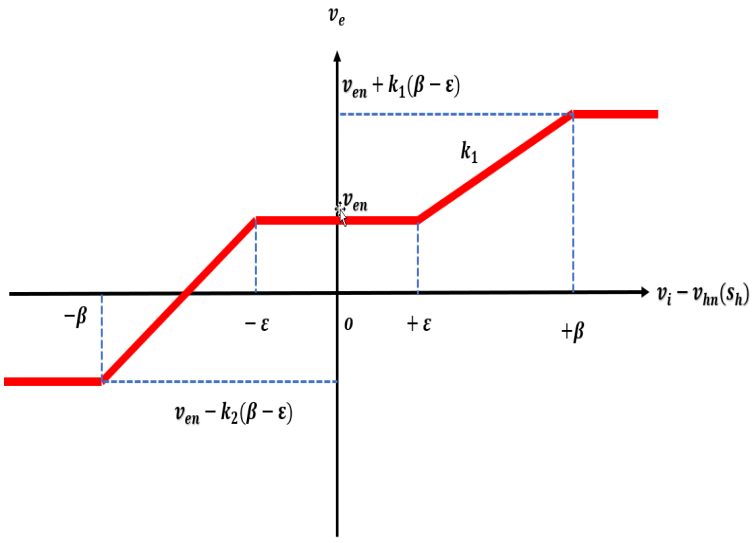

Figure 5.34 The target velocity profile of the robot end-effector trying to follow the human's intention.

$$
v_e = \begin{cases} v_{en}(s_e), \\ \quad \text{if } v_i \in [v_{hn}(s_h) - \varepsilon, v_{hn}(s_h) + \varepsilon] \\ v_{en}(s_e) + k_1(v_i - v_{hn}(s_h) - \varepsilon), \\ \quad \text{if } v_i \in (v_{hn}(s_h) + \varepsilon, v_{hn}(s_h) + \beta] \\ v_{en}(s_e) - k_2(-v_i + v_{hn}(s_h) - \varepsilon), \\ \quad \text{if } v_i \in [v_{hn}(s_h) - \beta, v_{hn}(s_h) - \varepsilon) \\ v_{en}(s_e) + k_1(\beta - \varepsilon), \\ \quad \text{if } v_i > \beta + v_{hn}(s_h) \\ v_{en}(s_e) - k_2(\beta - \varepsilon). \\ \quad \text{if } v_i < v_{hn}(s_h) - \beta \end{cases} \tag{5.44}
$$

(5.44) is formulated to modify the velocity of the robot end-effector v_e according to the human intended velocity v_i. In particular, if the difference between the human intended velocity and the nominal human motion velocity $v_{hn}(s_h)$ stays in the range of $[-\varepsilon, \varepsilon]$, where ε is a small positive constant, then the robot end-effector operates at the regular velocity $v_{en}(s_e)$. If the velocity difference $v_i - v_{hn}(s_h)$ lies in the range of $(\varepsilon, \beta]$, it indicates that the robot end-effector is assisting the human in getting up at a relative faster velocity than the nominal one. The maximum velocity $v_{hn}(s_h) + k_1(\beta - \varepsilon)$ can be reached if $v_i - v_{hn}(s_h) > \beta$. Where the slope k_1 is defined as a positive variable that affects how fast the robot end-effector moves along the positive direction of S_{en}. $\beta > \varepsilon$ is the cutoff value that determines the maximum forward velocity of the robot end-effect during the STS assistance. When the velocity difference $v_i - v_{hn}(s_h) < -\varepsilon$, the robot end-effector is either decelerating or running in the opposite direction along S_{en}. The maximum backward velocity is $v_{hn}(s_h) - k_2(\beta - \varepsilon)$, where k_2 is the slope value calculated as $v_{en}/(\varepsilon - v_{hn}(s_h))$ to ensure that the $v_e(0 - v_{hn}(s_h)) = 0$, i.e., the robot freezes if the human does not intend to move for safety consideration.

5.4.5 Simulation Result and Experimental Validation

Simulation and Experimental Verification of Knee Joint Load Reduction As a matter of fact, one critical functionality of robotic STS assistance is to decrease the joint load in STS process. To find out the effectiveness of the proposed approach of robotic STS assistance in knee joint load reduction, we implement a simulation and an experiment to validate the performance.

In the simulation section, we first construct human dynamic model in 'MATLAB'. Then, we acquire theoretical joint torque/load from simulations of three different scenarios of STS assistance:

(1) The human subject stands up without any assistance (abbreviated as 'without assistance').

(2) The human subject stands up with robotic assistance. While the trajectory of the robot end-effector is simplified as an obliquely straight line (abbreviated as 'simplified assistance').

(3) The human subject stands up with robotic assistance and the trajectory of the assistive robot end-effector is designed as the optimized trajectory, $X_{en}(t)$ (abbreviated as 'optimized assistance').

It is worth mentioning that the joint load/torque can be estimated from human dynamics [62]. Therefore, we evaluate and compare knee joint torque from (5.45) according to three scenarios.

As a result showing in Figure 5.35, it is clear that the human knee joint load is greatly alleviated when robot assists human in STS process in comparison with the scenario of 'without assistance'. This indicates that robot assistance is effective in STS motion. Furthermore, when the robot end-effector tracks the optimized trajectory $X_{en}(t)$, the knee joint torque can be further reduced in contrast to the 'simplified STS assistance' (scenario (2)), which validates the effectiveness of joint load deduction of the proposed method.

Next, to validate the simulation result, we conduct three tests corresponding to three scenarios ((1)-(3)). However, it is difficult to measure the joint/muscle force directly from a human being, therefore we use surface-detected electromyographic (S-EMG) sensors as

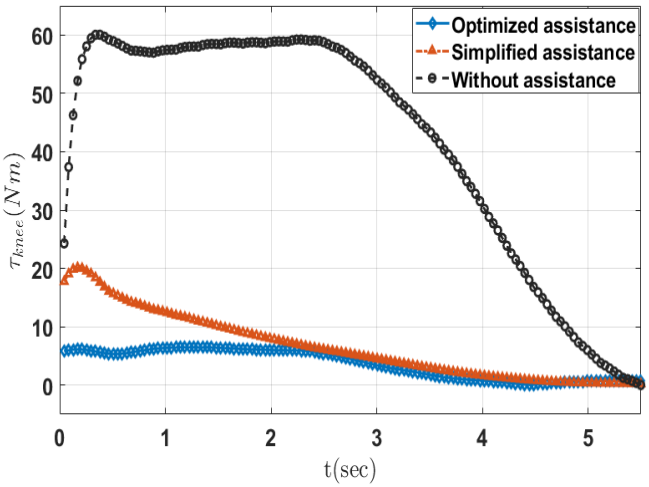

Figure 5.35 The simulation of knee joint load comparison in three different scenarios: optimized robot assistance reduces the most load acting on knee joint; Simplified robot assistance reduces some load acting on knee joint; Standing up without any assistance results in the heaviest load on knee joint.

an indirect method to measure the muscle activation. As variations in S-EMG signals are utilized to infer changes in neural activity related with a muscle contraction. For example, increasing S-EMG signal level can be associated with greater muscle force exerted [63–65].

The experimental setup is shown in Figure 5.36, where the human subject (a 70-year-old volunteer who had knee and waist injuries in the past), is requested to sit on a chair with an assistive robot (6-DOF 'AUBO' bot) placed nearby. The robot is arranged on an aclinic surface to ensure no inclination during operations. In scenario (1), the human subject is asked to stand up gradually with two arms overlapped on each other in front his/her chest. In scenarios (2) and (3), the robot assists the human in getting up. It is noted that since our robot does not have a hand with fingers, we require the subject to grasp the end-effector (the last joint) of the robot manipulator during the STS assistance, which is kinematically the same as the scenario of robot grasping human's hand if a robotic hand with fingers is available. Two S-EMG sensors are connected with 'Arduino Mega 2560' board and placed adjacent to the knee joint. Since the knee joint torque includes both flexion and extension motion torque, we attach S-EMG sensors on the positions of vastus lateralis muscles as well as semitendinosus muscle for signal recording [66].

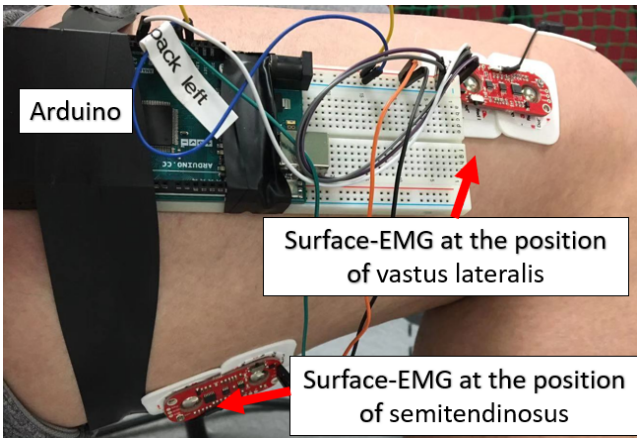

Figure 5.36 The experimental setup of joint load reduction testing using Surface-EMG (S-EMG) sensors.

The S-EMG signals measured for the three experiments are shown in Figure 5.37. When the subject stands up without any external assistance (scenario (1)), the output of S-EMG sensors shows a large peak signal which indicates a large joint load imposed on the knee joint during the STS process; While in scenario (2), the amplitude of the S-EMG signal is decreased, which shows that the knee joint load can be substantially reduced with a simple point-to-point assistance trajectory of the robot end-effector; In scenario (3), the output of S-EMG indicates that the knee joint load can be further reduced when the robot end-effector tracks the optimized trajectory $X_{en}(t)$ during STS assistance. In addition, the performance indices (euclidean norms) are calculated to express the energy levels corresponding to the scenarios (1), (2) and (3) as shown in Table. 5.3:

Table 5.3 Performance Index of Three STS Assistance Using Euclidean Norms

Scenarios/Norms (volts)	$\|v\|_2$:	$\|v\|_\infty$:
Without assistance	27.4	2.1
Simplified assistance	8.7	0.8
Optimized assistance	5.8	0.4

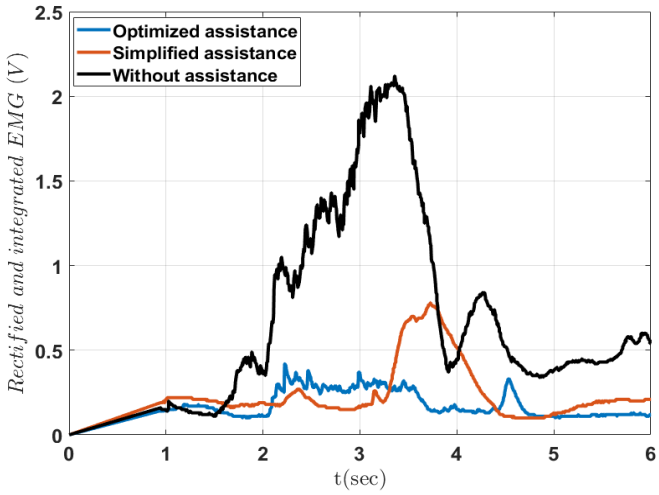

Figure 5.37 Rectified and integrated EMG signals obtained corresponding to the three scenarios of STS assistance.

As can be seen clearly in Table 5.3, the scenario of 'optimized assistance' using the trajectory generation proposed has the most energy efficiency among all the three scenarios, whereas standing up without any assistance has the most energy consumption.

Experiment on Human Intention Based Control In this experiment, we testify the applicability of the human intention recognition algorithm applied in the robot end-effector controller. Specifically, four STS tasks are implemented under four categories of human intentions:

(A) The human subject stands up normally (abbreviated as 'standard STS').

(B) The human subject intends to stand up slower than normal (abbreviated as 'slow STS').

(C) The human subject intends to stand up faster than normal (abbreviated as 'fast STS').

(D) The human subject changes his mind during STS assistance and tries to sit back down (abbreviated as 'sit back down').

The experimental setup is described as the follows: the human subject is asked for sitting naturally on a chair in the center of a matrix of 'Motive' motion capture cameras. These cameras record human joint angles in real-time for intention detection. It is worth

noting that the parameter selection corresponding to Equation (5.44) is given as follows: ε is assigned as 0.1 (rad/s); β is assigned as 1 (rad/s) and the slope k_1 is assigned as 1.

The screenshots of the four tasks are shown in Figure 5.38 and the actual trajectories of the robot end-effector are plotted in Figure 5.39. For (A), the human subject intends to

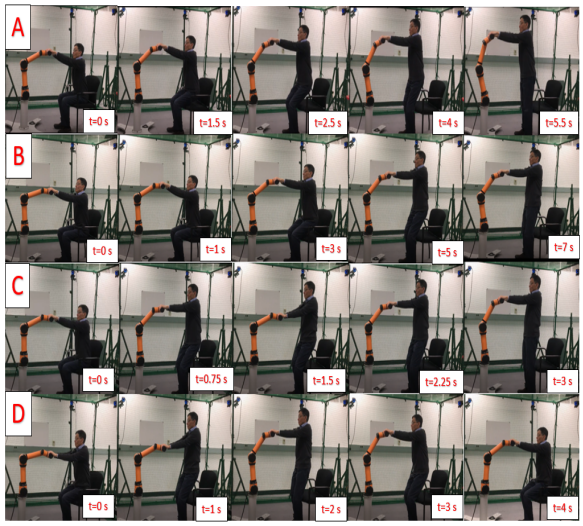

Figure 5.38 Four STS tasks with different human intentions: (A) standard STS, (B) slow STS, (C) fast STS, (D) human refuses to stand up and sits back down.

get up normally. The actual end-effector trajectories (a) in Figure 5.39 are almost the same as the nominal trajectories plotted in Figure 5.31. For (B), the human subject attempts to stand up slowly which leads to a slower movement of the robot end-effector in comparison to (a). For (C), since the human subject wants to stand up faster, the robot effector recognizes the human intention immediately and boosts the velocity of the end-effector along $X_{en}(t)$. For (D), the human tries to sit back down in order to adjust his posture. On the basis of the algorithm (5.44), the robot catches the human intention and controls its end-effector to move backward in the middle of the STS assistance. As a result, the human subject sits back down successfully in the end. Additionally, the tasks are recorded and attached to the link: `https://youtu.be/Esidf20hTtI`.

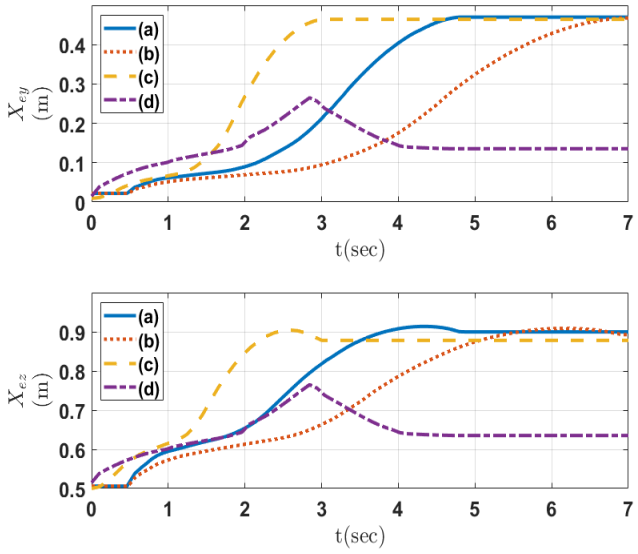

Figure 5.39 The actual end-effector trajectories (a)-(d) plotted for the tasks (A)-(D).

5.4.6 Conclusion

In this research, we proposed an integrated approach that accommodates human dynamics, robot control as well as LSTM network for the problem of Sit-To-Stand (STS) assistance using a robotic manipulator. In particular, we first observed and studied the human-to-human STS assistance. Then, on the basis of the observation and recorded data, we formulated the average intended motion trajectories of the human lower extremities. On the account of the joint trajectories and the formulated human body dynamics, we generated the optimal nominal trajectory of the robot end-effector $X_{en}(t)$. When the robot end-effector travels on $X_{en}(t)$ during STS assistance, the human knee joint load is greatly reduced. In reality, the person who receives the assistance may stand up faster or slower comparatively, or even sit back down due a sudden change of mind. Therefore, to deal with such situations in STS assistance, we utilized LSTM network to evaluate human intentions in STS process and used the human intention to regulate the velocity of the robot end-effector during the assistance. Finally, we implemented simulation and experiments to validate the proposed method in the aspects of joint load reduction and human intention recognition for robot control. The results verified the effectiveness of the proposed algorithm that it is able

to minimize the human joint load and deal with human's changing intention during STS assistance. The proposed method has a great potential in assisting the elderly, disabled, and injured individuals in their daily lives.

5.5 A General Control Framework for Robotic STS Assistance: Design a Novel Estimator for Human Intention Recognition and Human-Robot Contact Model Identification

5.5.1 Introduction

In this research, we propose a general control framework for STS assistance. The kernel of the research is to design a task-specified human intention recognition mechanism for assistive robots to understand different human intended motions and be able to identify the contact model between the human partner and the robot according to different situations. In particular, we first perform various Human-Human STS assistance. From observation of these tasks, we extract common features and construct assumptions. On the basis of the assumption made, we formulate the system dynamics as well as the contact model between the human and the robot. Second, based on the proposed dynamics, a NN-based control framework is designed to let the robot predict the contact model and the human intentions during STS process. Third, various simulations and experiments are performed to validate the proposed approach.

5.5.2 Dynamic Modeling of Contacts Between Human and Robot

In this section, we first perform diverse human-human STS assistance. Then, on the basis of the observation of the human-human collaborations, a number of assumptions are made. The system dynamics and the contact model are constructed on the account of the experimental results and assumptions.

Observation of human-human collaboration The reason of performing human-human collaborative experiments is that human beings naturally and deeply understand how to interact with other human beings safely and fast which is an excellent example for an assistive robot to learn from. On the other hand, we can also observe how a human being reacts when another person is cooperating with the person. This helps us understand the habits and motions of a person so that we can define and even re-shape the formulations of

the human robot contact model as well as the human intention recognition mechanism in a more accurate perspective. Therefore we implement the following experiments that can be summarized as:

A) Various human-human STS assistance with different initial sitting postures.

B) Observation and investigation of human-human interactions during collaborative STS assisted tasks.

In the first group of human-human STS assistance experiments, two volunteers are asked to perform STS assistance together. The person who is passively assisted is request for sitting on a stable chair comfortably with any initial postures. Then the another person is required to hold his/her hands and help the former getting up slowly until the entire STS process is accomplished. As can be seen in Figure 5.40.

Figure 5.40 Human-human STS assistance with different initial postures. 1. upright sitting posture; 2. lean backward sitting posture; 3. lean forward sitting posture.

In the second group of experiments, we ask for different human subjects to perform STS assistance, meanwhile we scrutinize and record the contact patterns as well as motions during each STS process. As shown in Figure 5.41. According to the observations,

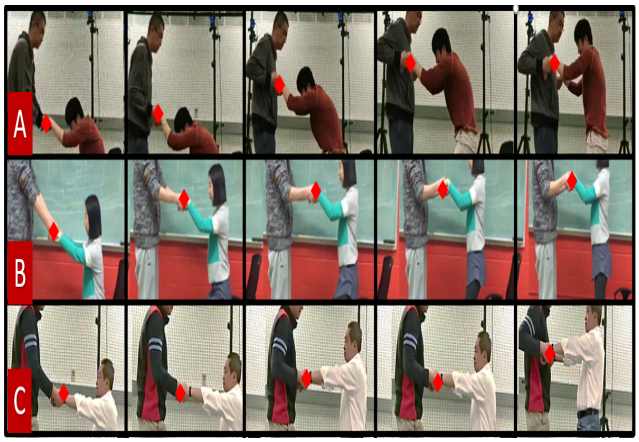

Figure 5.41 The Contact patterns in human-human STS assistance among various subjects. (A) assisting an male adult; (B) assisting a female adult; (C) assisting an elderly subject.

inquiries and analysis of the human-human collaborations, we found those experiments possess some common features that can be seen as:

- Feature 1: In the first group of STS assistance experiments, the motions of the subject who is assisted, stands up in a vertical 2D plane that the out-of-plane waggling motions can be ignored.
- Feature 2: In the second group of STS assistance experiments, the human subjects are always attempting to smooth as well as slow the assisted motions in order to alleviate the force applied along the arms and to anticipate the partners' movements ahead.

According to these common features obtained, some assumptions are made as the followings:

- *Assumption 1*: The human body dynamic is formulated using a five-link planar robot model that the ankle joint is fixated to a leveled ground and the wrist joint is always connected to the robot end-effector.
- *Assumption 2*: We assume an impedance contact model for human-human hand contacts. Furthermore, we also apply this contact model to human robot contacts at the location of the end-effectors.

Modeling of the system dynamics From above analyses, we introduce a general contact scenario for robotic assisted STS. We assume a person who is being assisted sits on a seated place where a commercial robotic manipulator is established firmly at the adjacent place

in font. The person uses two hands to grasp tightly on the robot end-effector. Then, the robot manipulator gradually assists the human in getting up from the seated place until the person completely stands up. The schematic diagram of the system is given in Figure 5.42:

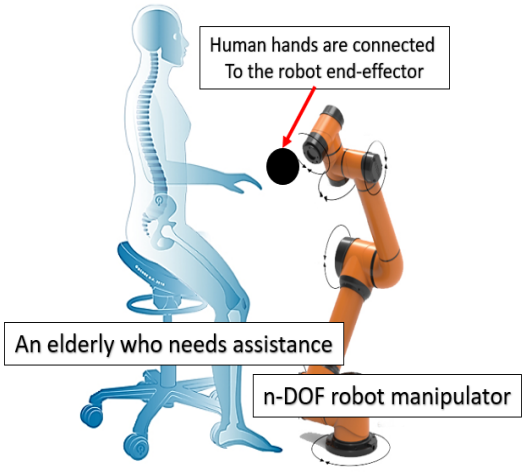

Figure 5.42 The schematic diagram of the system dynamic model.

On the human side, we assume that the human dynamics can be represented with a five-linked structure. The mathematics model is given by:

$$M_h(q)\ddot{q} + C_h(q,\dot{q})\dot{q} + G_h(q) = \tau_h + J_h(q)^T f(t). \tag{5.45}$$

Where the vector $q = [q_1, q_2, q_3, q_4, q_5]^T$ stands for the human joint angles. In particular, q_1 is the ankle angle, q_2 is the knee angle, q_3 is the hip angle, q_4 is the shoulder angle and q_5 is the elbow angle. $M_h(q) \in R^{5\times5}$ is a positive-definite symmetric matrix that represents the human inertia. $C_h(q,\dot{q})\dot{q} \in R^5$ represents the Coriolis and the centripetal forces. $G_h(q) \in R^5$ is the gravitational force. $\tau_h \in R^5$ is the human joint torques generated by muscles and $J_h(q) \in R^{3\times5}$ is the Jacobian matrix. $f(t) \in R^3$ describes the interactive force between the robot end-effector and the human hands.

Since the parameters, such as $M_h(q)$, $C_h(q,\dot{q})$ and $G_h(q)$ are difficult to be obtained directly from measurements. Therefore, we estimate the geometric and inertia parameters

of the human subject by referring to the table of human body segment parameters [49]. The parameters are listed in Table 5.4.

Table 5.4 Human Body Segment Parameters

Segment	$L(\%)$	$M(\%)$	$I_1(Kg-m^2)$	$I_2(Kg-m^2)$
Head	0.5358	0.0730	0.0248	0.3119
Upper arm	0.4360	0.0270	0.0213	0.3119
Forearm	0.4300	0.0160	0.0760	0.3119
Hand	0.5060	0.0066	0.0005	0.3119
Trunk	0.4383	0.5080	1.3080	0.3119
Thigh	0.4330	0.0988	0.1502	0.3119
Lower leg	0.4330	0.0465	0.0505	0.3119
Foot	0.4290	0.0145	0.0038	0.3119

Where $L(\%)$ is the segment length of human body which is defined as a percentage of the whole body length, $M(\%)$ is the segment weight of human body that is defined as a percentage of the whole body weight, I_1 is the mass moments of inertia of the segment along the transverse axis, and I_2 is the mass moments of inertia of along the longitudinal axis. It is worth noting that the parameters must be selected by referring to each individual.

On the robot side, we introduce the mathematical model for a general n-DOF robotic manipulator:

$$M_r(q_n)\ddot{q}_n + C_r(q_n,\dot{q}_n)\dot{q}_n + G_r(q_n) = \tau_r - J_r(q_n)^T f(t). \tag{5.46}$$

Where the vector q_n stands for the robot joint angles. $M_r(q_n) \in R^{n\times n}$ is a positive-definite symmetric matrix that represents the robot inertia. $C_r(q_n,\dot{q}_n)\dot{q}_n \in R^n$ represents the Coriolis and the centripetal forces. $G_r(q_n) \in R^n$ is the gravitational force. $\tau_r \in R^n$ is the robot joint

torques generated by motors and $J_r(q_n) \in R^{3\times n}$ is the Jacobian matrix. $f(t) \in R^3$ describes the interactive force between the robot end-effector and the human hands.

Consider that the robot kinematics in joint space has the following relationship in Cartesian space:

$$X(t) = \phi(q_n) \tag{5.47}$$

where $X(t) \in R^6$ and the $q_n \in R^n$ are the positions/orientations in Cartesian space and the joint space. The velocity profile can be obtained by differentiating equation (5.47):

$$\dot{X}(t) = J_r(q_n)\dot{q}_n, \tag{5.48}$$

Then, taking the time derivative of the equation $\dot{X}(t) = J_r(q_n)\dot{q}_n$ that represents the kinematic relationship between the robot joint space and work space. We can obtain the acceleration $\ddot{X}(t)$ by further derive (5.48):

$$\ddot{X}(t) = J_r(q_n)\ddot{q}_n + \dot{J}_r(q_n)\dot{q}_n, \tag{5.49}$$

Since the interaction occurs at the location between the robot end-effector and the human hands. Hence, we transform the robot dynamics (5.46) into Cartesian coordinate [43].

$$M_c(q_n)\ddot{X}(t) + C_c(q_n,\dot{q}_n)\dot{X}(t) + G_c(q_n) = U - f(t). \tag{5.50}$$

Where,

$$\begin{aligned}
&M_c(q_n) = J_r(q_n)^{-T} M_r(q_n) J_r(q_n)^{-1};\\
&C_c(q_n,\dot{q}_n) = J_r(q_n)^{-T}(C_r(q_n,\dot{q}_n)\\
&\qquad -M_r(q_n)J_r(q_n)^{-1}\dot{J}_r(q_n)J_r(q_n)^{-1})J_r(q_n)^{-1};\\
&G_c(q_n) = J_r(q_n)^{-1} G_r(q_n);\\
&U = J_r(q_n)^{-1}\tau_r.
\end{aligned} \tag{5.51}$$

Notice that $M_c(q_n)$ symmetric and positive definite. $C_c(q_n,\dot{q}_n)$ is a skew-symmetric matrix.

Contact model formulation We define the contact model between the human partner and the assistive robot as an impedance model governed by the equation below:

$$M_d(\ddot{X}(t)-\ddot{X}_d)+C_d(\dot{X}(t)-\dot{X}_d)+K_d(X(t)-X_d)=f(t). \tag{5.52}$$

where M_d, C_d and K_d are are the desired inertia, damping as well as stiffness matrices. $X(t)\in R^3$, $\dot{X}(t)\in R^3$ and $\ddot{X}(t)\in R^3$ describe the present state variables of the robot end-effector. $X_d(t)\in R^3$, $\dot{X}_d(t)\in R^3$ and $\ddot{X}_d(t)\in R^3$ are the desired targets marked at the human hands.

5.5.3 Contact Model Identification and Human Intention Estimation

This section is dedicated to elucidate the structure of the purposed estimator and the functionalities with respect to the contact model identification and human intention recognition for STS assistance.

Problem statement and optimizer design Human beings are naturally sensitive to the surroundings and be able to figure out the physical properties, such as rigidity as well as roughness and the movements of any objects, such as positions and velocities. Therefore, human beings are capable of interacting with surroundings safely and dexterously. This characteristic is validated in human-human STS assistance. Therefore, inspired by this human talent, we intend to train robots so that the robots are able to imitate what human strategy in STS assistance. In order to simplify the problem formulation, the following prerequisites are defined as:

1. We assume the human intended motion $\ddot{X}_d$, which is the desired acceleration term of the human hands is bounded and its variation frequency is slowly in STS assistance since the subjects being assisted are usually aged and sluggish.
2. Equation (5.52) is simplified as:

   $$C_d(\dot{X}(t)-\dot{X}_d)+K_d(X(t)-X_d)=f(t) \tag{5.53}$$

   in order to reduce the calculation complexity.

Hence, we propose a convex estimator for contact model identification and human intention recognition under the constrains of the prerequisites.

$$\min \sum \{||\ddot{X}_d||^2 + \lambda ||f(t) - (C_d(\dot{X}(t) - \dot{X}_d) + K_d(X(t) - X_d))||^2\} \tag{5.54}$$

where λ is a Lagrange multiplier.

To identify the contact model (5.53), we need to figure out the coefficients C_d as well as K_d. Meanwhile to estimate the human intended motions we need to figure out $\ddot{X}_d$. Therefore, as long as we substitute $f(t)$, $X(t)$ and $\dot{X}(t)$ into (5.54) using computational nonlinear solvers, we can get C_d, K_d and $\ddot{X}_d$.

NN-based human intended motion estimation To accomplish the general control framework for STS assistance, we create the structure, as shown in Figure 5.43. The working principle of the structure can be summarized into three procedures:

1. We first use the proposed estimator, which is given by (5.54) to identify the contact model parameters C_d, K_d and to predict the intended human motion $\widehat{\ddot{X}_d}$.
2. From $\widehat{\ddot{X}_d}$ we are able to get $\widehat{\dot{X}_d}$ and $\widehat{X_d}$. Then the historic data of contact force $f(t)$, $\widehat{\dot{X}_d}$ and $\widehat{X_d}$ are applied for training a Neural Network (NN).
3. Based on the NN developed, we design the robot end-effector controller for the manipulator to assist people in STS process.

Impedance control for the robot end-effector To control and achieve contact force between the robot end-effector and the human hands in the form of Equation (5.52), we design the control law for the robot end-effector as:

$$\begin{aligned} U = M_c(q_n)(\ddot{X}_d(t) + M_d^{-1}(C_d(\dot{X}_d(t) - \dot{X}(t)) + K_d(X_d(t) - X(t)) \\ + f(t)) + C_c(q_n, \dot{q}_n)\dot{X}(t) + G_c(q_n) + f(t) \end{aligned} \tag{5.55}$$

To accomplish the desired contact force in the form of Equation (5.53), we can set the value of $\ddot{X}(t)$ as $\ddot{X}_d(t)$ for the robot end-effector so that the robot end-effector can be controlled

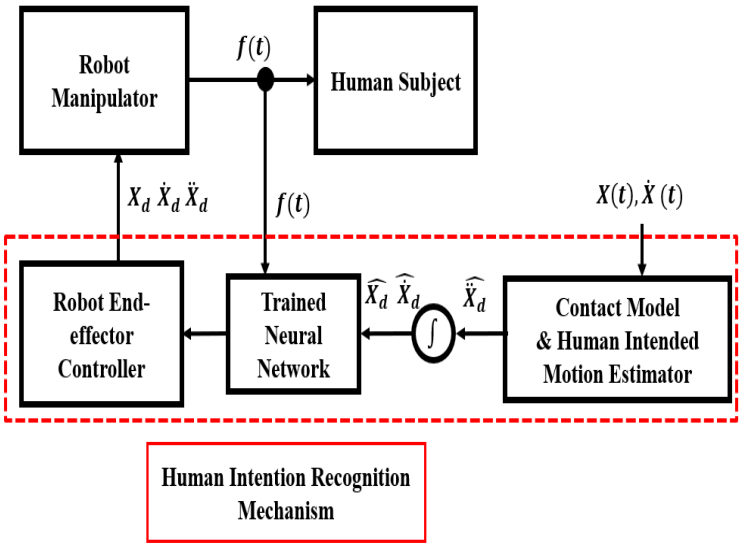

Figure 5.43 Schematic diagram of the control framework.

in velocity mode without losing the authenticity of the impedance control:

$$\dot{X}(t) = C_d^{-1}(f(t) - K_d(X(t) - X_d(t))) + \dot{X}_d(t) \tag{5.56}$$

However, the contact force $f(t)$ must be measured in real-time and feed into (5.56) as a compensation.

5.5.4 Simulation Results

Simulation: contact model parameters identification and human intended motion estimation Initially, we pre-generated a particular human intended motion profiles of X_d, $\dot{X}_d$ and $\ddot{X}_d$ in 1-D space. As can be seen in Figure 5.44.

Next, to testify the performance of the proposed estimator, we define the values of C_d and K_d for two verification groups. In the first group, we set $C_d = 250$ and $K_d = 200$; In the second group, we set $C_d = 200$ and $K_d = 200$. The results are shown in Figure. 5.45.

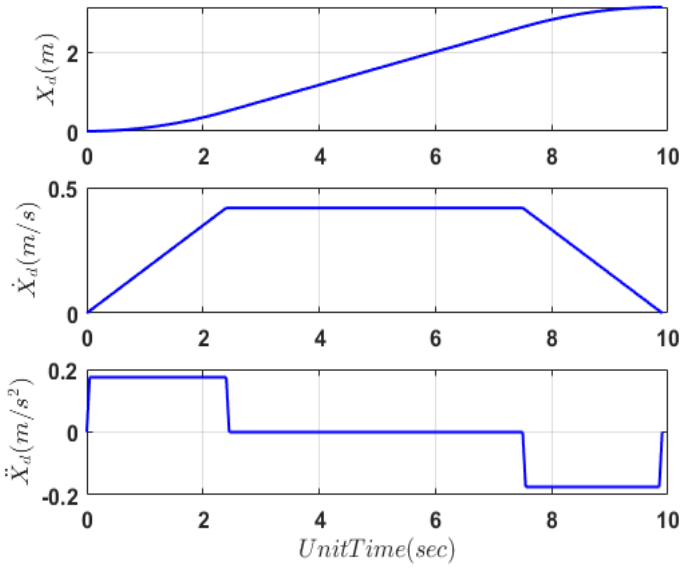

Figure 5.44 The 1D profile of the human intended motion trajectories.

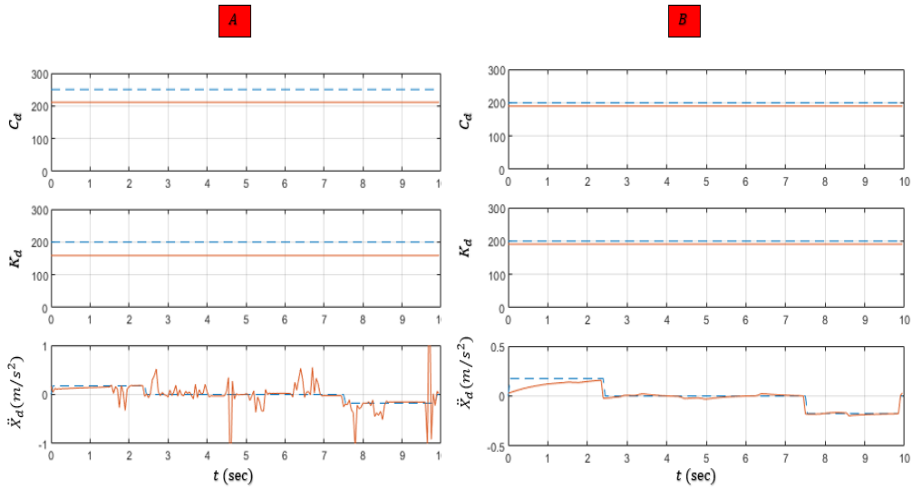

Figure 5.45 Test results of the contact model identification and the human intended motion estimation. (A) $C_d = 250$ and $K_d = 200$; (B) $C_d = 200$ and $K_d = 200$.

5.5.5 Conclusion

In this study, a general control framework for STS assistance is developed which is able to estimate human intention and to identify the contact model between the human partner and the robot. First of all, we conducted different Human-Human STS assistance. From observation of these experiments, we obtained common features and constructed assumptions. On the account of the assumption made, we formulated the human-robot manipulator system dynamics and the contact model. Then, based on the given dynamics, we designed a NN-based control framework which ia capable of identifying the contact model parameters as well as recognizing the human intentions during STS process. Finally, we preformed various simulations to validate the proposed approach.

CHAPTER 6

CONCLUSION

In these studies, the main direction of the research concentrates on Human-Robot Interaction (HRI), assistive robot for STS assistance and human intention estimation. The objective is to effectively assist individuals in need to stand up from a seated position using a robot manipulator. To achieve the goal, we propose a series studies of STS assistance, control framework design as well as human intention recognition. In particular, we performed and recorded a number of demonstrations of human-to-human STS assistance using motion capture system. On the account of the observation and recorded data. We constructed human dynamics, human limb control mechanism, impedance contact model and force optimization algorithms for the HRI. In actual STS assistance, we also considered that the human who is being assisted is likely to move faster or slower from the nominal trajectories, or even sit back down. Therefore, we also developed NNs-based controllers to estimate the ever-changing human's intention in STS assistance, and then adjust the motions of the robot end-effector on the basis of the predicted human intention. Simulations and experiments are conducted in research, which demonstrated that the proposed algorithm is indeed capable of minimizing joint load of human while following his/her intention during the course of STS motion. The proposed algorithms can potentially be applied to future home robots that assist elderly and disabled people with daily activities.

BIBLIOGRAPHY

[1] C. Heyer, "Human-robot interaction and future industrial robotics applications," in *Intelligent Robots and Systems (IROS)*. IEEE, 2010, pp. 4749–4754.

[2] P. A. Lasota, G. F. Rossano, and J. A. Shah, "Toward safe close-proximity human-robot interaction with standard industrial robots," in *2014 International Conference on Automation Science and Engineering (CASE)*. IEEE, 2014, pp. 339–344.

[3] K. Yamazaki, R. Ueda, S. Nozawa, M. Kojima, K. Okada, K. Matsumoto, M. Ishikawa, I. Shimoyama, and M. Inaba, "Home-assistant robot for an aging society," *Proceedings of the IEEE*, vol. 100, no. 8, pp. 2429–2441, 2012.

[4] A. J. Houtenville, D. L. Brucker, and E. A. Lauer, "2015 annual disability statistics compendium." *Institute on Disability, University of New Hampshire, Durham, NH*, 2016.

[5] R. Alqasemi, S. Mahler, and R. Dubey, "Design and construction of a robotic gripper for activities of daily living for people with disabilities," in *Rehabilitation Robotics, 2007. ICORR 2007.* IEEE, 2007, pp. 432–437.

[6] A. M. Okamura, N. Smaby, and M. R. Cutkosky, "An overview of dexterous manipulation," in *Robotics and Automation, 2000. Proceedings. ICRA'00. International Conference on*, vol. 1. IEEE, 2000, pp. 255–262.

[7] T. Hassan, M. Manti, G. Passetti, N. d'Elia, M. Cianchetti, and C. Laschi, "Design and development of a bio-inspired, under-actuated soft gripper," in *Engineering in Medicine and Biology Society (EMBC), 2015 37th Annual International Conference*. IEEE, 2015, pp. 3619–3622.

[8] B. Ward-Cherrier, N. Rojas, and N. F. Lepora, "Model-free precise in-hand manipulation with a 3d-printed tactile gripper," *IEEE Robotics and Automation Letters*, vol. 2, no. 4, pp. 2056–2063, 2017.

[9] C. Della Santina, C. Piazza, G. Grioli, M. G. Catalano, and A. Bicchi, "Toward dexterous manipulation with augmented adaptive synergies: The pisa/iit softhand 2," *IEEE Transactions on Robotics*, no. 99, pp. 1–16, 2018.

[10] F. Veiga, H. Van Hoof, J. Peters, and T. Hermans, "Stabilizing novel objects by learning to predict tactile slip," in *Intelligent Robots and Systems (IROS)*. IEEE, 2015, pp. 5065–5072.

[11] A. Rajeswaran, V. Kumar, A. Gupta, J. Schulman, E. Todorov, and S. Levine, "Learning complex dexterous manipulation with deep reinforcement learning and demonstrations," *arXiv preprint arXiv:1709.10087*, 2017.

[12] M. Liarokapis and A. M. Dollar, "Deriving dexterous, in-hand manipulation primitives for adaptive robot hands," in *Intelligent Robots and Systems (IROS)*. IEEE, 2017, pp. 1951–1958.

[13] X.-Z. Zheng, R. Nakashima, and T. Yoshikawa, "On dynamic control of finger sliding and object motion in manipulation with multifingered hands," *IEEE Transactions on Robotics and Automation*, vol. 16, no. 5, pp. 469–481, 2000.

[14] Y. Yin, Z. Luo, M. Svinin, and S. Hosoe, "Hybrid control of multi-fingered robot hand for dexterous manipulation," in *Systems, Man and Cybernetics*, vol. 4. IEEE, 2003, pp. 3639–3644.

[15] J. Shi, J. Z. Woodruff, P. B. Umbanhowar, and K. M. Lynch, "Dynamic in-hand sliding manipulation," *IEEE Transactions on Robotics*, vol. 33, no. 4, pp. 778–795, 2017.

[16] N. Chavan-Dafle, R. Holladay, and A. Rodriguez, "In-hand manipulation via motion cones," *Dynamics*, vol. 19, no. 31, p. 18, 2018.

[17] E. Lauer and A. Houtenville, "2017 annual disability statistics compendium." *Institute on Disability, University of New Hampshire, Durham, NH*, 2018.

[18] I. R. Molton and A. L. Terrill, "Overview of persistent pain in older adults." *American Psychologist*, vol. 69, no. 2, p. 197, 2014.

[19] B. Heidari, "Knee osteoarthritis prevalence, risk factors, pathogenesis and features: Part i," *Caspian journal of internal medicine*, vol. 2, no. 2, p. 205, 2011.

[20] O. Salah, S. Sessa, A. M. R. F. El-Bab, Y. Kobayashi, A. Takanishi, and M. Fujie, "Modeling and simulation for support robot tracking a human sit to stand motion," in *2016 28th International Conference on Microelectronics (ICM)*, Dec 2016, pp. 81–84.

[21] J. Schneider, W. Stork, S. Irgenfried, and H. Wörn, "A multimodal human machine interface for a robotic mobility aid," in *Automation, Robotics and Applications (ICARA), 2015 6th International Conference on*. IEEE, 2015, pp. 289–294.

[22] Z. Matjačić, M. Zadravec, and J. Oblak, "Sit-to-stand trainer: an apparatus for training "normal-like" sit to stand movement," *IEEE Transactions on Neural Systems and Rehabilitation Engineering*, vol. 24, no. 6, pp. 639–649, 2016.

[23] I. Kim, W. Cho, G. Yuk, H. Yang, B.-R. Jo, and B.-H. Min, "Kinematic analysis of sit-to-stand assistive device for the elderly and disabled," in *2011 IEEE International Conference on Rehabilitation Robotics*. IEEE, 2011, pp. 1–5.

[24] M. Shomin, J. Forlizzi, and R. Hollis, "Sit-to-stand assistance with a balancing mobile robot," in *Robotics and Automation (ICRA), 2015 IEEE International Conference on*. IEEE, 2015, pp. 3795–3800.

[25] M. Geravand, P. Z. Korondi, C. Werner, K. Hauer, and A. Peer, "Human sit-to-stand transfer modeling towards intuitive and biologically-inspired robot assistance," *Autonomous Robots*, vol. 41, no. 3, pp. 575–592, 2017.

[26] P. J. Millington, B. M. Myklebust, and G. M. Shambes, "Biomechanical analysis of the sit-to-stand motion in elderly persons," *Archives of Physical Medicine and Rehabilitation*, vol. 73, no. 7, pp. 609–617, 1992.

[27] Y. Li and S. S. Ge, "Human–robot collaboration based on motion intention estimation," *IEEE/ASME Transactions on Mechatronics*, vol. 19, no. 3, pp. 1007–1014, 2014.

[28] Y. Maeda, T. Hara, and T. Arai, "Human-robot cooperative manipulation with motion estimation," in *Intelligent Robots and Systems. 2001 IEEE/RSJ International Conference on*, vol. 4. IEEE, 2001, pp. 2240–2245.

[29] D. Vasquez, T. Fraichard, and C. Laugier, "Growing hidden markov models: An incremental tool for learning and predicting human and vehicle motion," *The International Journal of Robotics Research*, vol. 28, no. 11-12, pp. 1486–1506, 2009.

[30] L. Bascetta, G. Ferretti, P. Rocco, H. Ardö, H. Bruyninckx, E. Demeester, and E. Di Lello, "Towards safe human-robot interaction in robotic cells: an approach based on visual tracking and intention estimation," in *Intelligent Robots and Systems (IROS), 2011 IEEE/RSJ International Conference on*. IEEE, 2011, pp. 2971–2978.

[31] H. Shen, Q. Song, X. Deng, Y. Zhao, Y. Yu, and Y. Ge, "Recognition of phases in sit-to-stand motion by neural network ensemble (nne) for power assist robot," in *2007 IEEE International Conference on Robotics and Biomimetics (ROBIO)*. IEEE, 2007, pp. 1703–1708.

[32] F. Romano, G. Nava, M. Azad, J. Čamernik, S. Dafarra, O. Dermy, C. Latella, M. Lazzaroni, R. Lober, M. Lorenzini, *et al.*, "The codyco project achievements and beyond: Toward human aware whole-body controllers for physical human robot interaction," *IEEE Robotics and Automation Letters*, vol. 3, no. 1, pp. 516–523, 2018.

[33] Y. Cheng, L. Sun, C. Liu, and M. Tomizuka, "Towards efficient human-robot collaboration with robust plan recognition and trajectory prediction," *IEEE Robotics and Automation Letters*, vol. 5, no. 2, pp. 2602–2609, 2020.

[34] L. Sun, H. An, H. Ma, and J. Gao, "Real-time human intention recognition of multi-joints based on myo," *IEEE Access*, vol. 8, pp. 4235–4243, 2019.

[35] Y. Cheng, W. Zhao, C. Liu, and M. Tomizuka, "Human motion prediction using adaptable neural networks," *arXiv preprint arXiv:1810.00781*, 2018.

[36] P. Schydlo, M. Rakovic, L. Jamone, and J. Santos-Victor, "Anticipation in human-robot cooperation: A recurrent neural network approach for multiple action sequences

prediction," in *2018 IEEE International Conference on Robotics and Automation (ICRA)*, 2018, pp. 5909–5914.

[37] P. Wang, H. Liu, L. Wang, and R. X. Gao, "Deep learning-based human motion recognition for predictive context-aware human-robot collaboration," *The International Academy for Production Engineering*, vol. 67, no. 1, pp. 17–20, 2018.

[38] K. Wakita, J. Huang, P. Di, K. Sekiyama, and T. Fukuda, "Human-walking-intention-based motion control of an omnidirectional-type cane robot," *IEEE/ASME Transactions On Mechatronics*, vol. 18, no. 1, pp. 285–296, 2011.

[39] Y. Wang, Y. Sheng, J. Wang, and W. Zhang, "Human intention estimation with tactile sensors in human-robot collaboration," in *ASME 2017 Dynamic Systems and Control Conference*. American Society of Mechanical Engineers Digital Collection, 2017.

[40] J.-Y. Kuan, T.-H. Huang, and H.-P. Huang, "Human intention estimation method for a new compliant rehabilitation and assistive robot," in *Proceedings of SICE Annual Conference 2010*. IEEE, 2010, pp. 2348–2353.

[41] W. Chen, S. Wang, X. Zhang, L. Yao, L. Yue, B. Qian, and X. Li, "Eeg-based motion intention recognition via multi-task rnns," in *Proceedings of the 2018 SIAM International Conference on Data Mining*. SIAM, 2018, pp. 279–287.

[42] A. Ajoudani, A. M. Zanchettin, S. Ivaldi, A. Albu-Schäffer, K. Kosuge, and O. Khatib, "Progress and prospects of the human–robot collaboration," *Autonomous Robots*, vol. 42, no. 5, pp. 957–975, 2018.

[43] Y. Li and S. S. Ge, "Human–robot collaboration based on motion intention estimation," *IEEE/ASME Transactions on Mechatronics*, vol. 19, no. 3, pp. 1007–1014, 2014.

[44] X. Yu, W. He, Y. Li, C. Yang, and C. Sun, "Neural control for constrained human-robot interaction with human motion intention estimation and impedance learning," in *2017 Chinese Automation Congress (CAC)*, 2017, pp. 2682–2687.

[45] X. Yu, W. He, Y. Li, C. Xue, J. Li, J. Zou, and C. Yang, "Bayesian estimation of human impedance and motion intention for human-robot collaboration," *IEEE Transactions on Cybernetics*, pp. 1–13, 2019.

[46] D. Nicolis, A. M. Zanchettin, and P. Rocco, "Human intention estimation based on neural networks for enhanced collaboration with robots," in *International Conference on Intelligent Robots and Systems (IROS)*. IEEE, 2018, pp. 1326–1333.

[47] R. D. Howe and M. R. Cutkosky, "Practical force-motion models for sliding manipulation," *The International Journal of Robotics Research*, vol. 15, no. 6, pp. 557–572, 1996.

[48] S. Goyal, A. Ruina, and J. Papadopoulos, "Limit surface and moment function descriptions of planar sliding," in *Robotics and Automation, 1989. Proceedings., 1989 IEEE International Conference on*. IEEE, 1989, pp. 794–799.

[49] A. Tözeren, *Human body dynamics: classical mechanics and human movement, Washinton, DC*. Springer Science & Business Media, 1999.

[50] W. Zhao, R. F. Kirsch, R. J. Triolo, and S. Delp, "A bipedal, closed-chain dynamic model of the human lower extremities and pelvis for simulation-based development of standing and mobility neuroprostheses," in *Engineering in Medicine and Biology Society, 1998. Proceedings of the 20th Annual International Conference of the IEEE*, vol. 5. IEEE, 1998, pp. 2605–2608.

[51] J. Li, L. Lu, L. Zhao, C. Wang, and X. Huo, "A human-centered control framework for robotic sit-to-stand assistance," in *2018 IEEE/ASME International Conference on Advanced Intelligent Mechatronics (AIM)*. IEEE, 2018, pp. 845–850.

[52] S. Feng, E. Whitman, X. Xinjilefu, and C. G. Atkeson, "Optimization-based full body control for the DARPA robotics challenge," *Journal of Field Robotics*, vol. 32, no. 2, pp. 293–312, 2015.

[53] S. Mason, L. Righetti, and S. Schaal, "Full dynamics lqr control of a humanoid robot: An experimental study on balancing and squatting," in *Humanoid Robots (Humanoids), 2014 14th IEEE-RAS International Conference on*. IEEE, 2014, pp. 374–379.

[54] W. Li and E. Todorov, "Iterative linear quadratic regulator design for nonlinear biological movement systems." in *International Conference on Informatics in Control, Automation and Robotics (ICINCO)*, 2004, pp. 222–229.

[55] H. W. Kuhn and A. W. Tucker, "Nonlinear programming," in *Traces and emergence of nonlinear programming*. Pavia, Italy, Springer, 2014, pp. 247–258.

[56] P. Zhang, W. Ouyang, P. Zhang, J. Xue, and N. Zheng, "Sr-lstm: State refinement for lstm towards pedestrian trajectory prediction," in *Proceedings of the IEEE Conference on Computer Vision and Pattern Recognition*, 2019, pp. 12 085–12 094.

[57] A. Zyner, S. Worrall, J. Ward, and E. Nebot, "Long short term memory for driver intent prediction," in *2017 IEEE Intelligent Vehicles Symposium (IV)*. IEEE, 2017, pp. 1484–1489.

[58] R. Chellali *et al.*, "Predicting arm movements a multi-variate lstm based approach for human-robot hand clapping games," in *2018 27th IEEE International Symposium on Robot and Human Interactive Communication (RO-MAN)*. IEEE, 2018, pp. 1137–1142.

[59] B. Rohrer. Recurrent neural networks (rnn) and long short-term memory (LSTM), accessed on June 2017. Youtube. [Online]. Available: https://www.youtube.com/watch?v=WCUNPb-5EYI&list=PLVZqlMpoM6kbaeySxhdtgQPFEC5nV7Faa

[60] F. A. Gers, J. Schmidhuber, and F. Cummins, "Learning to forget: Continual prediction with lstm," 1999.

[61] F. A. Gers, N. N. Schraudolph, and J. Schmidhuber, "Learning precise timing with lstm recurrent networks," *Journal of Machine Learning Research*, vol. 3, no. Aug, pp. 115–143, 2002.

[62] E. B. Hutchinson, P. O. Riley, and D. E. Krebs, "A dynamic analysis of the joint forces and torques during rising from a chair," *IEEE Transactions on Rehabilitation Engineering*, vol. 2, no. 2, pp. 49–56, 1994.

[63] H. Suzuki, R. A. Conwit, D. Stashuk, L. Santarsiero, and E. J. Metter, "Relationships between surface-detected EMG signals and motor unit activation," *Medicine & Science in Sports & Exercise*, vol. 34, no. 9, pp. 1509–1517, 2002.

[64] A. Erfanian, H. J. Chizeck, and R. M. Hashemi, "Using evoked emg as a synthetic force sensor of isometric electrically stimulated muscle," *IEEE Transactions on Biomedical Engineering*, vol. 45, no. 2, pp. 188–202, 1998.

[65] H. Milner-Brown and R. Stein, "The relation between the surface electromyogram and muscular force." *The Journal of physiology*, vol. 246, no. 3, pp. 549–569, 1975.

[66] L. Liu, M. Lüken, S. Leonhardt, and B. J. Misgeld, "Emg-driven model-based knee torque estimation on a variable impedance actuator orthosis," in *2017 IEEE International Conference on Cyborg and Bionic Systems (CBS)*. IEEE, 2017, pp. 262–267.